

NONLINEAR DYNAMICS AND SYSTEMS THEORY

An International Journal of Research and Surveys

Volume 22 Number 2 2022

CONTENTS

The Geometry of Mass Distributions.....	117
<i>S. B. Davis</i>	
Lyapunov-Type Inequalities for a Fractional Boundary Value Problem with a Fractional Boundary Condition.....	133
<i>S. Dhar and J. T. Neugebauer</i>	
Performance Comparison of Some Two-Dimensional Chaotic Maps for Global Optimization.....	144
<i>A. Djaout, T. Hamaizia and F. Derouiche</i>	
Existence and Uniqueness of Solutions for a Semilinear Functional Dynamic Equation with Infinite Delay and Impulses.....	155
<i>C. Duque, H. Leiva and A. Tridane</i>	
Modification of the Trajectory Following Method for Asymptotic Stability in a System Nonlinear Control.....	169
<i>Firman, Syamsuddin Toaha, Kasbawati</i>	
Direct Torque Control of Three-Phase Induction Motor Powered by Three-Level Indirect Matrix Converter.....	178
<i>Ameur Khaldi, El Madjid Berkouk, Mohand Oulhadj Mahmoudi and Abdellah Kouzou</i>	
On the Existence of Periodic Solutions of a Degenerate Parabolic Reaction-Diffusion Model.....	197
<i>Amer Mesbahi and Salim Mesbahi</i>	
Active Fault Tolerant Synchronization of Two Hyper Chaos Lu Systems with Disturbance Input and Parametric Uncertainty.....	206
<i>Alireza Sabaghian and Saeed Balochian</i>	
Type-II Left Censoring of Some Finite Support Family Lifetime Distributions.....	218
<i>Mahmoud M. Smadi</i>	

NONLINEAR DYNAMICS & SYSTEMS THEORY

Volume 22, No. 2, 2022

Nonlinear Dynamics and Systems Theory

An International Journal of Research and Surveys

EDITOR-IN-CHIEF A.A.MARTYNYUK

*S.P.Timoshenko Institute of Mechanics
National Academy of Sciences of Ukraine, Kiev, Ukraine*

MANAGING EDITOR I.P.STAVROULAKIS

Department of Mathematics, University of Ioannina, Greece

REGIONAL EDITORS

P.BORNE, Lille, France
M.FABRIZIO, Bologna, Italy
Europe

M.BOHNER, Rolla, USA
HAO WANG, Edmonton, Canada
USA and Canada

T.A.BURTON, Port Angeles, USA
C.CRUZ-HERNANDEZ, Ensenada, Mexico
USA and Latin America

M.ALQURAN, Irbid, Jordan
Jordan and Middle East

K.L.TEO, Perth, Australia
Australia and New Zealand

Nonlinear Dynamics and Systems Theory

An International Journal of Research and Surveys

EDITOR-IN-CHIEF A.A.MARTYNYUK

The S.P.Timoshenko Institute of Mechanics, National Academy of Sciences of Ukraine,
Nesterov Str. 3, 03680 MSP, Kiev-57, UKRAINE / e-mail: journalndst@gmail.com

MANAGING EDITOR I.P.STAVROULAKIS

Department of Mathematics, University of Ioannina
451 10 Ioannina, HELLAS (GREECE) / e-mail: ipstav@cc.uoi.gr

ADVISORY EDITOR A.G.MAZKO

Institute of Mathematics of NAS of Ukraine, Kiev (Ukraine)
e-mail: mazko@imath.kiev.ua

REGIONAL EDITORS

M.ALQURAN (Jordan), e-mail: marwan04@just.edu.jo
P.BORNE (France), e-mail: Pierre.Borne@ec-lille.fr
M.BOHNER (USA), e-mail: bohner@mst.edu
T.A.BURTON (USA), e-mail: taburton@olympen.com
C. CRUZ-HERNANDEZ (Mexico), e-mail: ccruz@cicese.mx
M.FABRIZIO (Italy), e-mail: mauro.fabrizio@unibo.it
HAO WANG (Canada), e-mail: hao8@ualberta.ca
K.L.TEO (Australia), e-mail: K.L.Teo@curtin.edu.au

EDITORIAL BOARD

Aleksandrov, A.Yu. (Russia)	Jafari, H. (South African Republic)
Artstein, Z. (Israel)	Khusainov, D.Ya. (Ukraine)
Awrejcewicz, J. (Poland)	Kloedon, P. (Germany)
Benrejeb, M. (Tunisia)	Kokologiannaki, C. (Greece)
Braiek, N.B. (Tunisia)	Krishnan, E.V. (Oman)
Chen Ye-Hwa (USA)	Limarchenko, O.S. (Ukraine)
D'Anna, A. (Italy)	Nguang Sing Kiong (New Zealand)
De Angelis, M. (Italy)	Okninski, A. (Poland)
Denton, Z. (USA)	Peterson, A. (USA)
Vasundhara Devi, J. (India)	Radziszewski, B. (Poland)
Djemai, M. (France)	Shi Yan (Japan)
Dshalalow, J.H. (USA)	Sivasundaram, S. (USA)
Eke, F.O. (USA)	Sree Hari Rao, V. (India)
Gajic Z. (USA)	Staicu V. (Portugal)
Georgiou, G. (Cyprus)	Stavrakakis, N.M. (Greece)
Herlambang T. (Indonesia)	Vatsala, A. (USA)
Honglei Xu (Australia)	Zuyev, A.L. (Germany)
Izobov, N.A. (Belarusia)	

ADVISORY COMPUTER SCIENCE EDITORS

A.N.CHERNIENKO and A.S.KHOROSHUN, Kiev, Ukraine

ADVISORY LINGUISTIC EDITOR

S.N.RASSHYVALOVA, Kiev, Ukraine

INSTRUCTIONS FOR CONTRIBUTORS

(1) General. Nonlinear Dynamics and Systems Theory (ND&ST) is an international journal devoted to publishing peer-refereed, high quality, original papers, brief notes and review articles focusing on nonlinear dynamics and systems theory and their practical applications in engineering, physical and life sciences. Submission of a manuscript is a representation that the submission has been approved by all of the authors and by the institution where the work was carried out. It also represents that the manuscript has not been previously published, has not been copyrighted, is not being submitted for publication elsewhere, and that the authors have agreed that the copyright in the article shall be assigned exclusively to InforMath Publishing Group by signing a transfer of copyright form. Before submission, the authors should visit the website:

<http://www.e-ndst.kiev.ua>

for information on the preparation of accepted manuscripts. Please download the archive Sample_NDST.zip containing example of article file (you can edit only the file Samplefilename.tex).

(2) Manuscript and Correspondence. Manuscripts should be in English and must meet common standards of usage and grammar. To submit a paper, send by e-mail a file in PDF format directly to

Professor A.A. Martynyuk, Institute of Mechanics,
Nesterov str.3, 03057, MSP 680, Kiev-57, Ukraine
e-mail: journalndst@gmail.com

or to one of the Regional Editors or to a member of the Editorial Board. Final version of the manuscript must typeset using LaTeX program which is prepared in accordance with the style file of the Journal. Manuscript texts should contain the title of the article, name(s) of the author(s) and complete affiliations. Each article requires an abstract not exceeding 150 words. Formulas and citations should not be included in the abstract. AMS subject classifications and key words must be included in all accepted papers. Each article requires a running head (abbreviated form of the title) of no more than 30 characters. The sizes for regular papers, survey articles, brief notes, letters to editors and book reviews are: (i) 10-14 pages for regular papers, (ii) up to 24 pages for survey articles, and (iii) 2-3 pages for brief notes, letters to the editor and book reviews.

(3) Tables, Graphs and Illustrations. Each figure must be of a quality suitable for direct reproduction and must include a caption. Drawings should include all relevant details and should be drawn professionally in black ink on plain white drawing paper. In addition to a hard copy of the artwork, it is necessary to attach the electronic file of the artwork (preferably in PCX format).

(4) References. Each entry must be cited in the text by author(s) and number or by number alone. All references should be listed in their alphabetic order. Use please the following style:

Journal: [1] H. Poincare, Title of the article. *Title of the Journal* **volume**
(issue) (year) pages. [Language]

Book: [2] A.M. Lyapunov, *Title of the Book*. Name of the Publishers, Town, year.

Proceeding: [3] R. Bellman, Title of the article. In: *Title of the Book*. (Eds.).
Name of the Publishers, Town, year, pages. [Language]

(5) Proofs and Sample Copy. Proofs sent to authors should be returned to the Editorial Office with corrections within three days after receipt. The corresponding author will receive a sample copy of the issue of the Journal for which his/her paper is published.

(6) Editorial Policy. Every submission will undergo a stringent peer review process. An editor will be assigned to handle the review process of the paper. He/she will secure at least two reviewers' reports. The decision on acceptance, rejection or acceptance subject to revision will be made based on these reviewers' reports and the editor's own reading of the paper.

NONLINEAR DYNAMICS AND SYSTEMS THEORY

An International Journal of Research and Surveys
Published by InforMath Publishing Group since 2001

Volume 22

Number 2

2022

CONTENTS

The Geometry of Mass Distributions	117
<i>S. B. Davis</i>	
Lyapunov-Type Inequalities for a Fractional Boundary Value Problem with a Fractional Boundary Condition	133
<i>S. Dhar and J. T. Neugebauer</i>	
Performance Comparison of Some Two-Dimensional Chaotic Maps for Global Optimization	144
<i>A. Djaout, T. Hamaizia and F. Derouiche</i>	
Existence and Uniqueness of Solutions for a Semilinear Functional Dynamic Equation with Infinite Delay and Impulses	155
<i>C. Duque, H. Leiva and A. Tridane</i>	
Modification of the Trajectory Following Method for Asymptotic Stability in a System Nonlinear Control	169
<i>Firman, Syamsuddin Toaha, Kasbawati</i>	
Direct Torque Control of Three-Phase Induction Motor Powered by Three-Level Indirect Matrix Converter	178
<i>Ameur Khaldi, El Madjid Berkouk, Mohand Oulhadj Mahmoudi and Abdellah Kouzou</i>	
On the Existence of Periodic Solutions of a Degenerate Parabolic Reaction-Diffusion Model	197
<i>Amer Mesbahi and Salim Mesbahi</i>	
Active Fault Tolerant Synchronization of Two Hyper Chaos Lu Systems with Disturbance Input and Parametric Uncertainty	206
<i>Alireza Sabaghian and Saeed Balochian</i>	
Type-II Left Censoring of Some Finite Support Family Lifetime Distributions	218
<i>Mahmoud M. Smadi</i>	

Founded by A.A. Martynyuk in 2001.

Registered in Ukraine Number: KB No 5267 / 04.07.2001.

NONLINEAR DYNAMICS AND SYSTEMS THEORY

An International Journal of Research and Surveys

Impact Factor from SCOPUS for 2020: SJR – 0.360, SNIP – 1.040 and CiteScore – 1.4

Nonlinear Dynamics and Systems Theory (ISSN 1562–8353 (Print), ISSN 1813–7385 (Online)) is an international journal published under the auspices of the S.P. Timoshenko Institute of Mechanics of National Academy of Sciences of Ukraine and Curtin University of Technology (Perth, Australia). It aims to publish high quality original scientific papers and surveys in areas of nonlinear dynamics and systems theory and their real world applications.

AIMS AND SCOPE

Nonlinear Dynamics and Systems Theory is a multidisciplinary journal. It publishes papers focusing on proofs of important theorems as well as papers presenting new ideas and new theory, conjectures, numerical algorithms and physical experiments in areas related to nonlinear dynamics and systems theory. Papers that deal with theoretical aspects of nonlinear dynamics and/or systems theory should contain significant mathematical results with an indication of their possible applications. Papers that emphasize applications should contain new mathematical models of real world phenomena and/or description of engineering problems. They should include rigorous analysis of data used and results obtained. Papers that integrate and interrelate ideas and methods of nonlinear dynamics and systems theory will be particularly welcomed. This journal and the individual contributions published therein are protected under the copyright by International InforMath Publishing Group.

PUBLICATION AND SUBSCRIPTION INFORMATION

Nonlinear Dynamics and Systems Theory will have 5 issues in 2022, printed in hard copy (ISSN 1562–8353) and available online (ISSN 1813–7385), by InforMath Publishing Group, Nesterov str., 3, Institute of Mechanics, Kiev, MSP 680, Ukraine, 03057. Subscription prices are available upon request from the Publisher, EBSCO Information Services (<mailto:journals@ebSCO.com>), or website of the Journal: <http://e-ndst.kiev.ua>. Subscriptions are accepted on a calendar year basis. Issues are sent by airmail to all countries of the world. Claims for missing issues should be made within six months of the date of dispatch.

ABSTRACTING AND INDEXING SERVICES

Papers published in this journal are indexed or abstracted in: Mathematical Reviews / MathSciNet, Zentralblatt MATH / Mathematics Abstracts, PASCAL database (INIST–CNRS) and SCOPUS.



The Geometry of Mass Distributions

S. B. Davis *

*Research Foundation of Southern California,
8861 Villa La Jolla Drive #13595, La Jolla, CA 92037.*

Received: October 25, 2021; Revised: February 8, 2022

Abstract: Geometrical characteristics of mass distributions are defined and the relation with classical mechanics and general relativity is described. The classical stability of closed geodesic trajectories on surfaces of arbitrary genus is established. An iterative procedure for solving the N-body problem to a high degree of precision is introduced through a complexity minimization method.

Keywords: *center; geodesics; geometrical complexity; N-body problem.*

Mathematics Subject Classification (2010): 52C45, 58E10, 70S05.

1 Introduction

The equations of classical mechanics and general relativity describe the motion of particle in a geometry of three or four dimensions. The potential in general relativity is derived from the curvature of space-time which results from the energy-momentum tensor or mass distribution. The effect of the geometry of the mass distribution on the dynamics will be considered. A geometrical median will be given and verified for various curves and surfaces. It is proven in the two theorems of Section 2 that the geometrical median of a curve is located on the curve if it is a straight line in Euclidean space and a geodesic in curved space. These theorems remain valid for the barycentre which coincides with the center of mass of a uniform distribution. The role of the center of the mass distribution then will be described in classical mechanics and general relativity. It is known that mass distributions tend towards the center [8]. The local stability of geometrical configurations under the gravitational potential will follow for geodesics.

The stability of geodesics that can be identified with strings on a surface is considered. Given the tendency of uniform mass distributions towards the center of a geometrical configuration, it follows from the theorems of Section 2 that only closed geodesics will

* Corresponding author: <mailto:sbdavis@resfndsca.org>

be stable on a Riemann surface in a gravitational field. The geodesic flows on elliptic and hyperbolic surfaces are described. The effect of the flow on an elliptic surface is an infinitesimal displacement of the trajectory. On a hyperbolic surface, however, the transformation of the Jacobi field tends to introduce divergences. The geodesics are known to form a dense set on a hyperbolic Riemann surface [27] and the flow is metrically transitive [17]. The dynamics is invariant under quasi-isometries [12]. The stability of the geodesic flow under the action of the fundamental group has been proven for diffusion paths on a geometrically finite hyperbolic surface with finite [24] or infinite volume [10]. Gibbs measures for the dynamics of geodesic flow on negatively curved Riemannian manifolds have been developed to describe the equilibrium state in the presence of a potential [29]. It is related to the Patterson-Sullivan density at the boundary of Teichmüller space, which suffices for the Myrberg limit set with the full measure [33, 37], where singularities occur for an isometry in the interior.

Particles follow geodesics on the space-times shaped by energy-momentum tensors. A measure of geometrical complexity will be defined in Section 3 for spatial curves satisfying conditions of minimal complexity for geodesics and locally extremal values for curves of high symmetry in a neighbourhood in path space. A divergence is found to arise for the sets of points, with the same equivalence class of tangent vectors or covariant derivatives, having zero Lebesgue measure. The occurrence of these infinities is similar to that of the singularities in a theory of gravity or the elementary particles through point particles. A fundamental length scale may be introduced which would require, however, a theoretical basis. The sum representing this term in the intrinsic complexity is rendered finite through the removal of the singular term in a zeta function regularization method. Given this measure of the complexity, the geodesics paths of particles in curved spaces may be derived from an action principle with a Lagrange multiplier term.

The principle of complexity minimization in deterministic processes may be used to establish the time development of a configuration of masses. Its theoretical foundations are enunciated in the first law of classical mechanics and the geodesic free motion in general relativity. It is adapted in Section 3 to predict the dynamics of an N -body system of approximately equal masses, with an iterative procedure of replacing two masses by a single mass at the center of gravity. This subsequent motion can be placed in a general relativistic setting and the geodesics on the curved manifold representing the force fields would tend to reduce complexity of the system. The classical limit then would yield a configuration that also minimizes complexity.

2 The Geometrical Characteristic

The geometrical median of any continuous set S will be defined to be that point a which minimizes $\int_C r(s, a) ds$, where $r(s, a)$ is the distance from the point a to the point $s \in C$. For a discrete set of points, the sum $\sum_s r(s, a) ds$ is minimized [39] and a generalization to continuous sets has been given [13].

For a straight line of length L , $\int_0^L r(s) ds = 2 \int_0^{\frac{L}{2}} r dr = 2 \frac{(\frac{L}{2})^2}{2} = \frac{L^2}{4}$ from the midpoint, while $\int_0^L r(s) ds = \int_0^L r dr = \frac{L^2}{2}$ from the endpoint. For the vertices of an equilateral triangle with sides of length L , the sum of the distances from the center is $3 \frac{L}{\sqrt{3}} = \sqrt{3}L$, whereas the sum of the distances from any of the vertices equals $2L$.

From a point at a distance r_0 from the point of symmetry of a circle,

$$r(\theta) = \sqrt{R^2 + r_0^2 - 2r_0R \cos \theta}, \quad (1)$$

where θ is the angle subtended from the point of symmetry. When $r_0 = 0$, $\int r(\theta)ds = R^2 \int_{\theta=0}^{2\pi} d\theta = 2\pi R^2$. If $r_0 = R$,

$$\int r(\theta)ds = \sqrt{2}R^2 \int_0^{2\pi} (1 - \cos \theta)^{\frac{1}{2}} d\theta = 8R^2. \tag{2}$$

The geometrical median therefore coincides with the conventional definition of the center for these sets of points.

More generally, let $C(t) : [t_0, t_1] \rightarrow C[t_0, t_1]$ be a curve in Euclidean space. The distance from a point on the curve is

$$r(t) = \sqrt{(x(t) - x_c)^2 + (y - y_c)^2} \tag{3}$$

and the integral $\int_{t_0}^{t_1} r(t)dt$ is minimized when

$$\delta_{x_c} \int_{t_0}^{t_1} \sqrt{(x(t) - x_c)^2 + (y(t) - y_c)^2} dt = \delta_{y_c} \int_{t_0}^{t_1} \sqrt{(x(t) - x_c)^2 + (y(t) - y_c)^2} dt = 0. \tag{4}$$

Then

$$\begin{aligned} \int_{t_0}^{t_1} \frac{x(t) - x_c}{\sqrt{(x(t) - x_c)^2 + (y(t) - y_c)^2}} dt &= 0, \\ \int_{t_0}^{t_1} \frac{y(t) - y_c}{\sqrt{(x(t) - x_c)^2 + (y(t) - y_c)^2}} dt &= 0. \end{aligned} \tag{5}$$

The condition for the center to be a point on the curve is that there exists $t' \in [t_0, t_1]$ such that

$$\begin{aligned} \int_{t_0}^{t_1} \frac{x(t) - x(t')}{\sqrt{(x(t) - x(t'))^2 + (y(t) - y(t'))^2}} dt &= 0, \\ \int_{t_0}^{t_1} \frac{y(t) - y(t')}{\sqrt{(x(t) - x(t'))^2 + (y(t) - y(t'))^2}} dt &= 0. \end{aligned} \tag{6}$$

Theorem 2.1 *The only curves in two-dimensional Euclidean space with geometrical medians located on the curves are straight lines.*

Proof. The conditions (6) can be verified for a straight line $y = mx + b$. Let $x(t) = a_1t + b_1$ and $y(t) = a_2t + b_2$ such that $y(t) = \frac{a_2}{a_1}(a_1t + b_1) + (b_2 - \frac{a_2}{a_1}b_1)$. Substituting these linear relations into (6) gives

$$\int_{t_0}^{t_1} \frac{a_1(t - t')}{\sqrt{(a_1^2(t - t')^2 + a_2^2(t - t')^2}} dt = \frac{a_1}{\sqrt{a_1^2 + a_2^2}} \int_{t_0}^{t_1} \frac{t - t'}{|t - t'|} dt \tag{7}$$

$$= \frac{a_1}{\sqrt{a_1^2 + a_2^2}} \int_{t_0}^{t_1} [\theta(t - t') - \theta(t' - t)] dt = 0, \tag{8}$$

$$\int_{t_0}^{t_1} \frac{a_2(t - t')}{\sqrt{(a_1^2(t - t')^2 + a_2^2(t - t')^2}} dt = \frac{a_2}{\sqrt{a_1^2 + a_2^2}} \int_{t_0}^{t_1} \frac{t - t'}{|t - t'|} dt$$

$$= \frac{a_2}{\sqrt{a_1^2 + a_2^2}} \int_{t_0}^{t_1} [\theta(t - t') - \theta(t' - t)] dt = 0,$$

which can be satisfied if

$$-(t' - t_0) + (t_1 - t') = 0, \quad t' = \frac{t_0 + t_1}{2}.$$

The use of nonlinear parameters for the straight line does not alter the result.

If $y = mx^\alpha + b$, where $\alpha \neq 1$, then the conditions on t' will not be satisfied by a single value of $t' \in [t_0, t_1]$. Therefore, the center would not occur on the curve for $\alpha \neq 1$. A similar conclusion is reached for a sum of terms with different exponents $\{\alpha_1, \dots, \alpha_\ell\}$, where $\alpha_i \neq 1$, $i = 1, \dots, \ell$.

The generalization of the definition of the geometric median of the curve would be the point in a manifold which minimizes the integral $\int_{t_0}^{t_1} \sqrt{g_{\mu\nu}(x(t) - x_0^\mu)(x(t) - x_0^\nu)} dt$.

Theorem 2.2 *The geometrical median is located on a curve in a manifold if and only if it is a geodesic.*

Proof. The geodesic extremizes the arc length of the curve $\int_{t_0}^{t_1} \sqrt{g_{\mu\nu} \frac{dx^\mu}{dt} \frac{dx^\nu}{dt}} dt$ between two fixed points $x(t_0)$ and $x(t_1)$. Since $\frac{dx^\mu}{dt} = \lim_{t-t' \rightarrow 0} \frac{x^\mu(t) - x^\mu(t')}{t-t'}$ for any curve $x(t)$, the arc length equals

$$\lim_{t-t'' \rightarrow 0} \int_{t_0}^{t_1} \sqrt{\frac{g_{\mu\nu}(x^\mu(t) - x^\mu(t''))(x^\nu(t) - x^\nu(t''))}{(t-t'')^2}} dt. \quad (9)$$

Since $\frac{dx^\mu(t)}{dt}$ is a continuous function, one of the two sets of inequalities

$$\begin{aligned} \frac{x^\mu(t) - x^\mu(t - \delta t)}{\delta t} &< \frac{dx^\mu(t)}{dt} < \frac{x^\mu(t + \delta t) - x^\mu(t)}{\delta t}, \\ \frac{x^\mu(t) - x^\mu(t - \delta t)}{\delta t} &> \frac{dx^\mu(t)}{dt} > \frac{x^\mu(t + \delta t) - x^\mu(t)}{\delta t}, \end{aligned} \quad (10)$$

is valid when the second derivative $\frac{d^2 x^\mu(t)}{dt^2}$ does not vanish. It follows that, given a positive definite metric, either

$$\begin{aligned} &\int_{t-\frac{\delta t}{2}}^t \left(g_{\mu\nu} \frac{(x^\mu(t) - x^\mu(t - \frac{\delta t}{2}))(x^\nu(t) - x^\nu(t - \frac{\delta t}{2}))}{(\frac{\delta t}{2})^2} \right)^{\frac{1}{2}} dt \\ &< \lim_{t-t' \rightarrow 0} \int_{t-\frac{\delta t}{2}}^t \sqrt{\frac{g_{\mu\nu}(x^\mu(t) - x^\mu(t'))(x^\nu(t) - x^\nu(t'))}{(t-t')^2}} dt \\ &\lim_{t-t' \rightarrow 0} \int_t^{t+\frac{\delta t}{2}} \sqrt{\frac{g_{\mu\nu}(x^\mu(t) - x^\mu(t'))(x^\nu(t) - x^\nu(t'))}{(t-t')^2}} dt \\ &< \int_t^{t+\frac{\delta t}{2}} \left(g_{\mu\nu} \frac{(x^\mu(t + \frac{\delta t}{2}) - x^\mu(t))(x^\nu(t + \frac{\delta t}{2}) - x^\nu(t))}{(\frac{\delta t}{2})^2} \right)^{\frac{1}{2}} dt \end{aligned} \quad (11)$$

or

$$\begin{aligned}
 & \int_{t-\frac{\delta t}{2}}^t g_{\mu\nu} \frac{(x^\mu(t) - x^\mu(t - \frac{\delta t}{2}))(x^\nu(t) - x^\nu(t - \frac{\delta t}{2}))}{(\frac{\delta t}{2})^2} dt \\
 & > \lim_{t-t' \rightarrow 0} \int_{t-\frac{\delta t}{2}}^t \frac{g_{\mu\nu}(x^\mu(t) - x^\mu(t'))(x^\nu(t) - x^\nu(t'))}{(t-t')^2} dt, \\
 & \lim_{t-t' \rightarrow 0} \int_t^{t+\frac{\delta t}{2}} \frac{g_{\mu\nu}(x^\mu(t) - x^\mu(t'))(x^\nu(t) - x^\nu(t'))}{(t-t')^2} dt \\
 & > \int_t^{t+\frac{\delta t}{2}} g_{\mu\nu} \frac{(x^\mu(t + \frac{\delta t}{2}) - x^\mu(t))(x^\nu(t + \frac{\delta t}{2}) - x^\nu(t))}{(\frac{\delta t}{2})^2} dt.
 \end{aligned} \tag{12}$$

At the point $x^\mu(t)$, moving an infinitesimal distance δt in any other direction than the tangent vector to the geodesic will increase the integrals in the bounds (10) and (11). Therefore, by eliminating the fixed value of δt , the integral

$$\int_{t-\frac{\delta t}{2}}^{t+\frac{\delta t}{2}} (g_{\mu\nu}(x^\mu(t) - x^\mu(t'))(x^\nu(t) - x^\nu(t')))^{\frac{1}{2}} dt \tag{13}$$

is minimized with respect to x'^μ , defined by a change of δt in the affine parameter along a curve which is derived by exponentiation of a vector field at the point $x^\mu(t)$, when this curve is the same geodesic $\{x^\mu(s) | t - \frac{\delta t}{2} < s < t + \frac{\delta t}{2}\}$ in the neighbourhood $N_{exp \frac{\delta t}{2}}(x^\mu(t))$.

By overlapping neighbourhoods $(t - \frac{\delta t}{2}, t + \frac{\delta t}{2})$ throughout the interval (t_0, t_1) , it may be concluded that there exists a point x_0^μ on the path, equal to $x^\mu(t')$, with t' fixed, such that the integral

$$\int_{t_0}^{t_1} \sqrt{g_{\mu\nu}(x^\mu(t) - x_0^\mu)(x^\nu(t) - x_0^\nu)} dt \tag{14}$$

achieves a minimal value.

Suppose that x_0^μ is not located on the geodesic $x(t)$ between $x(t_0)$ and $x(t_1)$. That would be equivalent to the existence of a path $\hat{x}(t)$ including x_0^μ which is not a geodesic between $x(t_0)$ and $x(t_1)$. By triangulation of the interior region between the two curves $x(t)$ and $\hat{x}(t)$, with $x_0^\mu = \hat{x}^\mu(t')$,

$$\int_{t_0}^{t_1} \sqrt{g_{\mu\nu}(\hat{x}^\mu(t) - \hat{x}^\mu(t'))(x^\nu(t) - \hat{x}^\nu(t'))} dt < \int_{t_0}^{t_1} \sqrt{g_{\mu\nu}(x^\mu(t) - x_0^\mu)(x^\nu(t) - x_0^\nu)} dt. \tag{15}$$

The inequality

$$\begin{aligned}
 & \int_{t_0}^{t_1} \sqrt{g_{\mu\nu}(\hat{x}^\mu(t) - \hat{x}^\mu(t'))(\hat{x}^\nu(t) - \hat{x}^\nu(t'))} dt \\
 & > \int_{t_0}^{t_1} \sqrt{g_{\mu\nu}(x^\mu(t) - x^\mu(t''))(x^\nu(t) - x^\nu(t''))} dt
 \end{aligned} \tag{16}$$

for a choice of t'' is valid by the integral form of the mean value theorem and

the minimization of the integral by the geodesic. Then

$$\begin{aligned} & \int_{t_0}^{t_1} \sqrt{g_{\mu\nu}(x^\mu(t) - x_0^\mu)(x^\nu(t) - x_0^\nu)} dt \\ & > \int_{t_0}^{t_1} \sqrt{g_{\mu\nu}(x^\mu(t) - x^\mu(t'))(x^\nu(t) - x^\nu(t'))} dt \\ & > \int_{t_0}^{t_1} \sqrt{g_{\mu\nu}(x^\mu(t) - x^\mu(t''))(x^\nu(t) - x^\nu(t''))} dt, \end{aligned} \quad (17)$$

again, by triangulation. The inequality may be proven generally by overlapping neighbourhoods of the geodesic. It follows that $x(t''')$ is located on the geodesic, which, therefore, includes its center.

Paths which are not geodesics do not minimize the integral (14) for some x_0^μ on the curve, and therefore, by triangulation, there exists another curve through x_0^μ and the endpoints $x(t_0)$ and $x(t_1)$ which has a lesser integral. A slight perturbation of the second curve will produce a curve with nearly the same integral that does not include x_0^μ . Then x_0^μ will minimize the integral for a curve on which it is not located. Consequently, the only curves which include the geometrical medians are geodesics.

The centroid or center of mass has been defined for regions in Euclidean space and generalized to Riemannian manifolds [2,15,19]. The center of mass of an object occupying a volume in a Euclidean space has coordinates

$$x_{i,c.m} = \frac{\int \rho(x)x_i dV}{\int \rho(x)dV}. \quad (18)$$

The mass density $\rho(x)$ is constant for a uniform distribution and

$$x_{i,c.m} = \frac{\rho \int x_i dV}{\rho \int dV} = \frac{\int x_i dV}{\int dV}. \quad (19)$$

The barycenter minimizes the integral of the squared distance [20], [21] from a given point x_0 to the other points in the region

$$\int \sum_i (x_i - x_{i,0})^2 dV. \quad (20)$$

Extremizing this integral requires

$$\delta \int \sum_i (x_i - x_{i,0})^2 dV = 0. \quad (21)$$

Suppose $x_0 = x_{c.m.}$. Then

$$\begin{aligned} - \sum_i \int (x_i - x_{i,0}) \delta x_{i,0} dV &= - \sum_i \int x_i \delta x_{i,0} dV + \sum_i \int \frac{\int x_i dV'}{\int dV'} \delta x_{i,0} dV \\ &= - \sum_i \int x_i \delta x_{i,0} dV + \sum_i \int x_i \delta x_{i,0} dV \\ &= 0. \end{aligned}$$

Therefore, the center of mass of a uniform distribution coincides with the barycentre of the geometric configuration. It may be verified that the barycenter of a straight line $x(t) = a_1t + b_1$ and $y(t) = a_2t + b_2$ between two points $(x(t_0), y(t_0))$ and $(x(t_1), y(t_1))$ occurs at $\frac{t_0+t_1}{2}$. Similarly, the barycenter of a geodesic will be located on the geodesic since the integral $\int_{t_0}^{t_1} g_{\mu\nu}(x^\mu(t) - x_0^\mu)(x^\nu(t) - x_0^\nu) dt$ will be minimized when $x_0^\mu = x^\mu(t'')$, $t'' \in [t_0, t_1]$.

The geometrical median may be compared with the barycenter for various compact sets including the circle [4, 40]. The variational conditions for this integral in Euclidean space are

$$\delta_{x_c} \int_{t_0}^{t_1} [(x(t) - x_c)^2 + (y(t) - y_c)^2] dt = 0, \quad \delta_{y_c} \int_{t_0}^{t_1} [(x(t) - x_c)^2 + (y(t) - y_c)^2] dt = 0,$$

or

$$\int_{t_0}^{t_1} (x(t) - x_c) dt = 0, \quad \int_{t_0}^{t_1} (y(t) - y_c) dt = 0.$$

These equations generally differ from Eq. (5). For the circle, with (x_c, y_c) located at the center and $\sqrt{(x(t) - x_c)^2 + (y(t) - y_c)^2}$ equal to a constant, the conditions are equivalent.

The tendency of uniform mass distributions towards the centers would cause the linear density of a geodesic on a Riemann surface to move towards a point on the curve. When it is closed, there are no distinguished points on the geodesic, which should be stable against variations satisfying classical equations. It may be identified, therefore, with a closed string state. However, a closed curve that is not a geodesic would have a center of mass located away from the path, and if it tends towards this point, the configuration will not be stable. It follows that there is an equivalence between closed string states and closed geodesics only.

The linear Poincare mapping of a closed geodesic translates the Jacobi field and its covariant derivative from one curve to another. The eigenvalue of this transformation has magnitude one when the geodesic is elliptic and stable and it is not equal to one if the geodesic is hyperelliptic and unstable [31]. This variation does not cause a geodesic to disintegrate. Instead, it is moved to a neighbourhood in the first class and diverges in the second category. The transformation only would represent a form of propagation of closed string states along the surface. Consequently, the geodesic flows differ at genus $g = 1$ and $g \geq 2$.

3 Complexity of a Curve and the Relation to the Center

Consider the Frenet frame of a curve spanned by the tangent, normal and binormal vectors \vec{t} , \vec{n} and \vec{b} and the resultant $\vec{v} = \vec{t} + \vec{n} + \vec{b}$. The integrals

$$\frac{- \int_{\gamma} ds \left[\frac{(\vec{v} \cdot \vec{t})^2}{|\vec{v}|^2} \ln \frac{(\vec{v} \cdot \vec{t})^2}{|\vec{v}|^2} + \frac{(\vec{v} \cdot \vec{n})^2}{|\vec{v}|^2} \ln \frac{(\vec{v} \cdot \vec{n})^2}{|\vec{v}|^2} + \frac{(\vec{v} \cdot \vec{b})^2}{|\vec{v}|^2} \ln \frac{(\vec{v} \cdot \vec{b})^2}{|\vec{v}|^2} \right]}{\int ds} \tag{22}$$

and

$$\frac{1}{\int ds} \left[- \int_{\gamma} ds \left[\frac{(\nabla_{\vec{t}} \vec{t} \cdot \hat{t})^2}{|\nabla_{\vec{t}} \vec{t}|^2} \ln \left(\frac{(\nabla_{\vec{t}} \vec{t} \cdot \hat{t})^2}{|\nabla_{\vec{t}} \vec{t}|^2} \right) + \frac{(\nabla_{\vec{t}} \vec{t} \cdot \hat{n})^2}{|\nabla_{\vec{t}} \vec{t}|^2} \ln \left(\frac{(\nabla_{\vec{t}} \vec{t} \cdot \hat{n})^2}{|\nabla_{\vec{t}} \vec{t}|^2} \right) \right. \right. \quad (23)$$

$$\left. \left. + \frac{(\nabla_{\vec{t}} \vec{t} \cdot \hat{b})^2}{|\nabla_{\vec{t}} \vec{t}|^2} \ln \left(\frac{(\nabla_{\vec{t}} \vec{t} \cdot \hat{b})^2}{|\nabla_{\vec{t}} \vec{t}|^2} \right) \right] \right]$$

increase with the number of nonrepetitive windings of a spatial curve. When the curve γ is a geodesic, $\nabla_{\vec{t}} \vec{t} = 0$ or it is proportional to \vec{t} with a change of the affine parameter and $\ln \frac{(\nabla_{\vec{t}} \vec{t} \cdot \hat{t})^2}{|\nabla_{\vec{t}} \vec{t}|^2} = 0$, the integral vanishes.

The first integral for the circle is maximized amongst planar curves. Given the coordinates and the tangent vector

$$(x(t), y(t)) = (a \cos t, a \sin t), \quad (24)$$

$$\left(\frac{dx}{dt}, \frac{dy}{dt} \right) = (-a \sin t, a \cos t),$$

the normal vector is $\vec{n} = (-a \cos t, -a \sin t)$. Then

$$\vec{v} = (-a(\sin t + \cos t), a(\cos t - \sin t)), \quad (25)$$

$$|\vec{t} + \vec{n}|^2 = a^2((\sin t + \cos t)^2 + (\cos t - \sin t)^2) = 2a^2$$

and

$$\vec{t} \cdot \vec{v} = a^2, \quad (26)$$

$$\vec{n} \cdot \vec{v} = a^2.$$

It follows that

$$\frac{- \int_{\gamma} ds \left[\frac{(\vec{v} \cdot \vec{t})^2}{|\vec{v}|^2} \ln \frac{(\vec{v} \cdot \vec{t})^2}{|\vec{v}|^2} + \frac{(\vec{v} \cdot \vec{n})^2}{|\vec{v}|^2} \ln \frac{(\vec{v} \cdot \vec{n})^2}{|\vec{v}|^2} \right]}{\int ds} = \frac{2\pi a \left(-\frac{1}{2} \ln \frac{1}{2} - \frac{1}{2} \ln \frac{1}{2} \right)}{2\pi a} = \ln 2. \quad (27)$$

If a series expansion $\sum_k \frac{1}{k!} I_k$ is considered, where

$$I_k \quad (28)$$

$$= \frac{- \int_C \left[\frac{\vec{t}^{(k)} \cdot \vec{v}^{(k)}}{|\vec{v}^{(k)}|^2} \ln \left(\frac{\vec{t}^{(k)} \cdot \vec{v}^{(k)}}{|\vec{v}^{(k)}|^2} \right) + \frac{\vec{n}^{(k)} \cdot \vec{v}^{(k)}}{|\vec{v}^{(k)}|^2} \ln \left(\frac{\vec{n}^{(k)} \cdot \vec{v}^{(k)}}{|\vec{v}^{(k)}|^2} \right) + \frac{\vec{b}^{(k)} \cdot \vec{v}^{(k)}}{|\vec{v}^{(k)}|^2} \ln \left(\frac{\vec{b}^{(k)} \cdot \vec{v}^{(k)}}{|\vec{v}^{(k)}|^2} \right) \right] ds}{\int_C ds},$$

it may be verified that, by the Frenet equations,

$$\begin{aligned}
 \vec{t}' &= \frac{d|\vec{t}|}{ds} \hat{t} + \kappa|\vec{t}| \hat{n}, \\
 \vec{n}' &= -\kappa|\vec{n}| \hat{t} + \frac{d|\vec{n}|}{ds} \hat{n} + \tau|\vec{n}| \hat{b}, \\
 \vec{b}' &= -\tau|\vec{b}| \hat{n} + \frac{d|\vec{b}|}{ds} \hat{b}, \\
 \vec{v}' &= \left(\frac{d|\vec{t}|}{ds} - \kappa|\vec{n}| \right) \hat{t} + \left(\kappa|\vec{t}| + \frac{d|\vec{n}|}{ds} - \tau|\vec{b}| \right) \hat{n} + \left(\tau|\vec{n}| + \frac{d|\vec{b}|}{ds} \right) \hat{b},
 \end{aligned}
 \tag{29}$$

and

$$\begin{aligned}
 I_1 = & -\frac{1}{\int_C ds} \int_C ds \left\{ \frac{\left[\frac{d|\vec{t}|}{ds} \left(\frac{d|\vec{t}|}{ds} - \kappa|\vec{n}| \right) + \kappa|\vec{t}| \left(\kappa|\vec{t}| + \frac{d|\vec{n}|}{ds} - \tau|\vec{b}| \right) \right]}{\left[\left(\frac{d|\vec{t}|}{ds} - \kappa|\vec{n}| \right)^2 + \left(\kappa|\vec{t}| + \frac{d|\vec{n}|}{ds} - \tau|\vec{b}| \right)^2 + \left(\tau|\vec{n}| + \frac{d|\vec{b}|}{ds} \right)^2 \right]} \right. \\
 & \ln \left[\frac{\left[\frac{d|\vec{t}|}{ds} \left(\frac{d|\vec{t}|}{ds} - \kappa|\vec{n}| \right) + \kappa|\vec{t}| \left(\kappa|\vec{t}| + \frac{d|\vec{n}|}{ds} - \tau|\vec{b}| \right) \right]}{\left[\left(\frac{d|\vec{t}|}{ds} - \kappa|\vec{n}| \right)^2 + \left(\kappa|\vec{t}| + \frac{d|\vec{n}|}{ds} - \tau|\vec{b}| \right)^2 + \left(\tau|\vec{n}| + \frac{d|\vec{b}|}{ds} \right)^2 \right]} \right] \\
 & + \frac{\left[-\kappa|\vec{n}| \left(\frac{d|\vec{t}|}{ds} - \kappa|\vec{n}| \right) + \frac{d|\vec{n}|}{ds} \left(\kappa|\vec{t}| + \frac{d|\vec{n}|}{ds} - \tau|\vec{b}| \right) + \tau|\vec{n}| \left(\tau|\vec{n}| + \frac{d|\vec{b}|}{ds} \right) \right]}{\left[\left(\frac{d|\vec{t}|}{ds} - \kappa|\vec{n}| \right)^2 + \left(\kappa|\vec{t}| + \frac{d|\vec{n}|}{ds} - \tau|\vec{b}| \right)^2 + \left(\tau|\vec{n}| + \frac{d|\vec{b}|}{ds} \right)^2 \right]} \\
 & \ln \left[\frac{\left[-\kappa|\vec{n}| \left(\frac{d|\vec{t}|}{ds} - \kappa|\vec{n}| \right) + \frac{d|\vec{n}|}{ds} \left(\kappa|\vec{t}| + \frac{d|\vec{n}|}{ds} - \tau|\vec{b}| \right) + \tau|\vec{n}| \left(\tau|\vec{n}| + \frac{d|\vec{b}|}{ds} \right) \right]}{\left[\left(\frac{d|\vec{t}|}{ds} - \kappa|\vec{n}| \right)^2 + \left(\kappa|\vec{t}| + \frac{d|\vec{n}|}{ds} - \tau|\vec{b}| \right)^2 + \left(\tau|\vec{n}| + \frac{d|\vec{b}|}{ds} \right)^2 \right]} \right] \\
 & + \frac{\left[-\tau|\vec{b}| \left(\kappa|\vec{t}| + \frac{d|\vec{n}|}{ds} - \tau|\vec{b}| \right) + \frac{d|\vec{b}|}{ds} \left(\tau|\vec{n}| + \frac{d|\vec{b}|}{ds} \right) \right]}{\left[\left(\frac{d|\vec{t}|}{ds} - \kappa|\vec{n}| \right)^2 + \left(\kappa|\vec{t}| + \frac{d|\vec{n}|}{ds} - \tau|\vec{b}| \right)^2 + \left(\tau|\vec{n}| + \frac{d|\vec{b}|}{ds} \right)^2 \right]} \\
 & \left. \ln \left[\frac{\left[-\tau|\vec{b}| \left(\kappa|\vec{t}| + \frac{d|\vec{n}|}{ds} - \tau|\vec{b}| \right) + \frac{d|\vec{b}|}{ds} \left(\tau|\vec{n}| + \frac{d|\vec{b}|}{ds} \right) \right]}{\left[\left(\frac{d|\vec{t}|}{ds} - \kappa|\vec{n}| + \frac{d|\vec{n}|}{ds} - \tau|\vec{b}| \right)^2 + \left(\tau|\vec{n}| + \frac{d|\vec{b}|}{ds} \right)^2 \right]} \right] \right\}.
 \end{aligned}
 \tag{30}$$

For the circle,

$$\begin{aligned}
 I_1 &= -\frac{1}{\int ds} \int ds \left[\frac{\kappa^2|\vec{t}|^2}{\kappa^2|\vec{t}|^2 + \kappa^2|\vec{n}|^2} \ln \frac{\kappa^2|\vec{t}|^2}{\kappa^2|\vec{t}|^2 + \kappa^2|\vec{n}|^2} + \frac{\kappa^2|\vec{n}|^2}{\kappa^2|\vec{t}|^2 + \kappa^2|\vec{n}|^2} \ln \frac{\kappa^2|\vec{n}|^2}{\kappa^2|\vec{t}|^2 + \kappa^2|\vec{n}|^2} \right] \\
 &= -\frac{1}{\int ds} \int ds \left[\frac{1}{2} \ln \frac{1}{2} + \frac{1}{2} \ln \frac{1}{2} \right] = \ln 2,
 \end{aligned}
 \tag{31}$$

since $|\vec{t}| = |\vec{n}| = a$, $\frac{d|\vec{t}|}{ds} = \frac{d|\vec{n}|}{ds} = 0$ and $|\vec{b}| = 0$. Given equal magnitudes of the integrals I_k , $k \geq 0$, the entire measure would be $\sum_{k=0}^{\infty} \frac{1}{k!} \ln 2 = e \ln 2$, which is the maximal bound for planar curves.

The second integral is significantly reduced because the projection of the covariant derivative of the tangent vector onto the vectors would be given in a polar diagram by

$$\begin{aligned} \hat{t} &= \frac{1}{r} \hat{\theta}, & \hat{n} &= \hat{r}, \\ \nabla_{\vec{t}} \vec{t} &= \Gamma^{\theta}_{\theta\theta} \hat{\theta} + \Gamma^r_{\theta\theta} \hat{r}, \\ \Gamma^{\theta}_{\theta\theta} &= 0, & \Gamma^r_{\theta\theta} &= \frac{1}{2} g^{rr} (g_{\theta\theta,r}) = r. \end{aligned} \quad (32)$$

Then

$$C_{curve} = - \int ds \frac{(\nabla_{\vec{t}} \vec{t} \cdot \hat{n})^2}{|\nabla_{\vec{t}} \vec{t}|^2} \ln \left(\frac{(\nabla_{\vec{t}} \vec{t} \cdot \hat{n})^2}{|\nabla_{\vec{t}} \vec{t}|^2} \right) = 0. \quad (33)$$

Even though the circle has maximal symmetry, it is not a geodesic in Euclidean space, and therefore, given the changing direction of the tangent vector, the introduction of a non-zero measure, less than that of neighbouring winding curves, may be considered.

The intrinsic complexity of a curve has been defined to be

$$\begin{aligned} &\sum_{k=1}^{\infty} \frac{1}{k!} C_{int}^{(k)}, \\ C_{int}^{(k)} &= - \int_{\mu=L\delta} \frac{f_k(\ell) d\ell}{L} \ln \frac{f_k(\ell) \ell_{i' min}^{(k)}}{L} - \sum_{i'} \frac{\ell_{i'}^{(k)}}{L} \ln \frac{\ell_{i'}^{(k)}}{L}, \end{aligned} \quad (34)$$

where $f_k(\ell)$ equals the finite number of times that the $(k-1)^{th}$ covariant derivative of the tangent vector can be identified, the index i' labels arcs with identified $(k-1)^{th}$ derivatives and $\ell_{i' min}$ is the minimum length of these arcs of non-zero measure [9]. When the curve is a geodesic, $\nabla_{\vec{t}} \vec{t} = 0$, and the $(k-1)^{th}$ derivatives vanish for $k \geq 2$ and $C_{int} = C_{int}^{(1)} = 0$ because the tangent vectors may be identified through parallel transport. The angular component of this expression has been evaluated for a circle to be non-zero, while the radial component is found to vanish [9], representing a local minimum amongst neighbouring paths. If $\ell_{i' min} \neq 0$, it would be proportional to the arc length of the curve since a dilation of the curve increases $\ell_{i' min}$ and the length L by the same factor. When there are no points that can be identified, the second sum vanishes and $\ell_{i' min}$ would be set equal to $\delta\ell L$, where $\delta\ell = \frac{\delta\ell}{[\delta\ell]}$, which causes a divergence as $\delta\ell \rightarrow 0$. This infinity can be removed from the formula by equating $\ell_{i' min}$ to a constant for these curves, yielding a dependence on L that breaks dilatational invariance. Another possibility for $\ell_{i' min}$ would be $\lambda_{\delta} L$, where λ_{δ} is constant. Then, although dilatational invariance is preserved, the formula includes an arbitrary constant with no theoretical basis.

The measure $\delta\ell \ln \delta\ell$, however, tends to zero, in this limit. Suppose that the variable η is defined by

$$\delta\eta = -\delta\ell \ln \delta\ell. \quad (35)$$

The integral $\int_0^L d\ell = L$ may be regarded as the limit of a Riemann sum $\sum_{i=1}^{\{\frac{L}{\delta\ell}\}} 1 \cdot \delta\ell =$

$\left\{ \frac{L}{\delta \ell} \right\} \delta \ell$. By contrast, the sum of the infinitesimals $\frac{\delta \eta}{L}$ equals

$$-\sum_{i=1}^{\left\{ \frac{L}{\delta \ell} \right\}} \frac{1}{L} \cdot \delta \ell \ln \delta \ell = -\frac{1}{L} \left\{ \frac{L}{\delta \ell} \right\} \delta \ell \ln \delta \ell = -\ln \delta \ell. \tag{36}$$

Given the approximation $\psi(z) \sim \ln z$ for $z \gg 1$, this value may be replaced by

$$\sum_{k=1}^{\left\{ \frac{L}{\delta \ell} \right\}} \frac{1}{k} - \ln L \simeq \sum_{k=\{L\}}^{\left\{ \frac{L}{\delta \ell} \right\}} \frac{1}{k}. \tag{37}$$

Independence with respect to L requires equality with $\sum_{k=1}^{\left\{ \frac{1}{\delta \ell} \right\}} \frac{1}{k}$. Then, $\lim_{\delta \ell \rightarrow 0} \sum_{k=1}^{\left\{ \frac{1}{\delta \ell} \right\}} \frac{1}{k} = \lim_{s \rightarrow 1} \zeta(s)$. Zeta function regularization would consist of removing the singular term in the expansion of the zeta function around $s = 1$, yielding $\lim_{s \rightarrow 1} \left[\zeta(s) - \frac{1}{s-1} \right] = \gamma$.

At a point (x, y) on the circle $x^2 + y^2 = r^2$, the polar coordinates are (r, θ) , with r equal to a constant. The tangent vector has components $(-y, x)$ and

$$\begin{aligned} \vec{t} &= -y \frac{\partial}{\partial x} + x \frac{\partial}{\partial y} = -y \left(\frac{x}{r} \frac{\partial}{\partial r} - \frac{y}{r^2} \frac{\partial}{\partial \theta} \right) + x \left(\frac{y}{r} \frac{\partial}{\partial r} + \frac{x}{r^2} \frac{\partial}{\partial \theta} \right) \\ &= \frac{xy - xy}{r} \frac{\partial}{\partial r} + \frac{x^2 + y^2}{r^2} \frac{\partial}{\partial \theta} = \frac{\partial}{\partial \theta}. \end{aligned} \tag{38}$$

The r component of the gradient is $\frac{\partial}{\partial r}$, while the θ component is $\frac{1}{r} \frac{\partial}{\partial \theta}$. Therefore, the components of the tangent vector in this basis are $(0, r)$. There is no radial component of the tangent vector, the theta component is constant, and yet, the vector $\frac{\partial}{\partial \theta}$ keeps changing with θ_0 at the points $(1, \theta_0)$ since

$$\frac{\partial}{\partial \theta} \Big|_{\theta_0} = -r \sin \theta_0 \frac{\partial}{\partial x} + r \cos \theta_0 \frac{\partial}{\partial y} \tag{39}$$

in contrast with the fixed unit vectors $\frac{\partial}{\partial x}$, $\frac{\partial}{\partial y}$ and $\frac{\partial}{\partial z}$. The vanishing of the radial component of the tangent vector to the circle is sufficient to ensure a local minimum for C_r^{int} for this curve, while the angular component yields a non-zero value, without any further identification of the tangent vectors through Euclidean motions of the plane. The non-zero value is supported by the work that is required to move an object travelling at a constant velocity in a circular path, by contrast with a straight trajectory. It may be noted that this feature is evident also if the distances from the center constitute the sequence for the radial complexity. More generally, it would be necessary to evaluate the perpendicular component of the distance. Then, it would be equal to zero from the center to any other point on a straight line. Since the center is located on the geodesic in curved space by Theorem 2, it would follow that the perpendicular component of the distance to any point on this path and the radial complexity with respect to the center would vanish.

The reduction of the N -body problem to an $(N - 1)$ -body problem through the replacement of two masses by another centrally located mass introduces an approximation

in the description of the motion [26]. The error will be increased by the method of induction culminating in a three-body problem, which has an analytic formulation and can be solved in the plane, where it is equivalent to a system of geodesic equations [34]. It may be reduced through a complexity minimization procedure [9]. The tendency of mass distributions to the center is a transition to a more symmetric and less complex distribution about this point. The introduction of this variational principle selects a classical configuration with each error range.

Theorem 3.1 *The final motions in an N-body problem may be reduced to a three-body problem for equal masses under the condition of the minimization of the complexity of the configuration.*

Proof. Lagrange multiplier terms may be added to give

$$L_N = \frac{1}{2}m \sum_i \sum_{k=1}^N \dot{x}_{i,k}^2 + Gm^2 \sum_{k<\ell}^N \frac{1}{r_{k\ell}} + \sum_j \lambda_j \sum_{k=1}^N (x_{j,k}(t) - x_{c,N}(t)). \quad (40)$$

The minimization of complexity of the configuration of N masses is equivalent to the extremization of the sum of the distances to the center of mass for this system. When the masses of two bodies are replaced by the combined mass $m_{N-1,N}$, the geometrical center must be replaced by the center of mass $x_{c.m.,N-1}$ [18], and given a tendency towards this point, the Lagrangian may be formulated to be

$$\begin{aligned} L_{N-1} = & \frac{1}{2}m \sum_i \sum_{k=1}^{N-2} \dot{x}_{i,k}^2 + \frac{1}{2}m_{N-1,N} \sum_i \dot{x}_{i,(N-1,N)}^2 + Gm^2 \sum_{k<\ell}^{N-2} \frac{1}{r_{k\ell}} \\ & + Gmm_{N-1,N} \sum_{k=1}^{N-2} \frac{1}{r_{k,(N-1,N)}} \\ & + \sum_j \lambda_j \left[\sum_{k=1}^{N-2} (x_{j,k}(t) - x_{c.m.,N-1}(t)) + (x_{j,(N-1,N)}(t) - x_{c.m.,N-1}) \right]. \end{aligned} \quad (41)$$

This averaging technique may be applied to the equations of motion derived from the Lagrangian, the nonlinear equations may be formulated with generalized derivatives which yield estimates of deviations from the exact configurations and ensure existence and convergence to the solution [25].

Since there exists one mass in the new configuration with a different magnitude, the minimization of complexity would not coincide exactly with a tendency towards the center of mass. Nevertheless, the process can be continued over extended intervals progressing to a state of minimum complexity approximated by a tendency towards the location $x_{0,K}$ near the center of mass $x_{c.m.,K}$. Gradient transformation differential equation algorithms have been developed for the minimization of a scalar function that may be identified presently with the complexity [14].

Iteration of the process yields the Lagrangian

$$\begin{aligned}
 L_K = & \frac{1}{2}m \sum_i \sum_{k=1}^{K-1} \dot{x}_{i,k}^2 + \frac{1}{2}m_{K,\dots,N} \sum_i \dot{x}_{i,(K,\dots,N)}^2 + Gm^2 \sum_{k<\ell}^{K-1} \frac{1}{r_{k\ell}} \\
 & + Gmm_{K,\dots,N} \sum_{k=1}^{K-1} \frac{1}{r_{k,(K,\dots,N)}} \\
 & + \sum_j \lambda_j \left[\sum_{k=1}^{K-1} (x_{j,k}(t) - x_{0,K}(t)) + (x_{j,(K,\dots,N)} - x_{0,K}(t)) \right],
 \end{aligned} \tag{42}$$

where $m_{K,\dots,N}$ is the combined mass replacing the masses of $N - K + 1$ bodies, $\{x_{i,(K,\dots,N)}\}$ is the location of center of mass for this system and $x_{c.m.,K}$ is the center of mass derived from the $m_{K,\dots,N}$ and the remaining $K - 1$ masses.

When $K = 3$,

$$\begin{aligned}
 L_3 = & \frac{1}{2}m \sum_i \sum_{k=1}^2 \dot{x}_{i,k}^2 + \frac{1}{2}m_{3,\dots,N} \sum_i \dot{x}_{i,(3,\dots,N)}^2 + Gm^2 \sum_{k<\ell}^2 \frac{1}{r_{k\ell}} \\
 & + Gmm_{3,\dots,N} \sum_{k=1}^{K-1} \frac{1}{r_{k,(3,\dots,N)}} \\
 & + \sum_j \lambda_j \left[\sum_{k=1}^2 (x_{j,k}(t) - x_{0,3}(t)) + (x_{j,(3,\dots,N)} - x_{0,3}(t)) \right]
 \end{aligned} \tag{43}$$

with $m_{3,\dots,N}$ being the combined mass for $N - 2$ bodies, $\{x_{i,(3,\dots,N)}\}$ is the center of mass for this system and $x_{0,3}$ is an attractor for the configuration of minimal complexity for the mass $m_{3,\dots,N}$ and the two masses at x_1 and x_2 , amongst those motions that are allowed by the equations of motion. The equations derived from this Lagrangian would be solvable.

Series solutions to the three-body problem [35] and the N-body problem [38] converge sufficiently slowly, and approximations are necessary over brief time intervals. The general instability of solutions in the nonhierarchical three-body problem, where there is a stratification of the masses and distances, requires statistical methods for a theoretical solution. The method derived from Theorem 3 would allow the errors to be reduced over longer time intervals, especially through stable repeating trajectories including the Lagrange-Euler family of solutions for three masses [11,23]. The replacement of two masses by another mass at the center of gravity resembles the description of the restricted three-body problem as a two-point boundary value problem [30]. The approximation introduced in this theorem would increase in precision given a longer time interval. It is necessary, therefore, to minimize the error for each replacement by the center of mass.

The complexity minimization principle provides a method for determining final states of classical systems. These motions in the three-body problem have been classified, including existence of five relative equilibria representing planar central configuration [5]. The classification may be extended to the N-body problem qualitatively [28], and the addition of a mass yields only finitely many relative equilibria [16], the finiteness of the

number of equivalence classes of these critical points has not been determined generally for $N > 3$. By the above theorem, however, it would follow that this number is finite for equal masses since the calculation can be reduced to a three-body problem through an iteration of an algorithm consisting of the replacement of the location of two masses by the center of mass.

The simplification of calculations resulting from a minimization of complexity is similar to that of the virial theorem, equating the average total kinetic energy with half of the negative of the Newtonian potential energy [3]. The generalization of relative equilibrium motions to G -equivariant motions yields a classification of planar three-body motions by the symmetry groups. Given the action for a certain class of motions, its minimization for a certain subset of motions can be determined. It is found, for example, that the minimum of the action amongst motions with an isosceles symmetry of order 2 is achieved by the Lagrange configurations with a discrete invariance group of order 6 [36]. By contrast, the minimization of the action for choreographic motions is found to be given by relative equilibrium motion corresponding to a regular n -gon. The characterization of stable solutions to the N -body problem by symmetry has generated a classification of the equilibria [7]. The minimization of the gravitational action [6] may be supplemented by that of the complexity, which may be combined with integration techniques to give a description of the dynamics [1].

4 Conclusion

The complexity of a path in curved space would be minimized by geodesics. Prime geodesics are represented by closed curves on surfaces with handles. Consequently, it follows that the geodesic trajectories in two dimensions could represent the propagation of closed strings only on Riemann surfaces of arbitrary genus. The other curves would be unstable against classical perturbations given a tendency toward the center.

The consistency of the dynamics of closed string theory and gravitation therefore follows from the motion of free particles along geodesics on a metric which is a solution to the gravitational field equations. The string effective field equations that tend to the equations of general relativity coupled to matter in the classical limit represent conditions for the quantum conformal invariance. Given the propagation of the quantum string along the surface, the equilibrium configuration of the geodesic can be derived from the variation of an action that includes a Lagrange multiplier term for the minimization of complexity [9]. This auxiliary condition may be transferred from the worldsheet to geodesic motion in the embedding space.

The dynamics of mass distributions in classical mechanics and general relativity then can be described, given the condition of minimization of complexity. The initial motion of N masses in a gravitational field may be formulated in terms of an $(N - 1)$ -body problem after two masses are replaced by the combined system at the center of mass. The subsequent coordinates then can be computed by requiring the complexity of the configuration to be minimized, which would include the classical limit of geodesic trajectories in a manifold curved by a gravity. Iteration of this procedure eventually produces a Lagrangian for the solvable three-body problem. Then the motion of the N bodies is predicted by separating the combined masses and determining the time evolution of this and subsequent configurations along the geodesics on the curved manifold representing the gravitational field of the remaining masses.

Acknowledgment

This research is supported by a Microsoft grant 1984/0420.

References

- [1] S. V. Aarseth. *Gravitational N-Body Simulations*. Cambridge University Press, Cambridge, 2009.
- [2] B. Afsari. Riemannian L^p Center of Mass: Existence, Uniqueness and Convexity, *Proc. Amer. Math. Soc.* **139** (2011) 655–673.
- [3] D. Boccaletti and G. Pucacco. *The Theory of Orbits*, Springer, New York, 1996.
- [4] B. Charlier. Necessary and Sufficient Condition for the Existence of a Fréchet Mean on a Circle. *ESAIM: Probability and Statistics* **17** (2013) 635–649.
- [5] J. Chazy. Le probleme des trois corps. *Annales de l'Ecole Normale* **39** (1922) 29–130.
- [6] A. Chenciner. Action Minimizing Solutions of the Newtonian n -body Problem: From Homology to Symmetry. *Proceedings of the International Congress of Mathematicians, Vol. III*, Beijing, 20 - 28 August 2002, World Scientific Publishing, Singapore, 2002, 1–3.
- [7] A. Chenciner. Symmetries and "Simple" Solutions of the Classical N-Body Problem, *XIVth International Congress on Mathematical Physics*, Lisbon, 28 July - 2 August 2003, World Scientific Publishing, Singapore, 2006, 4–20.
- [8] H. C. Corben and P. Stehle. *Classical Mechanics*, 2nd ed., Dover, New York, 1977.
- [9] S. Davis and B. K. Davis. A Complexity Minimization Principle for Dynamical Processes. *Int. J. Math. Anal.* **4** (2010) 2243–2259.
- [10] N. Enriquez, J. Franchi and Y. Le Jan. Stable Windings on Hyperbolic Surfaces. *Probab. Theory Relat. Fields* **119** (2001) 213–255.
- [11] L. Euler. De Motu Rectilineo Trium Corporum se Mutuo Attrahentium. *Novi Comm. Acad. Sci. Imp. Petrop.* **11** (1767) 144–151.
- [12] K. Falk. Myrberg Type Dynamics are Preserved by Quasi-Isometries of Hyperbolic Space, *Math. Proc. Cambridge Phil. Soc.* **136** (2004) 413–428.
- [13] S. P. Fekete, J. S. B. Mitchell and K. Beurer. On the Continuous Fermat-Weber Problem. *Oper. Res.* **53** (2005) 61–76.
- [14] W. J. Grantham. Gradient Transformation Trajectory following Algorithms for Equality-Constrained Minimization. *Nonlinear Dynamics and Systems Theory* **10** (2010) 125–160.
- [15] K. Grove. Center of Mass and G -local Triviality of G -Bundles. *Proc. Amer. Math. Soc.* **34** (1976) 352–354.
- [16] M. Hampton and A. N. Jensen. Finiteness of Relative Equilibria in the Planar Generalized N -Body Problem with Fixed Subconfigurations, *J. Geom. Mech.* **7** (2015) 35–42.
- [17] G. A. Hedlund. The Dynamics of Geodesic Flows. *Bull. Amer. Math. Soc.* **45** (1939) 241–260.
- [18] T. E. Honein and O. M. O'Reilly. The Geometry of Equations of Motion: Particles in Equivalent Universes. *Nonl. Dyn.* **104** (2021) 2979–2994.
- [19] H. Karcher. Riemannian Center of Mass and Mollifier Smoothing. *Commun. Pure Appl. Math.* **30** (1977) 509–541.
- [20] D. Kazika and A. Srivastava. The Karcher Mean of a Class of Symmetric Distributions on the Circle. *Stat. Prob. Lett.* **78** (2008) 1314–1316.

- [21] W. S. Kendall and H. Le. Statistical Shape Theory. In: *New Perspectives in Stochastic Geometry*. (Eds: W. S. Kendall and I. S. Molchanov). Clarendon, Oxford, 2010, 348–373.
- [22] B. Kol. Flux-based Statistical Prediction of Three-Body Outcomes. *Cel. Mech. Dyn. Astron.* **133** (4) (2021) 17.
- [23] J. L. Lagrange. Essai sur le problème des trois corps. *Oeuvres* **6** (1772) 229–331 [French].
- [24] F. Ledrappier. Harmonic One-forms on the Stable Foliation. *Bol. Soc. Bras. Math.* **25** (1994) 121–138.
- [25] A. A. Martynyuk. Analysis of a Set of Trajectories of Generalized Standard Systems: Averaging Technique. *Nonlinear Dynamic and Systems Theory* **17** (2017) 29–41.
- [26] M. Modugno and R. Vitolo. The Geometry of Newton’s Law and Rigid Systems. *Arch. Mathematicum* **43** (2007) 197–229.
- [27] P. J. Myrberg. Ein Approximationssatz für die fuchsschen Gruppen. *Acta Math.* **57** (1931) 389–409.
- [28] H. Pollard. The Behavior of Gravitational Systems. *J. Math. Mech.* **17** (1967) 601–612.
- [29] F. Paulin, M. Pollicott and B. Schapira. Equilibrium States in Negative Curvature, *Astérisque* **373**, Soc. Math. France, Paris, 2015.
- [30] A. F. B. A. Prado. A Survey on Space Trajectories in the Model of Three Bodies. *Nonlinear Dynamics and Systems Theory* **6** (2006) 389–400.
- [31] H.-B. Rademacher. On a Generic Property of Geodesic Flows. *Math. Ann.* **298** (1994) 101–116.
- [32] N. C. Stone and N. W. C. Leigh. A Statistical Solution to the Chaotic, Non-hierarchical Three-Body Problem. *Nature* **576** (12) (2019) 406–410.
- [33] B. O. Stratmann. A Remark on Myrberg Initial Data for Kleinian Groups. *Geom. Dedicata* **65** (1997) 257–266.
- [34] E. Straume. Geometry and Behavior of n -Body Motion. *Int. J. Math. Mathem. Sci.* **28** (2001) 689–732.
- [35] K. Sundman. Mémoire sur le problème des trois corps. *Acta Mathematica* **36** (1912) 105–179 [French].
- [36] S. Terracini, n -Body Problem and Choreographies. In: *Mathematics of Complexity and Dynamical Systems*, (Ed. R. A. Myers). Springer, New York, 2012, 1043–1069.
- [37] P. Tukia. The Poincaré Series and the Conformal Measure of Conical and Myrberg Limit Points, *J. Anal. Math.* **62** (1994) 241–259.
- [38] Q. Wang. The Global Solution of the N -Body Problem. *Celestial Mechanics* **50** (1991) 73–88.
- [39] E. Weiszfeld. Sur le point pour lequel la somme des distances de n points données est minimum. *Tohoku Math. J.* **43** (1937) 355–386 [French].
- [40] Le Yang. Riemannian Median and its Estimation. *LMS Journal of Computation and Mathematics* **13** (2010) 461–479.



Lyapunov-Type Inequalities for a Fractional Boundary Value Problem with a Fractional Boundary Condition

S. Dhar ^{1*} and J. T. Neugebauer ²

¹ *Department of Mathematics, University of Connecticut, Storrs, CT 06269 USA.*

² *Department of Mathematics and Statistics, Eastern Kentucky University, Richmond, KY 40475 USA.*

Received: January 25, 2019; Revised: March 31, 2022

Abstract: In this paper, we consider a linear fractional differential equation with fractional boundary conditions. First, by obtaining Green's function, we derive the Lyapunov-type inequalities for such boundary value problems. Furthermore, we use the contraction mapping theorem to study the existence of a unique solution to a nonlinear problem.

Keywords: *fractional boundary value problem, Lyapunov-type inequalities, Green's function, contraction mapping theorem, uniqueness and existence of solutions.*

Mathematics Subject Classification (2010): 34A08, 26A33, 26D15, 70K75.

1 Introduction

For the second-order linear differential equation

$$u'' + q(t)u = 0, \quad t \in (a, b) \quad (1)$$

with $q \in C([a, b], \mathbb{R})$, it is known that if (1) has a nontrivial solution u with $u(a) = u(b) = 0$, then

$$\int_a^b |q(t)| dt > \frac{4}{b-a}. \quad (2)$$

This result is known as the Lyapunov inequality, see [1, 22].

It was first noticed by Wintner [28] and later by several other authors that inequality (2) can be improved by replacing $|q(t)|$ by $q_+(t) := \max\{q(t), 0\}$, the nonnegative part of $q(t)$.

* Corresponding author: <mailto:sougata.dhar@uconn.edu>

The Lyapunov inequality was extended by Hartman [19, Chapter XI] to the more general equation

$$(r(t)u')' + q(t)u = 0, \quad (3)$$

where $q, r \in C([a, b], \mathbb{R})$, when it was shown that if (3) has a nontrivial solution u satisfying $u(a) = u(b) = 0$ and $u(t) \neq 0$ for $t \in (a, b)$, then

$$\int_a^b q_+(t) dt > \frac{4}{\int_a^b r^{-1}(t) dt}.$$

These Lyapunov inequalities have been used as an important tool in oscillation, disconjugacy, control theory, eigenvalue problems, and many other areas of differential equations. Due to their importance in applications, they have been extended in various directions by many authors. For more on Lyapunov-type inequalities, we refer the reader to [6–15] and the references cited therein.

Recently, fractional differential equations have gained a considerable attention for their applications in the mathematical modeling of systems and processes in the fields of physics, mechanics, chemistry, aerodynamics, nonlinear dynamics, and system theory [2–5]. Due to useful applications in the boundary value problems (BVPs), a subsequent search for the Lyapunov-type inequalities has also begun in the direction of fractional calculus. Ferreira first obtained Lyapunov-type inequalities for fractional differential equations with pointwise boundary conditions (BCs). In [17], he considered the Riemann-Liouville fractional differential equation

$$D_{a+}^{\alpha} u + q(t)u = 0, \quad 1 < \alpha \leq 2, \quad (4)$$

where $q \in C([a, b], \mathbb{R})$, and showed that if (4) has a nontrivial solution u satisfying $u(a) = u(b) = 0$, then

$$\int_a^b |q(t)| dt > \Gamma(\alpha) \left(\frac{4}{b-a} \right)^{\alpha-1}. \quad (5)$$

In [10, Theorem 2.3], Dhar and Kong improved (5) by replacing $|q(t)|$ by $q_+(t)$. Moreover, they obtained the Lyapunov-type inequalities for a fractional BVP consisting of Eq. (4) and the integral BCs

$$I_{a+}^{2-\alpha} u(a^+) = I_{a+}^{2-\alpha} u(b) = 0, \quad (6)$$

where $I_{a+}^{2-\alpha} u$ is the Riemann-Liouville fractional integral of $u(t)$ of order $2 - \alpha$.

When $\alpha = 2$, the results in [17] and [10] lead to the classical Lyapunov inequality. For more Lyapunov-type inequalities involving the Riemann-Liouville and Caputo fractional derivatives, we refer the reader to [16, 20, 26] and the references cited therein.

In this paper, we consider a Riemann-Liouville fractional BVP consisting of the equation

$$D_{a+}^{\alpha} u + q(t)u = 0,$$

together with the boundary conditions (BCs)

$$u(a) = 0, \quad D_{a+}^{\beta} u(b) = 0,$$

where $\alpha \in (1, 2]$, $\beta \in [0, \alpha - 1]$, D_{a+}^{α} , D_{a+}^{β} are Riemann-Liouville derivatives of order α and β , respectively, and $q \in C([a, b], \mathbb{R})$. We obtain Lyapunov-type inequalities and use them to study the nonexistence of a nontrivial solution of certain BVPs. Furthermore,

by using the contraction mapping theorem, we also establish a criterion for the existence of a nontrivial solution for a nonlinear fractional BVP.

This paper is organized as follows. After this introduction, we recall some basic definitions of fractional calculus in Section 2. Section 3 contains the main results regarding the Lyapunov-type inequalities. Finally, in Section 4, we obtain a criterion for the nonexistence of nontrivial solutions of a linear BVP and the existence of a unique solution of a nonlinear fractional BVP.

2 Background Materials and Preliminaries

For the convenience of the reader, here we present the necessary definitions and lemmas from fractional calculus theory in the sense of Riemann-Liouville. These results can be found in the books [21, 23, 25, 27].

Definition 2.1 Let $\nu > 0$. The Riemann-Liouville fractional integral of the function $u : [a, b] \rightarrow \mathbb{R}$ of order ν , denoted $I_{a^+}^\nu u$, is defined as

$$I_{a^+}^\nu u(t) = \frac{1}{\Gamma(\nu)} \int_a^t (t - s)^{\nu-1} u(s) ds,$$

where $\Gamma(\nu) = \int_0^\infty t^{\nu-1} e^{-t} dt$ is the gamma function, provided the right-hand side is pointwise defined on \mathbb{R}^+ .

Definition 2.2 Let n denote a positive integer and assume $n - 1 < \alpha \leq n$. The Riemann-Liouville fractional derivative of order α of the function $u : [a, b] \rightarrow \mathbb{R}$, denoted $D_{a^+}^\alpha u$, is defined as

$$D_{a^+}^\alpha u(t) = \frac{1}{\Gamma(n - \alpha)} \frac{d^n}{dt^n} \int_a^t (t - s)^{n-\alpha-1} u(s) ds = D^n I_{a^+}^{n-\alpha} u(t),$$

provided the right-hand side is pointwise defined on \mathbb{R}^+ .

In the following, unless otherwise mentioned, we use $D_{a^+}^\alpha u(t)$ to denote the fractional derivative of $u(t)$ with order α and $D^j u(t)$ to denote the classical derivative of order j of $u(t)$ with j being a nonnegative integer. We recall a few well-known properties of the Riemann-Liouville fractional derivatives and integrals to construct and analyze the family of Green’s functions. Let $u \in L_1[a, b]$. Then

$$I_{a^+}^{\nu_1} I_{a^+}^{\nu_2} u(t) = I_{a^+}^{\nu_1 + \nu_2} u(t) = I_{a^+}^{\nu_2} I_{a^+}^{\nu_1} u(t), \quad \nu_1, \nu_2 > 0; \tag{7}$$

$$D_{a^+}^{\nu_1} I_{a^+}^{\nu_2} u(t) = I_{a^+}^{\nu_2 - \nu_1} u(t), \quad \text{if } 0 \leq \nu_1 \leq \nu_2; \tag{8}$$

$$D_{a^+}^\alpha I_{a^+}^\alpha u(t) = u(t);$$

and

$$I_{a^+}^\alpha D_{a^+}^\alpha u(t) = u(t) + \sum_{i=1}^n c_i (t - a)^{\alpha - n + (i-1)}, \tag{9}$$

where $c_i \in \mathbb{R}$ for $1 \leq i \leq n$. The property (7) is referred to as the semigroup property for the fractional integral.

It follows from Definition 2.1 and 2.2 that

$$I_{a+}^{\nu_2}(t-a)^{\nu_1} = \frac{\Gamma(\nu_1+1)}{\Gamma(\nu_2+\nu_1+1)}(t-a)^{\nu_2+\nu_1}, \quad \nu_1 > -1, \nu_2 \geq 0,$$

and

$$D_{a+}^{\nu_2}(t-a)^{\nu_1} = \frac{\Gamma(\nu_1+1)}{\Gamma(\nu_1+1-\nu_2)}(t-a)^{\nu_1-\nu_2}, \quad \nu_1 > -1, \nu_2 \geq 0, \quad (10)$$

where it is assumed that $\nu_2 - \nu_1$ is not a positive integer. If $\nu_2 - \nu_1$ is a positive integer, then the right-hand side of (10) vanishes. To see this, appeal to the convention that $\frac{1}{\Gamma(\nu_1+1-\nu_2)} = 0$ if $\nu_2 - \nu_1$ is a positive integer.

3 Main Results

We now consider the fractional boundary value problem consisting of the differential equation

$$D_{a+}^{\alpha}u + q(t)u = 0, \quad t \in [a, b], \quad (11)$$

together with the boundary conditions

$$u(a) = 0, \quad D_{a+}^{\beta}u(b) = 0, \quad (12)$$

where $\alpha \in (1, 2]$, $\beta \in [0, \alpha - 1]$, D_{a+}^{α} , D_{a+}^{β} are Riemann-Liouville derivatives of order α and β , respectively, and $q \in C([a, b], \mathbb{R})$. First, we present Green's function corresponding to the BVP (11), (12).

Lemma 3.1 *Let $h \in C([a, b], \mathbb{R})$, $\alpha \in (1, 2]$, and $\beta \in [0, \alpha - 1]$. Then the unique solution of the BVP consisting of the equation*

$$D_{a+}^{\alpha}u + h(t) = 0, \quad t \in [a, b], \quad (13)$$

and the BCs (12) is

$$u(t) = \int_a^b G(t, s)h(s)ds, \quad t \in [a, b],$$

where

$$G(t, s) = \frac{1}{\Gamma(\alpha)} \begin{cases} \frac{(t-a)^{\alpha-1}(b-s)^{\alpha-1-\beta}}{(b-a)^{\alpha-1-\beta}} - (t-s)^{\alpha-1}, & a \leq s \leq t \leq b, \\ \frac{(t-a)^{\alpha-1}(b-s)^{\alpha-1-\beta}}{(b-a)^{\alpha-1-\beta}}, & a \leq t \leq s \leq b. \end{cases} \quad (14)$$

Proof. We use (9) to reduce (13) to an equivalent integral equation

$$u(t) = -I_{a+}^{\alpha}h(t) + c_1(t-a)^{\alpha-2} + c_2(t-a)^{\alpha-1}.$$

The BC $u(a) = 0$ implies $c_1 = 0$, and hence

$$u(t) = -I_{a+}^{\alpha}h(t) + c_2(t-a)^{\alpha-1}.$$

Note that $0 \leq \beta < \alpha$. Applying D_{a+}^{β} on both sides and using (8) and (10), we have

$$\begin{aligned} D_{a+}^{\beta}u(t) &= -D_{a+}^{\beta}(I_{a+}^{\alpha}h(t) + c_2(t-a)^{\alpha-1}) \\ &= -I_{a+}^{\alpha-\beta}h(t) + c_2\frac{\Gamma(\alpha)}{\Gamma(\alpha-\beta)}(t-a)^{\alpha-1-\beta}. \end{aligned}$$

Since $D_{a^+}^\beta u(b) = 0$, it is easy to see that

$$c_2 = \frac{1}{\Gamma(\alpha)(b-a)^{\alpha-1-\beta}} \int_a^b (b-s)^{\alpha-1-\beta} h(s) ds.$$

Therefore, the unique solution of problem (13), (12) is

$$\begin{aligned} u(t) &= \frac{-1}{\Gamma(\alpha)} \int_a^t (t-s)^{\alpha-1} h(s) ds + \frac{(t-a)^{\alpha-1}}{\Gamma(\alpha)(b-a)^{\alpha-1-\beta}} \int_a^b (b-s)^{\alpha-1} h(s) ds \\ &= \frac{1}{\Gamma(\alpha)} \int_a^t \left\{ \frac{(t-a)^{\alpha-1}(b-s)^{\alpha-1}}{(b-a)^{\alpha-1-\beta}} - (t-s)^{\alpha-1} \right\} h(s) ds \\ &\quad + \frac{1}{\Gamma(\alpha)} \int_t^b \frac{(t-a)^{\alpha-1}(b-s)^{\alpha-1}}{(b-a)^{\alpha-1-\beta}} h(s) ds \\ &= \int_a^b G(t,s) h(s) ds. \end{aligned}$$

The proof is complete.

Lemma 3.2 *Green’s function $G(t, s)$ given in (14) satisfies the following properties.*

1. $G(t, s) \geq 0$ for $(t, s) \in [a, b] \times [a, b]$.
2. $\max_{t \in [a, b]} G(t, s) \leq G(s, s)$ for $s \in [a, b]$.
3. $G(s, s)$ has a unique maximum at $s^* = \frac{(\alpha-1)b + (\alpha-1-\beta)a}{2\alpha-2-\beta}$ given by

$$G(s^*, s^*) = \frac{1}{\Gamma(\alpha)} \left(\frac{(b-a)(\alpha-1)}{2\alpha-2-\beta} \right)^{\alpha-1} \left(\frac{\alpha-1-\beta}{2\alpha-2-\beta} \right)^{\alpha-1-\beta}. \tag{15}$$

Proof. Define

$$g_1(t, s) = \frac{(t-a)^{\alpha-1}(b-s)^{\alpha-1-\beta}}{(b-a)^{\alpha-1-\beta}} - (t-s)^{\alpha-1},$$

for $a \leq s \leq t \leq b$ and

$$g_2(t, s) = \frac{(t-a)^{\alpha-1}(b-s)^{\alpha-1-\beta}}{(b-a)^{\alpha-1-\beta}},$$

for $a \leq t \leq s \leq b$. First, we point out that

$$\frac{b-s}{b-a} - \frac{t-s}{t-a} = \frac{(b-s)(t-a) - (t-s)(b-a)}{(b-a)(t-a)} = \frac{(b-t)(s-a)}{(b-a)(t-a)} \geq 0,$$

or

$$\frac{b-s}{b-a} \geq \frac{t-s}{t-a},$$

for $a \leq s \leq t \leq b$.

Now,

$$\begin{aligned} g_1(t, s) &= \frac{(t-a)^{\alpha-1}(b-s)^{\alpha-1-\beta}}{(b-a)^{\alpha-1-\beta}} - (t-s)^{\alpha-1} \\ &= (t-a)^{\alpha-1} \left(\frac{b-s}{b-a} \right)^{\alpha-1-\beta} - (t-a)^{\alpha-1} \left(\frac{t-s}{t-a} \right)^{\alpha-1} \\ &= (t-a)^{\alpha-1} \left[\left(\frac{b-s}{b-a} \right)^{\alpha-1-\beta} - \left(\frac{t-s}{t-a} \right)^{\alpha-1} \right]. \end{aligned}$$

Since $0 \leq \frac{b-s}{b-a} \leq 1$, $0 \leq \frac{t-s}{t-a} \leq 1$, and $\alpha-1-\beta \leq \alpha-1$, one has

$$\left(\frac{b-s}{b-a} \right)^{\alpha-1-\beta} \geq \left(\frac{b-s}{b-a} \right)^{\alpha-1} \geq \left(\frac{t-s}{t-a} \right)^{\alpha-1}.$$

So $g_1(t, s) \geq 0$ for $a \leq s \leq t \leq b$.

Now

$$\begin{aligned} \frac{\partial}{\partial t} g_1(t, s) &= (\alpha-1) \frac{(t-a)^{\alpha-2}(b-s)^{\alpha-1-\beta}}{(b-a)^{\alpha-1}} - (\alpha-1)(t-s)^{\alpha-2} \\ &= (\alpha-1)(t-a)^{\alpha-2} \left(\frac{b-s}{b-a} \right)^{\alpha-1-\beta} - (\alpha-1)(t-a)^{\alpha-2} \left(\frac{t-s}{t-a} \right)^{\alpha-2} \\ &= (\alpha-1)(t-a)^{\alpha-2} \left[\left(\frac{b-s}{b-a} \right)^{\alpha-1-\beta} - \left(\frac{t-s}{t-a} \right)^{\alpha-2} \right]. \end{aligned}$$

Since $0 \leq \frac{b-s}{b-a} \leq 1$, $0 \leq \frac{t-s}{t-a} \leq 1$, $\alpha-1-\beta \geq \alpha-2$, and $\alpha-2 \leq 0$, we have

$$\left(\frac{b-s}{b-a} \right)^{\alpha-1-\beta} \leq \left(\frac{b-s}{b-a} \right)^{\alpha-2} \leq \left(\frac{t-s}{t-a} \right)^{\alpha-2}.$$

So $\frac{\partial}{\partial t} g_1(t, s) \leq 0$ for $a \leq s \leq t \leq b$. Thus $g_1(t, s)$ is a decreasing function with respect to t , implying $g_1(t, s) \leq g_1(s, s)$ for all $t \in [s, b]$.

It is easy to see that $g_2(t, s) \geq 0$. Moreover,

$$\frac{\partial}{\partial t} g_2(t, s) = (\alpha-1) \frac{(t-a)^{\alpha-2}(b-s)^{\alpha-1-\beta}}{(b-a)^{\alpha-1-\beta}} \geq 0,$$

for $a \leq t \leq s \leq b$. So $g_2(t, s)$ is increasing with respect to t implying $g_2(t, s) \leq g_2(s, s)$ for all $t \in [a, s]$. Thus (1) and (2) hold.

To prove (3), we define

$$g(s) := G(s, s) = \frac{(s-a)^{\alpha-1}(b-s)^{\alpha-1-\beta}}{(b-a)^{\alpha-1-\beta}\Gamma(\alpha)}. \quad (16)$$

Then $g(a) = g(b) = 0$ and $g(s) > 0$ on (a, b) . By Rolle's theorem, there exists $s^* \in (a, b)$ such that $g(s^*) = \max_{s \in [a, b]} g(s)$, i.e., $g'(s^*) = 0$. Note that

$$\begin{aligned} g'(s) &= \frac{(\alpha-1)(s-a)^{\alpha-2}(b-s)^{\alpha-1-\beta} - (\alpha-1-\beta)(s-a)^{\alpha-1}(b-s)^{\alpha-2}}{(b-a)^{\alpha-1-\beta}\Gamma(\alpha)} \\ &= \frac{(s-a)^{\alpha-2}(b-s)^{\alpha-2-\beta} [(\alpha-1)(b-s) - (\alpha-1-\beta)(s-a)]}{(b-a)^{\alpha-1-\beta}\Gamma(\alpha)}. \end{aligned}$$

Hence $g'(s^*) = 0$ when

$$s^* = \frac{(\alpha - 1)b + (\alpha - 1 - \beta)a}{2\alpha - 2 - \beta}.$$

Notice

$$s^* > \frac{(\alpha - 1)a + (\alpha - 1 - \beta)a}{2\alpha - 2 - \beta} = a,$$

and

$$s^* < \frac{(\alpha - 1)b + (\alpha - 1 - \beta)a}{2\alpha - 2 - \beta} < \frac{(\alpha - 1)b + (\alpha - 1 - \beta)b}{2\alpha - 2 - \beta} = b,$$

so s^* is well-defined. Replacing s^* in (16) we see that (15) holds.

We remark here that if $\beta \in (\alpha - 1, 1]$, then properties (1) and (2) from Lemma 3.2 still hold. However, the function $g(s)$ defined in the proof has a singularity at b when $\beta > \alpha - 1$. Hence $G(s, s)$ does not have a maximum value, which is not surprising, since in this case, $G(s, s)$ is only defined for $s \in [a, b)$.

Lemma 3.3 *Let $G(t, s)$ be given by (14). Then*

$$\int_a^b G(t, s)ds \leq \frac{(\alpha - 1)^{\alpha-1}}{(\alpha - \beta)^\alpha \Gamma(\alpha + 1)} (b - a)^\alpha. \tag{17}$$

Proof. When using the expression of $G(t, s)$ in (14), it follows that

$$\begin{aligned} \int_a^b G(t, s)ds &= \frac{1}{\Gamma(\alpha)} \left[\frac{(t - a)^{\alpha-1}}{(b - a)^{\alpha-1-\beta}} \int_a^b (b - s)^{\alpha-1-\beta} ds - \int_a^t (t - s)^{\alpha-1} ds \right] \\ &= \frac{1}{\Gamma(\alpha)} \left[\frac{(t - a)^{\alpha-1}}{(b - a)^{\alpha-1-\beta}} \frac{(b - a)^{\alpha-\beta}}{\alpha - \beta} - \frac{(t - a)^\alpha}{\alpha} \right] \\ &= \frac{(t - a)^{\alpha-1}}{\Gamma(\alpha + 1)} \left[\frac{\alpha}{\alpha - \beta} (b - a) - (t - a) \right]. \end{aligned} \tag{18}$$

We denote

$$f(t) := \frac{(t - a)^{\alpha-1}}{\Gamma(\alpha + 1)} \left[\frac{\alpha}{\alpha - \beta} (b - a) - (t - a) \right], \quad t \in [a, b]. \tag{19}$$

Let $c := a + \frac{\alpha}{\alpha - \beta}(b - a)$. Clearly, $f(a) = f(c) = 0$, and $f(t) > 0$ on (a, c) . Since $\alpha - \beta \leq \alpha$, we have $b \leq c$ with the equality holding only when $\beta = 0$. By Rolle's theorem, there exists $t^* \in (a, c)$ such that $f(t^*) = \max_{t \in [a, c]} f(t)$, i.e., $f'(t^*) = 0$. Note that

$$f'(t) = \frac{(t - a)^{\alpha-2}}{\Gamma(\alpha)} \left[\frac{\alpha - 1}{\alpha - \beta} (b - a) - (t - a) \right]. \tag{20}$$

It is easy to see that $f'(t) = 0$ only at $t = t^* = a + \frac{\alpha-1}{\alpha-\beta}(b - a)$. Again, $\alpha - 1 \leq \alpha - \beta$ implies $t^* \leq b$ with the equality holding only when $\beta = 1$. Hence $f(t)$ has a unique maximum at $t^* \in [a, b] \subseteq [a, c]$ given by

$$\max_{t \in [a, c]} f(t) = \max_{t \in [a, b]} f(t) = f(t^*) = \frac{(\alpha - 1)^{\alpha-1}}{(\alpha - \beta)^\alpha \Gamma(\alpha + 1)} (b - a)^\alpha.$$

The proof is complete.

Now we present a Lyapunov-type inequality for (11), (12).

Theorem 3.1 Assume (11) has a nontrivial solution u satisfying (12) and $u(t) \neq 0$ on (a, b) . Then

$$\int_a^b q_+(t)dt > \Gamma(\alpha) \left(\frac{2\alpha - 2 - \beta}{(b-a)(\alpha-1)} \right)^{\alpha-1} \left(\frac{2\alpha - 2 - \beta}{\alpha - 1 - \beta} \right)^{\alpha-1-\beta}. \quad (21)$$

Proof. Let u be a solution of (11), (12). Then u satisfies

$$u(t) = \int_a^b G(t, s)q(s)u(s)ds.$$

Without loss of generality, assume $u(t) > 0$ on (a, b) . Define $m = \max_{t \in [a, b]} u(t)$. Using Lemma 3.2 and the facts that $0 \leq u(t) \leq m$, $u(t) \not\equiv m$ on $[a, b]$, and $q(t) \leq q_+(t)$, we have

$$m < m \max_{t \in [a, b]} \int_a^b G(t, s)q_+(s)ds \leq m \int_a^b G(s, s)q_+(s)ds.$$

Canceling m from both sides and using Lemma 3.2 again, we see that

$$1 < \frac{1}{\Gamma(\alpha)} \left(\frac{(b-a)(\alpha-1)}{2\alpha-2-\beta} \right)^{\alpha-1} \left(\frac{\alpha-1-\beta}{2\alpha-2-\beta} \right)^{\alpha-1-\beta} \int_a^b q_+(t)dt,$$

which gives the desired result.

Remark 3.1 Notice when $\beta = 0$, we obtain the improved form (5) which was the result presented by Ferreira in [17] and later was noted by Dhar and Kong in [10]. Also, by setting $\alpha = 2$ and $\beta = 0$, we obtain the classical Lyapunov inequality.

4 Application to Boundary Value Problems

In the last section, we apply the obtained results in Section 3 to study the nonexistence, uniqueness, and existence-uniqueness of solutions of related fractional-order BVPs. First, we provide a sufficient condition for the nonexistence of a nontrivial solution of the BVP (11), (12).

Theorem 4.1 Assume

$$\int_a^b q_+(t)dt \leq \Gamma(\alpha) \left(\frac{2\alpha - 2 - \beta}{(b-a)(\alpha-1)} \right)^{\alpha-1} \left(\frac{2\alpha - 2 - \beta}{\alpha - 1 - \beta} \right)^{\alpha-1-\beta}. \quad (22)$$

Then (11), (12) has no nontrivial solutions.

Proof. Assume the contrary, i.e., BVP (11), (12) has a nontrivial solution u . Then by Theorem 3.1, (21) holds. This contradicts assumption (22).

Now we consider a nonlinear fractional BVP consisting of the equation

$$D_{a^+}^\alpha u + f(t, u) = 0, \quad (23)$$

together with the BCs (12), where $\alpha \in (1, 2]$, $\beta \in [0, \alpha - 1]$. Here we present a criterion for the existence of a unique solution for BVP (23), (12).

Theorem 4.2 Assume $f : [a, b] \times \mathbb{R} \rightarrow \mathbb{R}$ is continuous and satisfies a uniform Lipschitz condition with respect to the second variable on $[a, b] \times \mathbb{R}$ with Lipschitz constant K ; that is

$$|f(t, u_1) - f(t, u_2)| \leq K|u_1 - u_2|, \tag{24}$$

for all $(t, u_1), (t, u_2) \in [a, b] \times \mathbb{R}$. If

$$b - a < \left[\frac{(\alpha - \beta)^\alpha \Gamma(\alpha + 1)}{K(\alpha - 1)^{\alpha - 1}} \right]^{\frac{1}{\alpha}}, \tag{25}$$

then BVP (23), (12) has a unique solution on $[a, b]$.

Proof. Let \mathcal{B} be the Banach space of continuous functions defined on $[a, b]$ with the norm

$$\|u\| = \max_{t \in [a, b]} |u(t)|.$$

Now $u(t)$ is a solution of BVP (23) if and only if $u(t)$ satisfies the integral equation

$$u(t) = \int_a^b G(t, s) f(s, u(s)) ds.$$

Define the operator $T : \mathcal{B} \rightarrow \mathcal{B}$ by

$$Tu(t) = \int_a^b G(t, s) f(s, u(s)) ds.$$

Then T is completely continuous. We claim that T has a unique fixed point in \mathcal{B} . In fact, for any $u_1, u_2 \in \mathcal{B}$, we have

$$|Tu_1(t) - Tu_2(t)| \leq \int_a^b |G(t, s)| |f(s, u_1(s)) - f(s, u_2(s))| ds.$$

Since $G(t, s) \geq 0$ on $[a, b] \times [a, b]$ and f satisfies (24), we have

$$\begin{aligned} |Tu_1(t) - Tu_2(t)| &\leq K \int_a^b G(t, s) |u_1(s) - u_2(s)| ds \\ &\leq K \|u_1 - u_2\| \int_a^b G(t, s) ds. \end{aligned} \tag{26}$$

From Lemma 3.3, it follows that

$$|Tu_1(t) - Tu_2(t)| \leq K \frac{(\alpha - 1)^{\alpha - 1}}{(\alpha - \beta)^\alpha \Gamma(\alpha + 1)} (b - a)^\alpha \|u_1 - u_2\| < \|u_1 - u_2\|,$$

where we have used (25). Hence T is a contraction mapping on \mathcal{B} . By the contraction mapping theorem, we obtain the desired result.

Remark 4.1 It is easy to see that the results in Theorem 4.2 can be extended to a nonlinear fractional BVP consisting of the equation (23) and the following nonhomogeneous BC:

$$u(a) = 0, \quad D_{a^+}^\beta u(b) = k,$$

where $k \in \mathbb{R}$. We leave the details to the interested reader.

5 Conclusion

In this paper, we obtained a Lyapunov-type inequality for a fractional differential equation with a fractional boundary condition. The inequality obtained is an improvement and a generalization of inequalities that have been obtained in the past. The inequality was applied to show the existence and nonexistence of solutions to a nonlinear fractional boundary value problem.

References

- [1] G. Borg. On a Liapounoff criterion of stability. *Amer. J. Math.* **71** (1949) 67–70.
- [2] A. Boudaoui and A. Slama. Approximate controllability of nonlinear fractional impulsive stochastic differential equations with nonlocal conditions and infinite delay. *Nonlinear Dyn. Syst. Theory* **16** (2016) 35–48.
- [3] P. G. Chhetri and A. S. Vatsala. Generalized monotone method for Riemann-Liouville fractional reaction-diffusion equation with applications. *Nonlinear Dyn. Syst. Theory* **18** (2018) 259–272.
- [4] Z. Denton and J. D. Ramirez. Monotone method for finite systems of nonlinear Riemann-Liouville fractional integro-differential equations. *Nonlinear Dyn. Syst. Theory* **18** (2018) 130–143.
- [5] Z. Denton, P.W. Ng and A.S. Vatsala. Quasilinearization method via lower and upper solutions for Riemann-Liouville fractional differential equations. *Nonlinear Dyn. Syst. Theory* **11** (2011) 239–251.
- [6] S. Dhar and Q. Kong. Lyapunov-type inequalities for third-order half-linear equations and applications to boundary value problems. *Nonlin. Anal.* **110** (2014) 170–181.
- [7] S. Dhar and Q. Kong. Lyapunov-type inequalities for higher order half-linear differential equations. *Appl. Math. Comput.* **273** (2016) 114–124.
- [8] S. Dhar and Q. Kong. Lyapunov-type inequalities for third-order linear differential equations. *Math. Inequal. Appl.* **19** (2016) 297–312.
- [9] S. Dhar and Q. Kong. Lyapunov-type inequalities for odd order linear differential equations. *Electron. J. Differ. Equ.* **2016** (243) (2016) 1–10.
- [10] S. Dhar, Q. Kong and M. McCabe. Fractional boundary value problems and Lyapunov-type inequalities with fractional integral boundary conditions. *Electron. J. Qual. Theory Differ. Equ.* (43) **2016** 1–16.
- [11] S. Dhar and Q. Kong. Lyapunov-type inequalities for α -th order fractional differential equations with $2 < \alpha \leq 3$ and fractional boundary conditions. *Electron. J. Differ. Equ.* 2017 (203) (2017) 1–15.
- [12] S. Dhar. On linear and nonlinear fractional Hadamard boundary value problems. *Differ. Equ. Appl.* **10** (3) (2018) 329–339.
- [13] S. Dhar and J. S. Kelly. A non Green’s function approach to fractional Lyapunov-type inequalities with applications to multivariate domains. *Differential Equations & Applications* **11** (3) (2019) 409–425.
- [14] S. Dhar and Q. Kong. Fractional Lyapunov-type inequalities with mixed boundary conditions on univariate and multivariate domains. *J. Fract. Calc. Appl.* **11** (2) (2020) 148–159.
- [15] S. Dhar, J. S. Kelly, and Q. Kong. Lyapunov-type Inequalities for Third Order Linear and Half-Linear Difference Equations. *J. Difference Equ. Appl.* **27** (1) (2021) 61–80.
- [16] R. A. C. Ferreira. On a Lyapunov-type inequality and the zeros of a certain Mittag-Leffler function. *J. Math. Anal. Appl.* **412** (2014) 1058–1063.

- [17] R. A. C. Ferreira. A Lyapunov-type inequality for a fractional boundary value problem. *Fract. Calc. Appl. Anal.* **16** (2013) 978–984.
- [18] R. A. C. Ferreira. Existence and uniqueness of solutions for two-point fractional boundary value problems. *Electron. J. Differ. Equ.* **2016** (2016) 1–5.
- [19] P. Hartman. *Ordinary Differential Equations*. Wiley, New York, 1964, and Birkhauser, Boston, 1982.
- [20] M. Jleli and B. Samet. Lyapunov-type inequalities for fractional boundary value problems. *Elect. J. Diff. Eq.* **2015** (2015) 1–11.
- [21] A. A. Kibas, H.M. Srivastava and J.J. Trujillo. *Theory and Applications of Fractional Differential Equations*. North-Holland Mathematics Studies, 204, Elsevier Science B.V., Amsterdam, 2006.
- [22] A. M. Liapunov. Probleme general de la stabilite du mouvement. *Ann. Math Stud.* **17** (1947) 203–474.
- [23] K. S. Miller and B. Ross. *An Introduction to the Fractional Calculus and Fractional Differential Equations*. John Wiley and Sons, Inc., New York, 1993.
- [24] D. O'Regan and B. Samet. Lyapunov-type inequalities for a class of fractional differential equations. *J. Inequal. Appl.* (2015) **2015**:247.
- [25] I. Podlubny. *Fractional Differential Equations*. Academic Press, San Diego, 1999.
- [26] J. Rong and C. Bai. Lyapunov-type inequality for a fractional differential equation with fractional boundary conditions. *Adv. Diff. Eq.* (2015) **2015**:82.
- [27] S. G. Samko, A.A. Kilbas, O.I. Marichev. *Fractional Integrals and Derivatives, Theory and Applications*. Gordon and Breach, Yverdon, 1993.
- [28] A. Wintner. On the non-existence of conjugate points. *Amer. J. Math.* **73** (1951) 368–380.



Performance Comparison of Some Two-Dimensional Chaotic Maps for Global Optimization

A. Djaout¹, T. Hamaizia^{1*} and F. Derouiche²

¹ *Department of Mathematics, Faculty of Exact Sciences, University of Constantine 1, Algeria.*

² *Department of Mathematics, Faculty of Exact Sciences and Science of Nature and Life, University of Oum El-Bouaghi, Algeria.*

Received: December 5, 2021; Revised: April 4, 2022

Abstract: This paper studied the performance of a new class of evolutionary algorithms called the chaos optimization algorithms (COA). It was originally proposed to solve nonlinear optimization problems with bounded variables by Caponetto et al. [1, 2]. Different chaotic mappings have been considered, combined with several working strategies. We propose four different 2-D chaotic maps in the optimization algorithm using a two-stage chaos optimization method and compare them. This study surveys and compares the chaotic optimization algorithms in the literature. Furthermore, a two-phase strategy is a technique commonly used in the COA to fine tune the solution and help escaping from local optimums. The performance study is conducted to understand their impact on the chaos optimization algorithm.

Keywords: *chaos; global optimization; chaotic map; chaos optimization algorithm.*

Mathematics Subject Classification (2010): 34D45, 70K55.

1 Introduction

The existence of chaotic systems is an accepted fact of science [3]. Chaos is a kind of characteristics of nonlinear systems and chaos theory studies the behavior of systems that follow deterministic laws but appear random and unpredictable. This theory brings many qualitative and quantitative tools, namely, ergodicity, entropy, expansivity, and sensitive dependence on initial conditions. Theory of chaos, since its evolution, has found application in various important areas such as engineering, medicine, biology, economy and many others. The application of the Chaotic Search strategy in engineering had its peak of popularity over the last few years [3–8]. This approach configured as an

* Corresponding author: <mailto:el.tayyeb@umc.edu.dz>

attractive option for global optimization. One of the modern optimization algorithms is the chaos-based optimization [9, 10].

The chaos optimization search as a novel method of global optimization has attracted much attention in nonlinear fields. The chaos optimization algorithm (COA) is an effective way to solve the optimization problem of a nonlinear multimodal function with boundary constraint. Due to the nonrepetition of chaos, it can carry out overall searches at higher speeds than stochastic searches, which depend on probabilities. The application of chaotic sequences instead of random sequences in the COA is a powerful strategy to improve the COA's performance in preventing premature convergence to local minima [11, 14].

In the present paper, a robust chaos optimization algorithm is applied to efficiently solve the problem of optimizing a nonlinear multimodal function. In most of the chaos optimization algorithms, chaos variables are generated by logistic mapping [15, 16], but the uneven distribution will weaken the ergodicity of chaos variables. To overcome this problem, we select 5 different two-dimensional maps and replace the chaos variable generator in one of the existing COAs [17–20] with them. The remainder of this paper is organized as follows. Section 2 is made for Chaotic maps. Then in Section 3, the chaos optimization algorithm is introduced, experiments and simulation results are shown in Section 4, and finally, the conclusion is presented in Section 5.

2 Two-Dimensional Maps

Non-linear systems with complex dynamics have lately been the subject of intense research and exploration, giving birth to *chaos theory*. Chaotic systems are deterministic systems that exhibit irregular behavior and a sensitive dependence on the initial conditions. Chaos theory studies the behavior of systems that follow deterministic laws but appear random and unpredictable, i.e., dynamical systems. Chaotic variables can go through all states in certain ranges according to their own regularity without repetition [3, 8].

A chaotic map is a map that exhibits some type of chaotic behavior. In this work, we applied five different chaotic maps that are common in the literature, namely, the Hénon map, Lozi map, Duffing map, Gingerbreadman map, and Zeraoulia map. The mathematical form of a chaotic two-dimensional map, which maps the unit square $I \times I$, where $I = [0, 1]$, onto itself in a one-to-one manner, is chosen.

Later on, we will use these maps in the chaotic searches.

2.1 The Hénon map

The Hénon map is a discrete-time dynamical system [21]. It is one of the most studied examples of dynamical systems that exhibit chaotic behaviour. The Hénon map takes a point (x_n, y_n) in the plane and maps it to a new point

$$\begin{cases} y_1(k) = 1 - a(y_1(k-1))^2 + by(k-1), \\ y(k) = y_1(k-1), \end{cases} \quad (1)$$

where k is the iteration number.

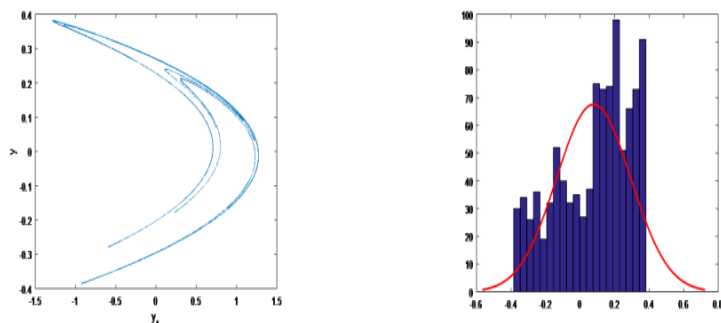


Figure 1: A chaotic Hénon attractor obtained for $a = 1.4$ and $b = 0.3$.

2.2 The Lozi map

Lozi map [22, 23] is a piecewise linear simplification of the Hénon map and it admits strange attractors. It is given by

$$\begin{cases} y_1(k) = 1 - a|y_1(k-1)| + by(k-1), \\ y(k) = y_1(k-1). \end{cases} \quad (2)$$

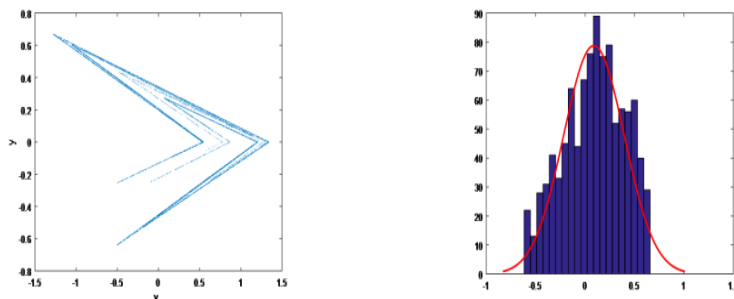


Figure 2: A chaotic Lozi attractor obtained for $a = 1.7$ and $b = 0.5$.

2.3 The Duffing map

The Duffing map (also called the 'Holmes map') [24] is a discrete-time dynamical system. It is an example of a dynamical system that exhibits chaotic behavior. The Duffing map takes a point (x_n, y_n) in the plane and maps it to a new point given by

$$\begin{cases} y_1(k) = y(k-1), \\ y(k) = -by_1(k-1) + y_1(k-1) - y(k-1)^3. \end{cases} \quad (3)$$

The map depends on two constants a and b . These are usually set to $a = 2.75$ and $b = 0.2$ to produce chaotic behaviour.

It is a discrete version of the Duffing equation.

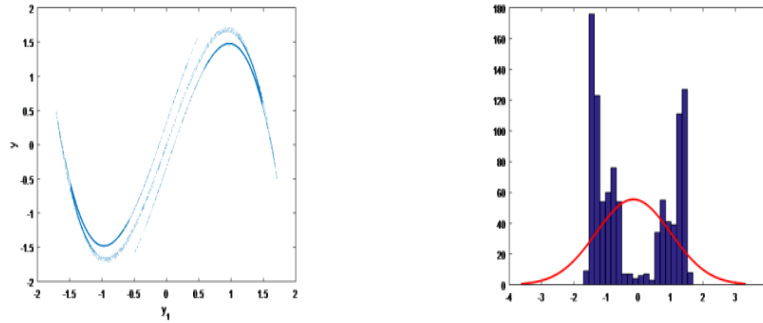


Figure 3: A chaotic Duffing attractor obtained for $a = 2.75$ and $b = 0.2$.

2.4 The Gingerbreadman map

In dynamical systems theory, the Gingerbreadman map [25] is a chaotic two-dimensional map. It is given by the piecewise linear transformation

$$\begin{cases} y_1(k) = 1 - a(y_1(k - 1))^2 + by_1(k - 1), \\ y_2(k) = y_1(k - 1). \end{cases} \quad (4)$$

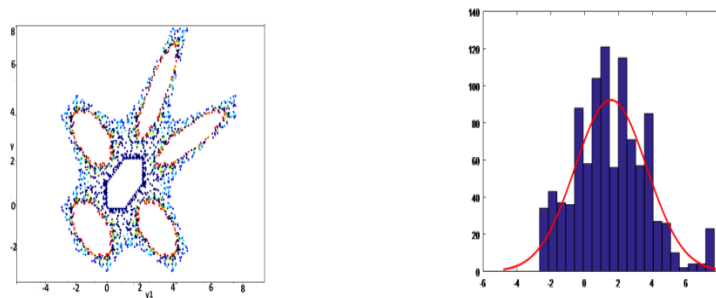


Figure 4: A chaotic Gingerbreadman attractor obtained for $a = 1$ and $b = 1$.

2.5 The Zeraoulia map

In dynamical systems theory, the Zeraoulia map [26] is a chaotic two-dimensional map. It is given by the piecewise linear transformation

$$\begin{cases} y_1(k) = 1 - a \sin(y_1(k-1)) + y_1(k-1), \\ y(k) = by_1(k-1). \end{cases} \quad (5)$$

The choice of the term $\sin(x)$ has an important role in that it makes the solutions bounded for the values of b such that $|b| \leq 1$, and all values of a , while they are unbounded for $|b| > 1$. The chosen parameter values are $a = 4$ and $b = 0.9$ as suggested in [26]. For these values the observed attractor shown in Figure 5.

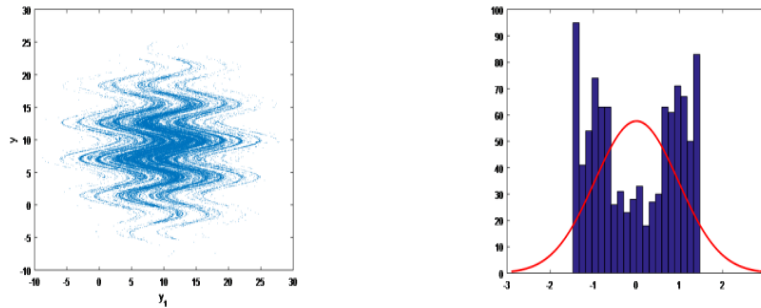


Figure 5: A chaotic Zeraoulia attractor obtained for $a = 4$ and $b = 0.9$.

3 Chaos Optimization Search

The study of chaos has been rapidly developed and attracted a great attention due to a variety of applications in science and technology, e.g., chaos-based global optimization. The chaos optimization algorithm (COA) is one of the hot topics in recent years. The COA is an effective method to solve the optimization problem of a nonlinear multimodal function with boundary constraint. Many chaotic strategies in the COA generally include two major stages [17–19]: the global phase and the local phase. Firstly, during the global phase, chaotic points are drawn from the domain of searches $[L, U]$ according to a certain 2-D chaotic model. Then, the objective function is evaluated at these points and the point with the minimum objective function as the current optimum is chosen. Secondly, during the local phase, the current optimum is assumed to be close to the global optimum after certain iterations and it is viewed as the center with a little chaotic perturbation and the global optimum is obtained through the fine search.

Consider the following optimization problem on the minimum of functions. If the target function $f(x_i)$ is continuous and differentiable, the object problem to be optimized is find x_i to minimize $f(x_i); x_i \in [L_i, U_i]; i = 1, 2, \dots, n$. The main procedures of this algorithm are shown as follows:

Input :

M_g : maximum number of iterations of the global search.

M_l : maximum number of iterations of the local search.

$M_l + M_g$: stopping criterion of the chaotic optimization method in iterations

λ : step size in the chaotic local search

Output :

X^* : best solution from the current run of the chaotic search.

f^* : best objective function (minimization problem).

- **Step 1 :** *Initialization* of the numbers M_g, M_l of steps of the chaotic search and initialization of the parameters λ and initial conditions. Set $k = 1, y(0), y_1(0)$. $a = 1.4$ and $b = 0.3$ of the Henon map, $a = 1.7$ and $b = 0.5$ of the Lozi map, $a = 2.75$ and $b = 0.2$ of the Duffing map, $a = 4$ and $b = 0.9$ of the Zraoulia map. Set the initial best objective function $f^* = \text{infini}$.

- **Step 2 :** *algorithm of the chaotic global search:*

Map the chaotic variables $z_i(k) = \frac{(x_i(k) - L_i)}{(U_i - L_i)}$ into the optimization variables $x_i(k)$ by the following equation in the chaotic map function:

$$x_i(k) = L_i + (U_i - L_i)z_i(k),$$

where $i = 1, 2, \dots, n$.

Equation $x_i(k) = L_i + (U_i - L_i)z_i(k)$ is suitable for most chaotic maps. It is determined by the range of the chaotic sequences generated by each chaotic map to select the equation. As the chaotic sequences generated by chaotic maps is the interval $(0, 1)$, equation $x_i(k) = L_i + (U_i - L_i)z_i(k)$ can map $(0, 1)$ into the interval (L, U) for optimization variables.

- **Step 3 :** compute the function value $f(x(k))$. If $f(x(k)) < f^*$, then $f^* = f(x(k))$ and the optimal solution $x^* = x(k)$.
- **Step 4 :** utilize a chaotic map function to generate next chaotic variables $z_i(k+1)$.
- **Step 5 :** $k = k + 1$. If $k \leq M_g$, turn to step 2, otherwise terminate the first stage search.
- **Step 6 :** *algorithm of the chaotic local search:*
If $r < 0.5$, then (where r is a uniformly distributed random)
Map the chaotic variables $z_i(k)$ into the optimization variables $x_i(k)$ by one of the following equations of the chaotic map function:

$$x_i(k+1) = x_i^* + \lambda \cdot z_i(k) \cdot |U_i - L_i^*|,$$

$$x_i(k+1) = x_i^* - \lambda \cdot z_i(k) \cdot |U_i - L_i^*|,$$

where $i = 1, 2, \dots, n$.

- **Step 7 :** compute the function value $f(x(k_1)), f(x(k_2))$. Take the minimum value of the two as $f(x(k))$. If $f(x(k_1)) < f(x(k_2))$, then $x(k) = x(k_1), f(x(k)) = f(x(k_1))$; otherwise $x(k) = x(k_2), f(x(k)) = f(x(k_2))$. Compare $f(x(k_1))$ with the optimal value, so far f^* . If $f(x(k)) < f^*$, then $f^* = f(x(k))$ and the optimal solution $x^* = x(k)$.
- **Step 8 :** utilize a chaotic map function to generate next chaotic variables $z_i(k+1)$.
- **Step 9 :** $k = k + 1$. If $k \leq M_g + M_l$, turn to step 6, otherwise terminate the second stage search.

4 Simulation Results

The proposed algorithm was tested on two benchmark functions, see Table 1, Figures 6, 7. All the programs were run on a 2 GHz Pentium IV processor with 2 GB of random access memory in the MATLAB. The algorithm used for comparison is a two-stage chaotic optimization algorithm with five chaotic maps. The algorithm was executed with 50 runs; $M_g=1000$, $M_l=400$, and different values for the step size λ (such $\lambda = 0.01$, $\lambda = 0.001$ and $\lambda \in]0.001, 0.01[$). Tables 2,3,4 show the best solution, the mean of the solution and standard deviation. From Tables 2, 3, 4, all of the best solutions are exactly equal to the exact solution of the function 2. From Tables 3, 4, the Hénon map and Zeraoulia map have better solutions for $\lambda = 0.001$ and $\lambda \in]0.001, 0.01[$ of function 1 than other maps according to the best solution. The Hénon map, Lozi map and Gingerbreadman map have better solutions for $\lambda = 0.001$ and $\lambda \in]0.001, 0.01[$ of function 2 than other maps according to the best solution.

Function name	Expression	bounds	Opt	Modality
The Schaffer	$F_1(x_1, x_2) = -0.5 \frac{(\sin \sqrt{(x_1^2 + x_2^2)}) - 0.5}{(1 + 0.001(x_1^2 + x_2^2))^2}$	$[-100, 100]$	-1	Multimodal
The Easom	$F_2(x_1, x_2) = \cos(x_1) \cos(x_2) \exp(-(x_1 - \pi)^2 - (x_2 - \pi)^2)$	$[-20, 20]$	-1	unimodal

Table 1: Properties of benchmark functions.

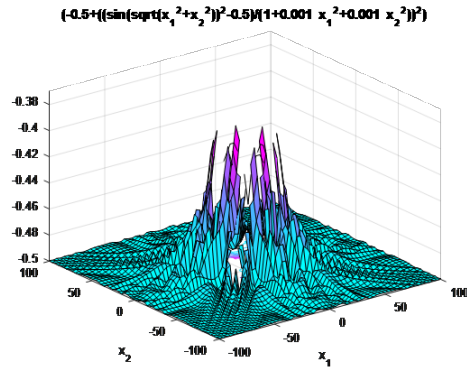


Figure 6: Plot of F_1 .

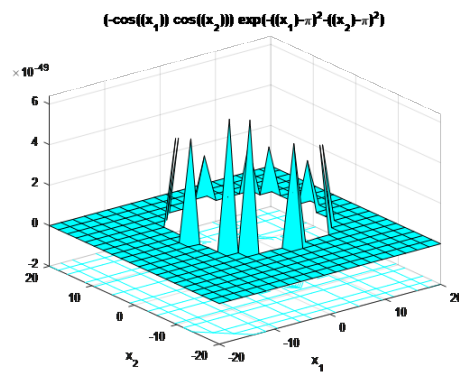


Figure 7: Plot of F_2 .

$\lambda = 0.01$					
Fun- ction	Maps	Best fit	(Xbest,Ybest)	Mean fit	standard fit
F_1	Hénon	-0.9897	(3.1331,0.4282)	-0.9897	$1.0e-15 \times 0.1121$
	Lozi	-0.8304	(5.7743,10.8775)	-0.8304	$1.0e-14 \times 0.1009$
	Duffing	-0.9398	(0.4017,-6.1062)	-0.9398	$1.0e-14 \times 0.0224$
	Gingerbreadman	-0.8217	(-11.7448,-11.7448)	-0.8217	0.0000
	Zraoulia	-0.9870	(3.1432,-0.5825)	-0.9870	$1.0e-15 \times 0.6729$
F_2	Hénon	-0.9961	(3.1739 ,3.1812)	-09960	$1.0e-03 \times 0.0452$
	Lozi	-0.9859	(3.0529,3.1054)	-0.9818	0.0021
	Duffing	-0.9963	(3.1819,3.1128)	-0.9961	0.0002
	Gingerbreadman	-0.9918	(3.0893,3.0893)	-0.9918	$1.0e-15 \times 0.4486$
	zraoulia	-0.9961	(3.1006,3.1736)	-0.9960	$1.0e-03 \times 0.0718$

Table 2: COA based five chaotic saerches so that $M_g=1000$, $M_l=400$, for 50 run.

$\lambda = 0.001$					
Function	Maps	Best fit	(Xbest,Ybest)	Mean fit	standard fit
F_1	Hénon	-0.9899	(3.1432,0.4698)	-0.9899	$1.0e-14 \times 0.0336$
	Lozi	-0.8727	(5.4511 ,11.0601)	-0.8726	0.0001
	Duffing	-0.9628	(0.2366,-6.2706)	-0.9627	0.0001
	Gingerbreadman	-0.8218	(-11.4213,-11.4217)	-0.8214	0.0004
	Zeraoulia	-0.9903	(3.0870,-0.6231)	-0.9902	0.0001
F_2	Hénon	-1	(3.0706,3.0244)	-0.9983	0.0053
	Lozi	-0.9999	(3.1335,3.1428)	-0.9999	0.001
	Duffing	-1	(3.1393,3.1363)	-1	0.0000
	Gingerbreadman	-1	(3.0303,3.030)	-0.9971	0.0072
	Zeraoulia	-1	(3.1421,3.1388)	-1	$1.0e-0.3 \times 0.0020$

Table 3: COA based five chaotic searches so that $M_g=1000$, $M_l=400$, for 50 run.

$\lambda \in]0.01, 0.001[$					
Function	Maps	Best fit	(Xbest,Ybest)	Mean fit	standard fit
F_1	Hénon	-0.9899	(3.0829,0.4698)	-0.9899	$1.0e-14 \times 0.0336$
	Lozi	-0.8727	(5.4511 ,11.0601)	-0.8726	0.0001
	Duffing	-0.9628	(0.2366,-6.2706)	-0.9627	0.0001
	Gingerbreadman	-0.8218	(-11.4213,-11.4217)	-0.8214	0.0004
	Zeraoulia	-0.9903	(3.0870,-0.6231)	-0.9902	0.0001
F_2	Hénon	-1	(3.0706,3.0244)	-0.9984	0.0053
	Lozi	-0.9999	(3.1303,3.1385)	-0.9999	0.0001
	Duffing	-1	(3.1399,3.1363)	-1	0.0000
	Gingerbreadman	-1	(2.9741,2.9741)	-0.9931	0.0179
	Zeraoulia	-1	(3.1424,3.1388)	-1	$1.0e-03 \times 0.0020$

Table 4: COA based five chaotic searches so that $M_g=1000, M_l=400$, for 50 run.

5 Conclusion

In this paper, we have proposed some two-dimensional maps which can be used as search patterns in the chaos optimization algorithm. We use five chaotic map searches. Our main conclusion is made by comparing different search patterns based on the numerical simulation results. We exhibited the generated chaotic sequences and the obtained best chaotic sequences. Further, this algorithm is tested on a benchmark consisting of two known nonlinear objective functions.

References

- [1] M. Bucolo, R. Caponetto, L. Fortuna, M. Frasca and A. Rizzo. Does chaos work better than noise? *IEEE Circuits and Systems, Magazine* **2** (3) (2002) 4–19.

- [2] R. Caponetto, L. Fortuna, S. Fazzino and M. G. Xibilia. Chaotic sequences to improve the performance of evolutionary algorithms. *IEEE Trans. on Evolutionary Computation* **7** (3) (2003) 289–304.
- [3] J. Gleick. *Chaos: Making a New Science*. New York, NY, USA: Viking, 1987.
- [4] X. X. Wu and Z. Chen. *Introduction of Chaos Theory*, Shanghai Science and Technology, Bibliographic Publishing House, 1996.
- [5] K. T. Alligood, T. D. Sauer and J. A. Yorke. *Chaos: an Introduction to Dynamical Systems*. London, UK: Springer, 1996.
- [6] T. Y. Li and J. A. Yorke. *Period Three Implies Chaos*. *Amer. Math. Monthly* **82** (1975) 985–992.
- [7] S. H. Strogatz. *Nonlinear Dynamics and Chaos*. Massachusetts: Perseus Publishing, 2000.
- [8] J. C. Sprott. *Chaos and Times-Series Analysis*. Oxford University Press, Oxford, UK, 2003.
- [9] J. S. Arora, O. A. Elwakeil, A. I. Chahande and C. C. Hsieh. Global optimization methods for engineering application: a review. *Struct Optimization* **9** (1995) 137–159.
- [10] L. X. Li, Y. X. Yang, H. Peng and X. D. Wang. An optimization method inspired by chaotic ant behavior. *Int. J. Bifurcat Chaos* **16** (2006) 2351–2364.
- [11] B. Li and W. S. Jiang. Chaos optimization method and its application. *Journal of Control Theory and Application* **14** (4) (1997) 613–615.
- [12] B. Li and W. S. Jiang. Optimizing complex function by chaos search. *Cybernetics and Systems* **29** (4) (1998) 409–419.
- [13] D. X. Yang, G. Li and G. D. Cheng. On the efficiency of chaos optimization algorithms for global optimization. *Chaos, Soli. Fract.* **34** (4) (2007) 1366–1375.
- [14] M. S. Tavazoei and M. Haeri. An optimization algorithm based on chaotic behavior and fractal nature. *Journal of Computational and Applied Mathematics* **206** (2) (2007) 1070–1081.
- [15] M. S. Tavazoei and M. Haeri. Comparison of Different One-Dimensional Maps as Chaotic Search Pattern in Chaos Optimization Algorithms. *Applied Mathematics and Computation* **187** (2) (2007) 1076–1085.
- [16] R. Jahani and Nejad H. Chahkandi. Comparison of chaotic optimization algorithm and other evolutionary techniques for optimal unit commitment of power system. *Australian Journal of Basic and Applied Sciences* **5** (2011) 923–929.
- [17] L. S. Coelho. Tuning of PID controller for an automatic regulator voltage system using chaotic optimization approach. *Chaos, Solitons and Fractals* **39** (2009) 1504–1514.
- [18] H. Shayeghi, S. Jalilzadeh, H. A. Shayanfar and A. Safari. Robust PSS design using chaotic optimization algorithm for a multimachine power system. In: *ECTI-CON 2009*. Pattaya, Thailand, May 2009, 40–43.
- [19] H. Shayeghi, H. A. Shayanfar, S. Jalilzade and A. Safari. A PSO based unified power controller for damping of power system oscillations. *Energy Conversion and Management* **50** (10) (2009) 2583–2592.
- [20] T. Hamaizia and R. Lozi. An improved chaotic optimization algorithm using a new global locally averaged strategy. *Journal of Nonlinear Systems and Applications* **3** (2) (2012) 58–63.
- [21] M. Hénon. A two dimensional mapping with a strange attractor. *Commun. Math. Phys.* **50** (1) (1976) 69–77.
- [22] R. Lozi. Un attracteur étrange? du type attracteur de Hénon. *J. Phys.* **39** (C5) (1978) 9–10.

- [23] A. Aziz-Alaoui, C. Robert and C. Grebogi. Dynamics of a Hénon-Lozi map. *Chaos, Solitons Fractals* **12** (11) (2001) 2323–2341.
- [24] G. Duffing. *Erzwungene Schwingungen bei Vernderlicher Eigenfrequenz*. F. Vieweg u. Sohn, Braunschweig, 1918.
- [25] R. L. Devaney. A piecewise linear model for the zones of instability of an area-preserving map. *Physica D* **10** (1989) 387–393.
- [26] E. Zeraoulia and J. C. Sprott. A two-dimensional discrete mapping with C1-multifold chaotic attractors. *Electronic Journal of Theoretical Physics* **5** (17) (2008) 107–120.
- [27] S. K. Mishra. Some New Test Functions For Global Optimization And Performance of Repulsive Particle Swarm Method. 23 August 2006, Online at <https://mpa.ub.uni-muenchen.de/2718/> MPRA Paper No. 2718, posted 13 Apr. 2007 UTC.
- [28] Marcin Molga and Czesaw Smutnicki. *Test Functions for Optimization Needs*, 3, Kwietnia, 2005.



Existence and Uniqueness of Solutions for a Semilinear Functional Dynamic Equation with Infinite Delay and Impulses

C. Duque¹, H. Leiva² and A. Tridane^{3*}

¹ *Department of Mathematics, Faculty of Sciences, Los Andes University, Mérida, Venezuela.*

² *School of Mathematical and Computational Science, Yachay Tech. University, San Miguel de Urcuqui, Imbabura, Ecuador.*

³ *Department of Mathematical Sciences, United Arab Emirates University, Al Ain, UAE.*

Received: November 15, 2021; Revised: March 20, 2022

Abstract: This work is devoted to the prove of the existence of solutions for a semilinear retarded differential equation with infinite delay and impulses on time-scales, which is done by using a version of the Arzela-Ascoli theorem on time-scales, and applying the Leray-Schauder alternative. After that, the uniqueness of solutions is proved by applying a version of Gronwall's inequality for impulsive differential equations, and finally, the continuation of solutions is proved.

Keywords: *semilinear functional dynamic equations; infinite delay; infinite impulses; Leray-Schauder alternative; existence; uniqueness; continuation; time-scales.*

Mathematics Subject Classification (2010): 93C10, 93C23, 34N05, 34K45.

1 Introduction

In the last decades, the theory of time scales has occupied an important space within the mathematical community, attracting the interest of many researchers since it is a powerful tool for continuous and discrete analysis from a unified point of view (see, for instance, [1–3] and references therein).

The time scales theory has made possible to create models in population dynamics, physics, chemical technology, economics, control theory, among others, that allow the study of certain phenomena and processes where the temporal variable can vary both continuously and discretely (see [3, 6–9] and references therein). However, there exists

* Corresponding author: <mailto:a-tridane@uaeu.ac.ae>

the possibility that these processes and phenomena on time scales could undergo drastic changes of their states at given times. These alterations in state might be due to certain external factors and these changes can be represented in mathematical notation in the form of impulses, which cannot be well described by pure time scales models, therefore, the influence of these impulses on the system could be investigated by introducing impulses effects, see, for instance, [10–12] and references therein.

In these order of ideas, in this paper we are going to study the existence, uniqueness and continuation of solutions for the following semilinear functional dynamic equation with infinite delay and impulses:

$$\begin{cases} z^\Delta(t) = A(t)z(t) + f(t, z_t), & t \in [0, \infty)_{\mathbb{T}} \setminus \bigcup_{k=1}^{\infty} \{t_k\}, \\ z(s) = \phi(s), & s \in (-\infty, 0]_{\mathbb{T}}, \\ z(t_k^+) = z(t_k^-) + J_k(t_k, z(t_k^-)), & k = 1, 2, \dots \end{cases} \quad (1)$$

For system (1), we are assuming that $0 \in \mathbb{T}$, $\inf \mathbb{T} = -\infty$, $\sup \mathbb{T} = \infty$ and $t + \tau \in \mathbb{T}$ if $t, \tau \in \mathbb{T}$. $0 < t_1 < t_2 < t_3 \cdots < t_k \rightarrow +\infty$, $t_k \in \mathbb{T}$. Here $z(t_k^+)$ and $z(t_k^-)$ represent the right and left limits with respect to the time scale, and, in addition, if t_k is right-scattered, then $z(t_k^+) = z(t_k)$, whereas if t_k is left-scattered, then $z(t_k^-) = z(t_k)$. Moreover, it is usually assumed that the solution z should be left-continuous (see [10]), in this case $z(t_k^+) = z(t_k) + J_k(t_k, z(t_k))$, $k = 1, 2, \dots$. On the other hand, if t_k is right-scattered, then $J(t_k, z(t_k)) = 0$, in other words, it makes sense to consider impulses at right-dense points only (see [11]). Here $A(t) \in \mathcal{R}(\mathbb{T}, \mathbb{R}^{n \times n})$ and $\phi \in \mathcal{C}_{hp}$, where \mathcal{C}_{hp} is called the phase space that will be defined later. For this type of problems, the phase space for initial functions plays an important role in the study of both qualitative and quantitative theory, for more details, in the continuous case and without impulses, we refer to Hale and Kato [13], Hino et al. [14] and Shin [15]. In the case of functional dynamic equations on time scales with and without impulses, there are a few works in this directions, we can cite Benchohra et al. [16] and Li et al. [17]. Particularly in this work we will use a modified version of the phase space defined in [17] since the initial function $\phi : (-\infty, 0]_{\mathbb{T}} \rightarrow \mathbb{R}^n$ has a fixed number of points of discontinuity, where the side limits exist and the function ϕ is left-continuous at such points. The function $z_t(\theta) = z(t + \theta)$ for $\theta \in (-\infty, 0]_{\mathbb{T}}$ illustrates the history of the state up to the time t , and also remembers much of the historical past of ϕ , carrying part of the present to the past. $f : [0, \infty)_{\mathbb{T}} \times \mathcal{C}_{hp} \rightarrow \mathbb{R}^n$ is an rd-continuous function on t and continuous on \mathcal{C}_{hp} , $J_k : [0, \infty)_{\mathbb{T}} \times \mathbb{R}^n \rightarrow \mathbb{R}^n$ are rd-continuous on t and continuous on \mathbb{R}^n .

The paper is organized as follows. In Section 2, we present a summary on dynamical systems on time scale, particularly the concept of rd-continuity, the exponential function, the variation of constants formula and a generalization of Gronwall's inequality to be applied to impulsive differential equations. In Section 3, we define the phase space for our problem, which satisfies the Hale and Kato Axiomatic Theory for Retarded Differential Equations with Infinite Delay. Section 4 is devoted to the proof of our main results, the existence and the uniqueness of solutions, which is done in two theorems, one for the existence using the Arzela-Ascoli theorem on time-scale (see [18]) and applying the Leray-Schauder alternative; and the other theorem for the uniqueness of solutions. Section 5 is dedicated to the study of the continuation of the solutions of our system, introducing the concept of maximal interval of existence of solutions on time scale and applying the generalization of Gronwall's inequality. Section 6 is devoted to an example, where we

can apply our results. Finally, Section 7 presents the conclusion and final remark, where we formulate future problems to investigate.

2 Preliminaries

In this section, we will make a brief introduction to the calculus on time scales, especially to clarify the notations and definitions, for a better understanding by the reader. For more details about time scales theory, we recommend the excellent monograph [3].

The time scales theory was introduced by Stefan Hilger (see [4]), and defined a time scale as any arbitrary nonempty closed subset of \mathbb{R} , this set is denoted by \mathbb{T} . For every $t \in \mathbb{T}$, the forward and backward jump operators $\sigma, \rho : \mathbb{T} \rightarrow \mathbb{T}$ are defined, respectively, as $\sigma(t) = \inf\{s \in \mathbb{T} : s > t\}$ and $\rho(t) = \sup\{s \in \mathbb{T} : s < t\}$. A point $t \in \mathbb{T}$ is said to be right-dense if $\sigma(t) = t$, right-scattered if $\sigma(t) > t$, left-dense if $\rho(t) = t$, left-scattered if $\rho(t) < t$, isolated if $\rho(t) < t < \sigma(t)$. The function $\mu : \mathbb{T} \rightarrow [0, \infty)$ defined by $\mu(t) := \sigma(t) - t$ is known as the graininess function. It is assumed that \mathbb{T} has the topology inherited from standard topology on the real numbers. The time scale interval $[a, b]_{\mathbb{T}}$ is defined by $[a, b]_{\mathbb{T}} = \{t \in \mathbb{T} : a \leq t \leq b\}$, with $a, b \in \mathbb{T}$, and is similarly defined by open intervals and open neighborhoods.

Definition 2.1 [3] A function $f : \mathbb{T} \rightarrow \mathbb{R}^n$ is said to be right-dense continuous or just rd-continuous if f is continuous at every right-dense point $t \in \mathbb{T}$ and $\lim_{s \rightarrow t^-} f(s)$ exists (finite) for every left-dense point $t \in \mathbb{T}$.

The class of all rd-continuous functions $f : \mathbb{T} \rightarrow \mathbb{R}^n$ is denoted by $C_{rd}(\mathbb{T}, \mathbb{R}^n)$. If $f : \mathbb{T} \rightarrow \mathbb{R}^n$ is a function, then we define the function $f \circ \sigma : \mathbb{T} \rightarrow \mathbb{R}^n$ by $f^\sigma(t) = f(\sigma(t))$ for all $t \in \mathbb{T}$, i.e., $f^\sigma = f \circ \sigma$. We define the set \mathbb{T}^κ by $\mathbb{T}^\kappa = \mathbb{T} \setminus (\rho(\sup \mathbb{T}), \sup \mathbb{T})$ if \mathbb{T} has a left-scattered maximum, and $\mathbb{T}^\kappa = \mathbb{T}$ otherwise.

Definition 2.2 [3] A function $f : \mathbb{T} \rightarrow \mathbb{R}^n$ is called delta differentiable (or simply Δ -differentiable) at $t \in \mathbb{T}^\kappa$ provided there exists $f^\Delta(t)$ with the property that given $\varepsilon > 0$, there is a neighborhood $U = (t - \delta, t + \delta)_{\mathbb{T}}$ for some $\delta > 0$ such that

$$\|f^\sigma(t) - f(s) - f^\Delta(t)(\sigma(t) - s)\| \leq |\sigma(t) - s|, \text{ for all } s \in U.$$

In this case, $f^\Delta(t)$ will be call the Δ -derivative of f in t .

If f is Δ -differentiable at $t \in \mathbb{T}^\kappa$, then it is easy to show that (see [3], Thm. 1.16)

$$f^\Delta(t) = \begin{cases} \frac{f^\sigma(t) - f(t)}{\sigma(t) - t} & \text{if } \sigma(t) > t, \\ \lim_{s \rightarrow t} \frac{f(t) - f(s)}{t - s} & \text{if } \sigma(t) = t. \end{cases}$$

Definition 2.3 [3] A function $F : \mathbb{T} \rightarrow \mathbb{R}^n$ is called an antiderivative of $f : \mathbb{T} \rightarrow \mathbb{R}^n$ if $F^\Delta(t) = f(t)$ for $t \in \mathbb{T}^\kappa$. The Cauchy integral is defined by

$$\int_s^t f(\tau) \Delta\tau = F(t) - F(s), \quad t, s \in \mathbb{T},$$

where F is an antiderivative of f .

A function $p : \mathbb{T} \rightarrow \mathbb{R}$ is said to be regressive if $1 + \mu(t)p(t) \neq 0$, $t \in \mathbb{T}$, and positively regressive if $1 + \mu(t)p(t) > 0$, $t \in \mathbb{T}$. We will denote by \mathcal{R} the set of all regressive and rd-continuous functions and by \mathcal{R}^+ the set of all positive regressive and rd-continuous functions.

Definition 2.4 [3] If $p \in \mathcal{R}$, then the generalized exponential function is defined by

$$e_p(t, s) = \exp \left(\int_s^t \xi_{\mu(\tau)}(p(\tau)) \Delta \tau \right),$$

where

$$\xi_{\mu}(z) := \begin{cases} \frac{1}{\mu} \text{Log}(1 + \mu z) & \text{if } \mu > 0, \\ z, & \text{if } \mu = 0. \end{cases}$$

Here $z \in \mathbb{C}_{\mu} := \{z \in \mathbb{C} : z \neq 1/\mu\}$ and $\text{Log}z = \log|z| + i \arg z$, $-\pi < \arg z \leq \pi$.

Let A be an $n \times n$ -matrix valued function on \mathbb{T} .

Definition 2.5 [3] We say that A is rd-continuous on \mathbb{T} if each entry of A is rd-continuous on \mathbb{T} , and the class of all such rd-continuous $n \times n$ matrix-valued functions on \mathbb{T} is denoted by $C_{rd}(\mathbb{T}, \mathbb{R}^{n \times n})$. A is called regressive (with respect to \mathbb{T}) provided $I + \mu(t)A(t)$ is invertible for all $t \in \mathbb{T}^{\kappa}$, and the class of all such regressive and rd-continuous functions is denoted by $\mathcal{R}(\mathbb{T}, \mathbb{R}^{n \times n})$.

Let $t_0 \in \mathbb{T}$ and A be an $n \times n$ regressive matrix-valued function defined on \mathbb{T} . Then the unique solution of the initial value problem

$$X^{\Delta} = A(t)X, \quad X(t_0) = I,$$

is called the matrix exponential function and it is denoted by $e_A(t, t_0)$. The matrix exponential function has the following properties.

Theorem 2.1 ([3], Thm. 5.24) Let $A \in \mathcal{R}(\mathbb{T}, \mathbb{R}^{n \times n})$ and suppose that $f : \mathbb{T} \rightarrow \mathbb{R}^n$ is rd-continuous. Let $t_0 \in \mathbb{T}$ and $x^0 \in \mathbb{R}^n$. Then the initial value problem

$$\begin{cases} x^{\Delta}(t) = A(t)x(t) + f(t), \\ x(t_0) = x^0 \end{cases} \quad (2)$$

has a unique solution $x : \mathbb{T} \rightarrow \mathbb{R}^n$. Moreover, this solution is given by

$$x(t) = e_A(t, t_0)x^0 + \int_{t_0}^t e_A(t, \sigma(s))f(s)\Delta s.$$

We will need the following fixed theorem to prove the existence of solutions of system (1).

Theorem 2.2 (Leray-Schauder alternative ([5], Thm. 5.4)) Let \mathcal{D} be a closed convex subset of a Banach space \mathcal{X} with $0 \in \mathcal{D}$. Let $\mathcal{P} : \mathcal{D} \rightarrow \mathcal{D}$ be a completely continuous operator. Then either \mathcal{P} has a fixed point in \mathcal{D} or the set

$$\{z \in \mathcal{D} : z = \lambda \mathcal{P}(z), \quad 0 < \lambda < 1\}$$

is unbounded.

Following Corollary 6.7 in [3] and Theorem 1.5.1 in [10], it is possible to prove the following Gronwall’s inequality with impulses on time scales.

Theorem 2.3 (Gronwall’s inequality) *Assume that*

1. *the sequence $\{t_k\}$ satisfies $0 \leq t_0 < t_1 < \dots < t_k \dots$, $\lim_{k \rightarrow \infty} t_k = \infty$,*
2. *$u \in C_{rd}(\mathbb{T}, \mathbb{R})$ and u is left continuous at t_k , $k = 1, 2, \dots$,*
3. *$p \in \mathcal{R}^+$, $p \geq 0$, $\beta_k \geq 0$, and $\alpha \in \mathbb{R}$.*

Then

$$u(t) \leq \alpha + \int_{t_0}^t p(s)u(s)\Delta s + \sum_{t_0 < t_k < t} \beta_k u(t_k), \quad t \geq t_0,$$

implies

$$u(t) \leq \alpha \prod_{t_0 < t_k < t} (1 + \beta_k) e_p(t, t_0), \quad t \geq t_0.$$

3 The Phase Space

In this section, we will introduce an adequate phase space that will permit us to solve our problem. This phase space is a modification of the phase space presented in [17].

We denote by $\mathbb{T}^- = (-\infty, 0]_{\mathbb{T}}$. Now, we shall define the functions space

$$\mathcal{PW}_p = \{ \phi : \mathbb{T}^- \rightarrow \mathbb{R}^n : \phi \text{ is rd-continuous except on } s_k \in \mathbb{T}^-, k = 1, 2, \dots, \text{ and such that } \phi(s_k^-), \phi(s_k^+) \text{ exist with } \phi(s_k^-) = \phi(s_k) \}.$$

Following [17], we consider $h \in C_{rd}(\mathbb{T}^-, \mathbb{R}^n)$, $h(s) > 0$ for all $s \in \mathbb{T}^-$ and

$$\int_{-\infty}^0 h(s)\Delta s = 1.$$

Now, we define the following space of functions:

$$\mathcal{C}_{hp} = \left\{ \phi \in \mathcal{PW}_p : \int_{-\infty}^0 h(s) |\phi|^{[s, 0]_{\mathbb{T}}} \Delta s < \infty \right\},$$

where $|\phi|^{[a, b]_{\mathbb{T}}} = \sup_{a \leq \theta \leq b} |\phi(\theta)|$, and $|\cdot|$ is a norm in \mathbb{R}^n .

It is clear that \mathcal{C}_{hp} is a linear subspace of \mathcal{PW}_p , and for $\phi \in \mathcal{C}_{hp}$,

$$\|\phi\|_{\mathcal{C}_{hp}} = \int_{-\infty}^0 h(s) |\phi|^{[s, 0]_{\mathbb{T}}} \Delta s.$$

Define a norm on \mathcal{C}_{hp} . Furthermore, analogously to Theorem 3.1 in [17], the space $(\mathcal{C}_{hp}, \|\cdot\|_{\mathcal{C}_{hp}})$ is a Banach space.

Next, for $\tau \in (0, \infty)_{\mathbb{T}}$ being arbitrary but fixed, we consider the space

$$\mathcal{PW}_{h\tau} = \mathcal{PW}_{h\tau}((-\infty, \tau]_{\mathbb{T}}, \mathbb{R}^n)$$

given by

$$\mathcal{PW}_{h\tau} = \{z : (-\infty, \tau]_{\mathbb{T}} \longrightarrow \mathbb{R}^n : z|_{\mathbb{T}^-} \in \mathcal{C}_{hp} \text{ and } z|_{[0, \tau]_{\mathbb{T}}} \text{ is rd-continuous except at } t_k, k = 1, \dots, p \text{ with } t_p < \tau, \text{ where } z(t_k^+), z(t_k^-) \text{ exist and } z(t_k^-) = z(t_k)\}.$$

Note that $\mathcal{PW}_{h\tau}$ is a Banach space endowed with the norm

$$\|z\|_{\mathcal{PW}_{h\tau}} = \|z|_{\mathbb{T}^-}\|_{\mathcal{C}_{hp}} + |z|^{[0, \tau]_{\mathbb{T}}}.$$

By using Theorem 3.2 in [17], it is possible to show that if $\phi \in \mathcal{C}_{hp}$, then

P1) If $z \in \mathcal{PW}_{h\tau}$ and $z_0 = \phi$, then for every $t \in [0, \tau]_{\mathbb{T}}$ we have that

- i) z_t is in \mathcal{C}_{hp} ,
- ii) z_t is rd-continuous with respect to t ,
- iii) there exists $H > 0$ such that $|z(t)| \leq H \|z_t\|_{\mathcal{C}_{hp}}$.

P2) $\|z_t\|_{\mathcal{C}_{hp}} \leq 2 \|z\|_{\mathcal{PW}_{h\tau}}$.

4 Main Result

In this section we will show the existence of solutions for system (1). In order to accomplish this, we shall assume the following hypotheses:

H1) $|f(t, \phi) - f(t, \varphi)| \leq \eta(t) \|\phi - \varphi\|_{\mathcal{C}_{hp}}$, for all $\phi, \varphi \in \mathcal{C}_{hp}$ and $t \in [0, \tau]_{\mathbb{T}}$, where $\eta \in C_{rd}([0, \tau]_{\mathbb{T}}, \mathbb{R}^+)$.

H2) $|f(t, \phi)| \leq \nu(t)(1 + \|\phi\|_{\mathcal{C}_{hp}})$, for $\phi \in \mathcal{C}_{hp}$ and $t \in [0, \tau]_{\mathbb{T}}$, $\nu \in C_{rd}([0, \tau]_{\mathbb{T}}, \mathbb{R}^+)$.

H3) $|J_k(t, x) - J_k(t, y)| \leq d_k |x - y|$, $J_k(t, 0) = 0$, $k = 1, 2, \dots$ and $\sum_{k \geq 1} d_k < \infty$.

A straightforward computation shows that

Theorem 4.1 $z(\cdot)$ is a solution of system (1) on $(-\infty, \tau]_{\mathbb{T}}$ if and only if $z(\cdot)$ satisfies

$$z(t) = \begin{cases} \phi(t), & t \in \mathbb{T}^-, \\ e_A(t, 0)\phi(0) + \int_0^t e_A(t, \sigma(s))f(s, z_s)\Delta s + \sum_{0 < t_k < t} e_A(t, t_k)J_k(t_k, z(t_k)), & t \in [0, \tau]_{\mathbb{T}}. \end{cases} \quad (3)$$

Now, for a given $\phi \in \mathcal{C}_{hp}$ being arbitrary but fixed, define $\phi^* : (-\infty, \tau]_{\mathbb{T}} \longrightarrow \mathbb{R}^n$ by

$$\phi^*(t) = \begin{cases} \phi(t), & t \in \mathbb{T}^-, \\ e_A(t, 0)\phi(0), & t \in [0, \tau]_{\mathbb{T}}. \end{cases} \quad (4)$$

Note that $\phi_0^* = \phi$. Let $x(t) = z(t) - \phi^*(t)$, then $x(t)$ satisfies

$$x(t) = \begin{cases} 0, & t \in \mathbb{T}^-, \\ \int_0^t e_A(t, \sigma(s))f(s, x_s + \phi_s^*)\Delta s + \sum_{0 < t_k < t} e_A(t, t_k)J_k(t_k, x(t_k) + \phi^*(t_k)), & t \in [0, \tau]_{\mathbb{T}}. \end{cases} \tag{5}$$

Finding a solution of system (1) on $(-\infty, \tau]_{\mathbb{T}}$ is equivalent to solving the integral equation (5), and this is equivalent to finding a fixed point of the operator

$$\mathcal{T} : \mathcal{PW}_{h\tau}^0 \longrightarrow \mathcal{PW}_{h\tau}^0$$

defined by

$$(\mathcal{T}x)(t) = \begin{cases} 0, & t \in \mathbb{T}^-, \\ \int_0^t e_A(t, \sigma(s))f(s, x_s + \phi_s^*)\Delta s + \sum_{0 < t_k < t} e_A(t, t_k)J_k(t_k, x(t_k) + \phi^*(t_k)), & t \in [0, \tau]_{\mathbb{T}}, \end{cases} \tag{6}$$

where $\mathcal{PW}_{h\tau}^0 = \{x \in \mathcal{PW}_{h\tau} : x_0 = 0\}$, with $\|x\|_{\mathcal{PW}_{h\tau}^0} = \|x|_{\mathbb{T}^-}\|_{\mathcal{C}_{hp}} + |x|^{[0, \tau]_{\mathbb{T}}} = |x|^{[0, \tau]_{\mathbb{T}}}$. Notice that $(\mathcal{PW}_{h\tau}^0, \|\cdot\|_{\mathcal{PW}_{h\tau}^0})$ is a Banach space.

Theorem 4.2 *Suppose that H1), H2) and H3) hold, then system (1) has at least one solution on $(-\infty, \tau]_{\mathbb{T}}$.*

Proof. To prove that the operator (6) has a fixed point, we will use the Leray-Schauder alternative. We denote by $M = \sup\{\|e_A(t, \xi)\| : t, \xi \in [0, \tau]_{\mathbb{T}}\}$, $\eta^* = \sup\{\eta(t) : t \in [0, \tau]_{\mathbb{T}}\}$ and $\nu^* = \sup\{\nu(t) : t \in [0, \tau]_{\mathbb{T}}\}$.

First, we will show that in three steps the operator \mathcal{T} is completely continuous.

Step 1: \mathcal{T} is continuous. If $t \in [0, \tau]_{\mathbb{T}}$, then

$$\begin{aligned} |(\mathcal{T}x)(t) - (\mathcal{T}y)(t)| &\leq \int_0^t \|e_A(t, \sigma(s))\| |f(s, x_s + \phi_s^*) - f(s, y_s + \phi_s^*)| \Delta s \\ &\quad + \sum_{0 < t_k < t} \|e_A(t, s(s))\| |J_k(t_k, x(t_k) + \phi^*(t_k)) - J_k(t_k, y(t_k) + \phi^*(t_k))| \\ &\leq M \left\{ \int_0^t |f(s, x_s + \phi_s^*) - f(s, y_s + \phi_s^*)| \Delta s \right. \\ &\quad \left. + \sum_{0 < t_k < t} |J_k(t_k, x(t_k) + \phi^*(t_k)) - J_k(t_k, y(t_k) + \phi^*(t_k))| \right\} \\ &\leq M \left\{ \int_0^t \eta(s) \|x_s - y_s\|_{\mathcal{C}_{hp}} \Delta s + \sum_{k=1}^p d_k |x(t_k) - y(t_k)| \right\} \\ &\leq M \left\{ 2\eta^* \int_0^\tau \|x - y\|_{\mathcal{PW}_{h\tau}} \Delta s + \sum_{k=1}^p d_k |x(t_k) - y(t_k)| \right\} \\ &\leq M \left\{ 2\eta^* \tau + \sum_{k=1}^\infty d_k \right\} \|x - y\|_{\mathcal{PW}_{h\tau}^0}. \end{aligned}$$

Therefore,

$$\|\mathcal{T}x - \mathcal{T}y\|_{\mathcal{PW}_{h\tau}^0} \leq M \left\{ 2\eta^*\tau + \sum_{k=1}^{\infty} d_k \right\} \|x - y\|_{\mathcal{PW}_{h\tau}^0}.$$

So, we have proved that \mathcal{T} is locally Lipschitz and therefore it is continuous.

Step 2: \mathcal{T} maps bounded sets of $\mathcal{PW}_{h\tau}^0$ into bounded sets of $\mathcal{PW}_{h\tau}^0$. It is enough to show that for any $R > 0$, there exists $r > 0$ such that for each $x \in B_R = \{x \in \mathcal{PW}_{h\tau}^0 : \|x\|_{\mathcal{PW}_{h\tau}^0} \leq R\}$, we have that $\|\mathcal{T}x\|_{\mathcal{PW}_{h\tau}^0} \leq r$. Indeed,

$$\begin{aligned} |(\mathcal{T}x)(t)| &\leq M \left\{ \int_0^t |f(s, x_s + \phi_s^*)| \Delta s + \sum_{k=1}^p d_k |x(t_k) + \phi^*(t_k)| \right\} \\ &\leq M \left\{ \int_0^t \nu(s)(1 + \|x_s + \phi_s^*\|_{\mathcal{E}_{hp}}) \Delta s + \sum_{k=1}^p d_k (|x(t_k)| + |\phi^*(t_k)|) \right\} \\ &\leq M \left\{ \int_0^t \nu(s)(1 + \|x_s\|_{\mathcal{E}_{hp}} + \|\phi_s^*\|_{\mathcal{E}_{hp}}) \Delta s + \sum_{k=1}^p d_k (|x(t_k)| + \|e_A(t_k, 0)\| |\phi(0)|) \right\} \\ &\leq M \left\{ \int_0^\tau \nu^*(1 + 2\|x\|_{\mathcal{PW}_{h\tau}^0} + 2\|\phi^*\|_{\mathcal{PW}_{h\tau}}) \Delta s + \sum_{k=1}^p d_k (\|x\|_{\mathcal{PW}_{h\tau}^0} + M|\phi(0)|) \right\} \\ &\leq M \left\{ \nu^*(1 + 2R + 2\|\phi^*\|_{\mathcal{PW}_{h\tau}}) \tau + (R + M|\phi(0)|) \sum_{k=1}^{\infty} d_k \right\} = r, \end{aligned}$$

Step 3: \mathcal{T} maps bounded sets into equicontinuous sets. Let us consider B_R as in step 2. We shall prove that $\mathcal{T}(B_R)$ is equicontinuous on the interval $[0, \tau]_{\mathbb{T}}$. If $t', t'' \in [0, \tau]_{\mathbb{T}}$ with $t' < t''$, then

$$\begin{aligned} |(\mathcal{T}x)(t'') - (\mathcal{T}x)(t')| &\leq \int_0^{t'} \|e_A(t'', \sigma(s)) - e_A(t', \sigma(s))\| |f(s, x_s + \phi_s^*)| \Delta s \\ &\quad + \sum_{0 < t_k < t'} \|e_A(t'', t_k) - e_A(t', t_k)\| |J_k(t_k, x(t_k) + \phi^*(t_k))| \\ &\quad + \sum_{t' < t_k < t''} \|e_A(t'', t_k)\| |J_k(t_k, x(t_k) + \phi^*(t_k))| \\ &\leq \int_0^{t'} \|e_A(t'', \sigma(s)) - e_A(t', \sigma(s))\| \nu(s)(1 + \|x_s + \phi_s^*\|_{\mathcal{E}_{hp}}) \Delta s \\ &\quad + \int_{t'}^{t''} \|e_A(t'', \sigma(s))\| \nu(s)(1 + \|x_s + \phi_s^*\|_{\mathcal{E}_{hp}}) \Delta s \\ &\quad + \sum_{0 < t_k < t'} d_k \|e_A(t'', t_k) - e_A(t', t_k)\| |x(t_k) + \phi^*(t_k)| \\ &\quad + \sum_{t' < t_k < t''} d_k \|e_A(t'', t_k)\| |x(t_k) + \phi^*(t_k)| \end{aligned}$$

$$\begin{aligned}
 &\leq \int_0^\tau \|e_A(t'', \sigma(s)) - e_A(t', \sigma(s))\| \nu(s)(1 + 2\|x\|_{\mathcal{PW}_{h\tau}} + 2\|\phi^*\|_{\mathcal{PW}_{h\tau}}) \Delta s \\
 &\quad + \int_{t'}^{t''} \|e_A(t'', \sigma(s))\| \nu(s)(1 + 2\|x\|_{\mathcal{PW}_{h\tau}} + 2\|\phi^*\|_{\mathcal{PW}_{h\tau}}) \Delta s \\
 &\quad + \sum_{0 < t_k < t'} d_k \|e_A(t'', t_k) - e_A(t', t_k)\| (\|x\|_{\mathcal{PW}_{h\tau}^0} + M|\phi(0)|) \\
 &\quad + \sum_{t' < t_k < t''} d_k \|e_A(t'', t_k)\| (\|x\|_{\mathcal{PW}_{h\tau}^0} + M|\phi(0)|) \\
 &\leq \nu^*(1 + 2R + 2\|\phi^*\|_{\mathcal{PW}_{h\tau}}) \int_0^\tau \|e_A(t'', \sigma(s)) - e_A(t', \sigma(s))\| \Delta s \\
 &\quad + M\nu^*(1 + 2R + 2\|\phi^*\|_{\mathcal{PW}_{h\tau}}) |t'' - t'| \\
 &\quad + (R + M|\phi(0)|) \sum_{0 < t_k < t'} d_k \|e_A(t'', t_k) - e_A(t', t_k)\| \\
 &\quad + M(R + M|\phi(0)|) \sum_{t' < t_k < t''} d_k.
 \end{aligned}$$

Since $e_A(\cdot, \sigma(s))$ is continuous, we have $|(\mathcal{T}x)(t'') - (\mathcal{T}x)(t')| \rightarrow 0$ as $t' \rightarrow t''$, independently of $x \in B_R$.

Therefore, $\mathcal{T}(B_R)$ is equicontinuous. From the Arzela-Ascoli theorem we have that $\mathcal{T}(B_R)$ is relatively compact, so \mathcal{T} is completely continuous.

Now, let us consider the set

$$\mathcal{D} = \{x \in \mathcal{PW}_{h\tau}^0 : x = \lambda \mathcal{T}x, \quad 0 < \lambda < 1\}.$$

If $x \in \mathcal{D}$, then for $t \in [0, \tau]_{\mathbb{T}}$, we get

$$\begin{aligned}
 |x(t)| &= \lambda \left| \int_0^t e_A(t, \sigma(s)) f(s, x_s + \phi_s^*) \Delta s + \sum_{0 < t_k < t} e_A(t, t_k) J_k(t_k, x(t_k) + \phi(t_k)^*) \right| \\
 &\leq \int_0^t \|e_A(t, \sigma(s))\| \|f(s, x_s + \phi_s^*)\| \Delta s + \sum_{0 < t_k < t} \|e_A(t, t_k)\| |J_k(t_k, x(t_k) + \phi^*(t_k))| \\
 &\leq M\nu^* \int_0^t (1 + \|x_s\|_{\mathcal{E}_{hp}} + \|\phi_s^*\|_{\mathcal{E}_{hp}}) \Delta s + M \sum_{0 < t_k < t} d_k (|x(t_k)| + |\phi(t_k)^*|) \\
 &\leq M \left(\nu^*(1 + 2\|\phi^*\|_{\mathcal{PW}_{h\tau}}) \tau + M|\phi(0)| \sum_{k=1}^\infty d_k \right) + M\nu^* \int_0^t \|x_s\|_{\mathcal{E}_{hp}} \Delta s \\
 &\quad + M \sum_{0 < t_k < t} d_k |x(t_k)|.
 \end{aligned}$$

If we put $\alpha = M \left(\nu^*(1 + 2\|\phi^*\|_{\mathcal{PW}_{h\tau}}) \tau + M|\phi(0)| \sum_{k=1}^\infty d_k \right)$, then

$$|x(t)| \leq \alpha + M\nu^* \int_0^t \|x_s\|_{\mathcal{E}_{hp}} \Delta s + MH \sum_{0 < t_k < t} d_k \|x_{t_k}\|_{\mathcal{E}_{hp}}.$$

Thus

$$\|x_t\|_{\mathcal{C}_{hp}} \leq \alpha + M\nu^* \int_0^t \|x_s\|_{\mathcal{C}_{hp}} \Delta s + MH \sum_{0 < t_k < t} d_k \|x_{t_k}\|_{\mathcal{C}_{hp}}.$$

By applying Gronwall's inequality with impulses on time scales, we get that

$$\|x_t\|_{\mathcal{C}_{hp}} \leq \alpha \prod_{0 < t_k < t} (1 + MHd_k) e_{M\nu^*}(t, 0) \leq \alpha \prod_{k=1}^p (1 + MHd_k) e_{M\nu^*}(t, 0).$$

Then

$$\|x\|_{\mathcal{D}\mathcal{W}_{h\tau}^0} \leq \alpha H \prod_{k=1}^p (1 + MHd_k) e_{M\nu^*}(t, 0).$$

Therefore, \mathcal{D} is a bounded set, and by the Leray-Schauder alternative, the operator \mathcal{T} has a fixed point.

Theorem 4.3 *Under the conditions of Theorem 4.2, the solution of system (1) on $(-\infty, \tau]_{\mathbb{T}}$ is unique.*

Proof. Let $\phi \in \mathcal{C}_{hp}$, and suppose that for some $\tau_0 \in (0, \tau]_{\mathbb{T}}$, there are two solutions z and \tilde{z} mapping $(-\infty, \tau_0]_{\mathbb{T}} \rightarrow \mathbb{R}^n$ with $z \neq \tilde{z}$. Let

$$\tau^* = \inf\{t \in (0, \tau_0)_{\mathbb{T}} : z(t) \neq \tilde{z}(t)\}.$$

Then, for $-\infty < t < \tau^*$, $z(t) = \tilde{z}(t)$. On the other hand

$$z(t) = e_A(t, 0)\phi(0) + \int_0^t e_A(t, \sigma(s))f(s, z_s)\Delta s + \sum_{0 < t_k < t} e_A(t, t_k)J_k(t_k, z(t_k))$$

and

$$\tilde{z}(t) = e_A(t, 0)\phi(0) + \int_0^t e_A(t, \sigma(s))f(s, \tilde{z}_s)\Delta s + \sum_{0 < t_k < t} e_A(t, t_k)J_k(t_k, \tilde{z}(t_k)).$$

Therefore,

$$\begin{aligned} |z(t) - \tilde{z}(t)| &\leq \int_{\tau^*}^t \|e_A(t, \sigma(s))\| |f(s, z_s) - f(s, \tilde{z}_s)| \Delta s \\ &\quad + \sum_{\tau^* < t_k < t} \|e_A(t, t_k)\| |J_k(t_k, z(t_k)) - J_k(t_k, \tilde{z}(t_k))| \\ &\leq \int_{\tau^*}^t M\eta(s) \|z_s - \tilde{z}_s\|_{\mathcal{C}_{hp}} \Delta s + \sum_{\tau^* < t_k < t} Md_k |z(t_k) - \tilde{z}(t_k)| \\ &\leq \varepsilon + \int_{\tau^*}^t M\eta^* \|z_s - \tilde{z}_s\|_{\mathcal{C}_{hp}} \Delta s + \sum_{\tau^* < t_k < t} Md_k H \|z_{t_k} - \tilde{z}_{t_k}\|_{\mathcal{C}_{hp}}, \end{aligned}$$

for $\varepsilon > 0$ being arbitrary. So,

$$\|z_t - \tilde{z}_t\|_{\mathcal{C}_{hp}} \leq \varepsilon + \int_{\tau^*}^t M\eta^* \|z_s - \tilde{z}_s\|_{\mathcal{C}_{hp}} \Delta s + \sum_{\tau^* < t_k < t} Md_k H \|z_{t_k} - \tilde{z}_{t_k}\|_{\mathcal{C}_{hp}}.$$

By using Gronwall’s inequality, we get that

$$\|z_t - \tilde{z}_t\|_{\mathcal{C}_{hp}} \leq \varepsilon \prod_{\tau^* < t_k < t} (1 + MHd_k)e_{M\eta^*}(t, \tau^*) \leq \varepsilon \prod_{\tau^* < t_k < \tau} (1 + MHd_k)e_{M\eta^*}(\tau, \tau^*).$$

Therefore,

$$|z(t) - \tilde{z}(t)| \leq \varepsilon H \prod_{\tau^* < t_k < \tau} (1 + MHd_k)e_{M\eta^*}(\tau, \tau^*).$$

Since ε is arbitrary, one has $|z(t) - \tilde{z}(t)| = 0$ for $t \in (\tau^*, \tau)_{\mathbb{T}}$, contradicting the definition of τ^* .

5 Continuation of Solutions

In this section, we will show that $z(t)$ is defined on $(-\infty, \infty)_{\mathbb{T}}$.

Definition 5.1 We shall say that $(-\infty, \tau)_{\mathbb{T}}$ is a maximal interval of existence of the solution $z(\cdot)$ of system (1) if there is no solution of (1) on $(-\infty, \tau^*)_{\mathbb{T}}$ with $\tau^* > \tau$.

Theorem 5.1 *Suppose that the conditions of existence and uniqueness hold. If z is a solution of problem (1) on $(-\infty, \tau)_{\mathbb{T}}$ and τ is maximal, then either $\tau = +\infty$ or $z(t)$ is not bounded in any neighborhood of τ .*

Proof. Suppose that $\tau < \infty$ and there is a neighborhood U of τ such that $|z(t)| \leq R$ for $t \in U \cap (-\infty, \tau)_{\mathbb{T}}$, then we can suppose that $|z(t)| \leq R$ for all $t \in (-\infty, \tau)_{\mathbb{T}}$. Let t_p be such that $t_p \leq \tau$. Suppose first that $t_p < \tau$.

If τ is left-dense, then there is a sequence $\{\tau_n\}$ such that $t_p < \tau_1 < \tau_2 < \dots < \tau_n < \dots$, $\lim_{n \rightarrow \infty} \tau_n = \tau$ and $\lim_{n \rightarrow \infty} z(\tau_n) = z^*$ for some $z^* \in \mathbb{R}^n$. We shall see that $\lim_{t \rightarrow \tau^-} z(t) = z^*$.

Since $\lim_{n \rightarrow \infty} \tau_n = \tau$, then there is $\tau_N \in (\tau - \varepsilon, \tau)_{\mathbb{T}}$ such that $|z(\tau_N) - z^*| < \varepsilon$. So, for $t \in (\tau - \varepsilon, \tau)_{\mathbb{T}}$ with $t > \tau_N$, we have that $|z(t) - z^*| \leq |z(t) - z(\tau_N)| + |z(\tau_N) - z^*|$. Now

$$\begin{aligned} |z(t) - z(\tau_N)| &\leq \|e_A(t, 0) - e_A(\tau_N, 0)\| |\phi(0)| + \int_0^{\tau_N} \|e_A(t, \sigma(s)) - e_A(\tau_N, \sigma(s))\| |f(s, z_s)| \Delta s \\ &\quad + \int_{\tau_N}^t \|e_A(\tau_N, \sigma(s))\| |f(s, z_s)| \Delta s + \sum_{k=1}^p d_k \|e_A(t, t_k) - e_A(\tau_N, \sigma(s))\| |z(t_k)| \\ &\leq \|e_A(t, 0) - e_A(\tau_N, 0)\| |\phi(0)| + \int_0^{\tau_N} \|e_A(t, \sigma(s)) - e_A(\tau_N, \sigma(s))\| \nu(s)(1 + \|z_s\|_{\mathcal{C}_{hp}}) \Delta s \\ &\quad + \int_{\tau_N}^t M \nu(s)(1 + \|z_s\|_{\mathcal{C}_{hp}}) \Delta s + \sum_{k=1}^p d_k \|e_A(t, t_k) - e_A(\tau_N, t_k)\| R \end{aligned}$$

$$\begin{aligned}
&\leq \|e_A(t, 0) - e_A(\tau_N, 0)\| |\phi(0)| + \int_0^{\tau_N} \|e_A(t, \sigma(s)) - e_A(\tau_N, \sigma(s))\| \nu(s) (1 + 2 \|z\|_{\mathcal{PW}_{h\tau}}) \Delta s \\
&\quad + \int_{\tau_N}^t M \nu(s) (1 + 2 \|z\|_{\mathcal{PW}_{h\tau}}) \Delta s + \sum_{k=1}^p d_k \|e_A(t, t_k) - e_A(\tau_N, t_k)\| R \\
&\leq \|e_A(t, 0) - e_A(\tau_N, 0)\| |\phi(0)| + \int_0^{\tau} \|e_A(t, \sigma(s)) - e_A(\tau_N, \sigma(s))\| \nu(s) (1 + 2R) \Delta s \\
&\quad + \int_{\tau_N}^{\tau} M \nu(s) (1 + 2R) \Delta s + \sum_{k=1}^p d_k \|e_A(t, t_k) - e_A(\tau_N, t_k)\| R.
\end{aligned}$$

Hence, we get that if $\tau_N \rightarrow \tau$, then $|z(t) - z(\tau_N)| \rightarrow 0$, so $\lim_{t \rightarrow \tau^-} z(t) = z^*$ and therefore $z(t)$ can be continued beyond τ , contradicting our assumption.

If τ is left-scattered, then $\rho(\tau) \in (0, \tau)_{\mathbb{T}}$ and since t_p is right-dense, we have $t_p < \rho(\tau)$, then the solution z exists also at τ , namely, by putting

$$z(\tau) = z(\rho(\tau)) + \mu(\rho(\tau)) [A(\rho(\tau))z(\rho(\tau)) + f(\rho(\tau), z_{\rho(\tau)})],$$

we get a contradiction.

Now, if $\tau = t_p$ and t_p is left-dense, then we set $z^+ = z^* + J_p(t_p, z^*)$. By using the same argument as previously, we can show that $\lim_{t \rightarrow \tau^-} z(t) = z^*$, and therefore $z(t)$ can be continued beyond τ .

If $\tau = t_p$ is left-scattered, then

$$\begin{aligned}
z(t_p) &= z(\rho(t_p)) + \mu(\rho(t_p)) [A(\rho(t_p))z(\rho(t_p)) + f(\rho(t_p), z_{\rho(t_p)})], \\
z(t_p^+) &= z(t_p) + J_p(t_p, z(t_p))
\end{aligned}$$

and therefore $z(t)$ can be extended beyond τ to the right. This is a contradiction.

Corollary 5.1 *If hypothesis H2) is replaced by*

$$|f(t, \phi)| \leq \nu(t) (1 + |\phi(0)|), \quad \phi \in \mathcal{C}_{hp}, t \in \mathbb{T},$$

then the system (1) has a unique solution defined on all \mathbb{T} .

Proof. Suppose that $z(t)$ is defined on $(-\infty, \tau)_{\mathbb{T}}$ with $\tau < \infty$, then

$$\begin{aligned}
|z(t)| &\leq \left| e_A(t, 0)\phi(0) + \int_0^t e_A(t, \sigma(s))f(s, z_s)\Delta s + \sum_{0 < t_k < t} e_A(t, t_k)J_k(t_k, z(t_k)) \right| \\
&\leq M |\phi(0)| + \int_0^t M \nu(s) (1 + |z(s)|) \Delta s + M \sum_{k=1}^p d_k |z(t_k)| \\
&\leq M (|\phi(0)| + \nu^* \tau) + M \nu^* \int_0^t |z(s)| \Delta s + M \sum_{k=1}^p d_k |z(t_k)|.
\end{aligned}$$

So

$$\begin{aligned}
|z(t)| &\leq M (|\phi(0)| + \nu^* \tau) \prod_{k=1}^p (1 + M d_k) e_{M \nu^*}(t, 0) \\
&\leq M (|\phi(0)| + \nu^* \tau) \prod_{k=1}^p (1 + M d_k) e_{M \nu^*}(\tau, 0).
\end{aligned}$$

This implies that $|z(t)|$ stays bounded in any neighborhood of τ . So, for Theorem 5.1 we have that $\tau = \infty$.

6 Example

Consider the following semilinear functional dynamic equation with infinite delay and impulses on time scales:

$$\begin{cases} z^\Delta(t) = a(t)z(t) + b(t) \tanh(z_t) + c(t), & t \in [0, \infty)_{\mathbb{T}} \setminus \bigcup_{k=1}^{\infty} \{t_k\}, \\ z(s) = \phi(s), & s \in (-\infty, 0]_{\mathbb{T}}, \\ z(t_k^+) = z(t_k^-) + \frac{1}{2^k} \sin(z(t_k^-)), & k = 1, 2, \dots, \end{cases} \tag{7}$$

with $a \in \mathcal{R}(\mathbb{T}, \mathbb{R})$ and $b, c \in C_{rd}(\mathbb{T}, \mathbb{R})$. Then we have that

- i) $|f(t, \phi) - f(t, \varphi)| = |b(t)| |\tanh(\phi) - \tanh(\varphi)| \leq |b(t)| \|\phi - \varphi\|_{\mathcal{C}_{hp}}$;
- ii) $|f(t, \phi)| = |b(t) \tanh(\phi) + c(t)| \leq \nu(t)(1 + \|\phi\|_{\mathcal{C}_{hp}})$, where $\nu(t) = \max\{|b(t)|, |c(t)|\}$;
- iii) $|J_k(t, x) - J_k(t, y)| \leq \frac{1}{2^k} |x - y|$, $J_k(t, 0) = 0$, for $k = 1, 2, \dots$ and $\sum_{k=1}^{\infty} \frac{1}{2^k} < \infty$.

Therefore hypotheses H1), H2) and H3) hold, so, by Theorems 4.2 and 4.3, we get that the problem (7) has a unique solution $z(t)$ defined on $(-\infty, \tau]_{\mathbb{T}}$.

7 Conclusion and Final Remarks

In this work, first of all, we prove the existence of solutions for a semilinear retarded differential equation with infinite delay and impulses on time-scale, by using a version of the Arzela-Ascoli theorem on time-scale and applying the Leray-Schauder alternative. Secondly, we prove the uniqueness of solutions by applying a version of Gronwall’s inequality for impulsive differential equations, and finally, we study the continuation of solutions. Of course, once we have an Arzela-Ascoli version on time-scale (see [18]), we can apply other fixed point theorems to prove the existence of solutions for such equations, perhaps one can apply Karakosta’s fixed point theorem like in [19]. Our next work is devoted to the study of the exact controllability for this type of equations on time-scales by using Rothe’s fixed point theorem like in [20].

References

- [1] R. Agarwal, D. O’Regan and S. Saker. *Dynamic Inequalities on Time Scales*. Springer International Publishing, Switzerland, 2014.
- [2] S. G. Georgiev, *Functional Dynamic Equations on Time Scales*. Springer Nature, Switzerland, AG 2019.
- [3] M. Bohner and A. Peterson. *Dynamics Equations on Time Scales. An Introduction with Applications*, Birkhäuser Boston Inc., Boston MA, 2001.
- [4] S. Hilger. *Ein Maßkettenkalkül mit Anwendung auf Zentrumsmannigfaltigkeiten*. PhD thesis, Universität Würzburg, 1988.
- [5] A. Granas and J. Dugundji. *Fixed point Theory*. Springer Monographs Mathematics, New York, 2003.

- [6] C. Tisdell and A. Zaidi. Basic qualitative and quantitative results for solutions to nonlinear dynamic equations on time scales with application to economic modeling. *Nonlinear Anal.* **68** (11) (2008) 3504–3524.
- [7] M. Bohner, M. Fan and J. Zhang. Existence of periodic solutions in predator-prey and competition dynamic systems. *Nonlinear Analysis: Real World and Applications* **7** (2006) 1193–1204.
- [8] C. Duque, J. Uzcátegui and H. Leiva. Approximate controllability of semilinear dynamic equations on time scale. *Asian Journal of Control* **21** (5) (2019) 1–7.
- [9] O. Lavrova, V. Mogylova, O. Stanzhytskyi and O. Misiats. Approximation of the optimal control problem on an interval with a family of optimization problems on time scales. *Nonlinear Dynamics and Systems Theory* **17** (3) (2017) 303–314.
- [10] V. Lakshmikantham, D. Bainov and P. Simeonov. *Theory of Impulsive Differential Equations*. Series in Modern Applied Mathematics, Vol 6, World Scientific, 1989.
- [11] M. Federson, J.G. Mesquita and A. Slavík. Basic results for functional differential and dynamic equations involving impulses. *Math. Nachr.* **286** (2-3) (2013) 181–204.
- [12] T.A. lukyanova and A.A. Martynyuk. Stability analysis of impulsive Hopfield-type neuron system on time scale. *Nonlinear Dynamics and Systems Theory* **13** (3) (2017) 315–326.
- [13] J. Hale and J. Kato. Phase space for retarded equations with infinite delay. *Funkcial. Ekvac.* **1** (1978) 11–41.
- [14] Y. Hino, S. Murakami and T. Naito. *Functional Differential Equations with Infinite Delay*, Lecture Notes in Mathematics, Vol. 1473, Springer-Verlag, Berlin, 1991.
- [15] J.S. Shin. On the uniqueness of solutions for functional differential equations with infinite delay. *Funkcial Ekvac.* **30** (1987) 225–236.
- [16] M. Benchohra, J. Henderson, S. Ntouyas and A. Ouahab. Impulsive functional dynamic equations on time scales. *Dynamic Systems and Applications* **15** (2006) 43–52.
- [17] L. Bi, M. Bohner and M. Fan. Periodic solutions of functional dynamic equations with infinite delay. *Nonlinear Analysis.* **68** (2008) 1226–1245.
- [18] Z. Zhu and Q. Wang. Existence of nonoscillatory solutions to neutral dynamic equations on time scales. *J. Math. Anal. Appl.* **335** (2007) 751–762.
- [19] M. Ayala, H. Leiva and D. Tallana. Existence of solutions for retarded equations with infinite delay, impulses, and nonlocal conditions. *Journal of Mathematical Control Science and Applications* **6** (1) (2020) 43–61.
- [20] D. Cabada, R. Gallo and H. Leiva. Roughness of the controllability for time varying systems under the influence of impulses, delays and nonlocal conditions. *Nonauton. Dyn. Syst.* **7** (2020) 126–139.



Modification of the Trajectory Following Method for Asymptotic Stability in a System Nonlinear Control

Firman^{*}, Syamsuddin Toaha, Kasbawati

Department of Mathematics, Faculty of Mathematics and Natural Science, Hasanuddin University, Indonesia

Received: November 9, 2021; Revised: April 4, 2022

Abstract: In this paper, we present the asymptotic stability for a class of nonlinear control systems. To achieve the asymptotic stability, we will design a dynamic feedback control. The design of the dynamic feedback control is based on the modification of the trajectory following method. To apply the modification of the trajectory following method, the system will be transformed through the input state linearization.

Keywords: *relative degree of system; input state linearization; zero dynamics; modified trajectory following method.*

Mathematics Subject Classification (2010): 93C10, 93D20.

1 Introduction

In the analysis for nonlinear control systems, there is no general method which can be applied to any nonlinear control system in designing the control input for solving the stability problems. Therefore, in general, the researchers describe some particular nonlinear classes only. Recently, stability problems for nonlinear control systems have been intensively investigated. Daizhan Cheng [1] has discussed the stability problem for a nonlinear system, where the zero dynamic has a multiplicity eigenvalue of 2. Zhengtao Ding [2] has discussed the stability of a nonlinear system through backstepping, where the backstepping design starts from the estimation of the output transformation. In 2004, Chen P *et al.* [3] and Diao L *et al.* [4] introduced the problem of stability through the system transformation, where the transformation of the system is made through dynamic feedback. In 2019, Erkan Kayacan [5] has discussed the Sliding Mode Learning Control (SMLC) of uncertain nonlinear systems with the Lyapunov stability analysis.

^{*} Corresponding author: <mailto:firman.math11@gmail.com>

One of popular methods for solving stability problems is the input-output linearization method. Some research on the stability problems of a nonlinear control system using the input-output linearization method was carried out by: Ricardo Marino and Patrizio Tomei [6], who discussed the stability of lower triangular nonlinear control system. Its stability control was the dynamic feedback of order $n + 2(r - 1)$ (n is the system order, r is the relative degree). Results on stabilization of nonlinear lower triangular systems with uncertainties in the output feedback form have been presented in [7] and [8]. In [9], Naiborhu J. *et al.* discussed the asymptotic stability problem for a nonlinear class, where its control design used the exact linearization. Furthermore, Firman *et al.* [10] have introduced the problem of stabilization for a class of nonlinear systems with uncertainty. Then, in [11], Firman *et al.* have introduced the problem of stabilization for some class of affine nonlinear control systems with the relative degrees of the system being 1 and $n-1$. For the design of input controls, the system will be transformed through the partial feedback linearization. Naiborhu J. and Shimizu K. [12] have proposed a dynamic feedback control for the asymptotic stability of a nonlinear class where its unforced dynamic is asymptotically stable.

In this paper, we will propose a dynamic feedback control for asymptotic stability in a system nonlinear control, even though its unforced dynamic is not asymptotically stable. The proposed dynamic feedback control is a modification of the trajectory following method.

2 Problem Formulation

Consider the affine nonlinear control system

$$\dot{x}(t) = f(x(t)) + g(x(t))u, \quad (1)$$

$$y(t) = h(x(t)), \quad (2)$$

where $x(t) \in \mathcal{R}^n$, $u(t) \in \mathcal{R}$. $f : D \rightarrow \mathcal{R}^n$, $f(\vec{0}) = \vec{0}$ and $g : D \rightarrow \mathcal{R}^n$ are sufficiently smooth in a domain $D \subset \mathcal{R}^n$. Let a state $y(t) = h(x(t))$, $h : D \rightarrow \mathcal{R}$ is sufficiently smooth in a domain $D \subset \mathcal{R}^n$, $h(\vec{0}) = 0$.

Our objective is to make the output $y(t)$ go to zero as $t \rightarrow \infty$. The main task is to design the input control u such that the system (1) has an asymptotically stable equilibrium at $x = 0$.

For designing the control input u , we need a system transformation based on the relative degree of the system. In the following, we present the method of the input state linearization by Isidori [13].

Let the relative degree of the system (1) with respect to the state y be r , $r \leq n$. If the relative degree of the system (1)-(2) is n , the system (1) with respect to the state y can be transformed to

$$\dot{z}_k = z_{k+1}, \quad k = 1, 2, \dots, n-1, \quad (3)$$

$$\dot{z}_n = f(z) + g(z)u, \quad (4)$$

$$y = z_1.$$

If $g(z) \neq 0$, $\forall t$, then the relative degree of the system with respect to the state y is well defined.

Let the relative degree of the system (1)-(2) be r , $r < n$, the system (1) with respect to the state y can be transformed to

$$\dot{z}_k = z_{k+1}, k = 1, 2, \dots, r - 1, \tag{5}$$

$$\dot{z}_r = f(z, \eta) + g(z, \eta)u, \tag{6}$$

$$\dot{\eta} = q(z, \eta), \tag{7}$$

$$y = z_1$$

with the internal dynamic

$$\dot{\eta} = q(z, \eta), \tag{8}$$

where $(z, \eta) = (z_1, z_2, \dots, z_r, \eta_1, \eta_2, \dots, \eta_{n-r})$. If $g(z, \eta) \neq 0, \forall t$, then the relative degree of the system with respect to the state y is well defined. Then if $z_1 = 0$, for all t , the system (8) is said to be zero dynamic with respect to the state $y = z_1$.

Consider a function $G : \mathcal{R}^{r+1} \rightarrow \mathcal{R}$, where $G = G(z_1, \dot{z}_1, \dots, z_1^{(r)})$ is a positive definite function and $\frac{\partial G}{\partial x_i}$ exists for $i = 1, 2, \dots, n$. Our objective is to find a dynamic feedback control $\dot{u}(t)$, for all t such that the function G becomes minimum. In this case, if the function G becomes minimum, then the state $y(t)$ goes to zero. The main task is to design the control input u such that $y(t) \rightarrow \infty 0$ as $t \rightarrow \infty$. Then our problem is formulated as follows:

$$\min G(z_1, \dot{z}_1, \dots, z_1^{(r)}), \tag{9}$$

$$\text{subj. to } \dot{x}(t) = f(x(t)) + g(x(t))u(t), \tag{10}$$

$$y(t) = h(x(t)). \tag{11}$$

The dynamic feedback control is designed based on the trajectory following method [14] as follows:

$$\dot{u} = -\frac{\partial G}{\partial u}. \tag{12}$$

When using the dynamic feedback control (12), the value of time derivative of function G along the trajectory of the system can not be guaranteed to be less than zero, $\forall t \geq 0$.

In this paper, we present the asymptotic stability of some class of affine nonlinear control systems by modifying the dynamic feedback control (12), i.e., by adding an artificial input.

3 Main Results

Consider the system (1)-(2). Let the relative degree of the system (1)-(2) be r , $r \leq n$. We design an input control u through the properties of the solution of a higher order ordinary differential equation. Consider a differential equation

$$a_r y^{(r)}(t) + a_{r-1} y^{(r-1)}(t) + \dots + a_1 \dot{y} + a_0 y(t) = 0, \tag{13}$$

with $y^{(i)} = \frac{d^i y}{dt^i}$, $i = 1, 2, \dots, r$, where r is the relative degree of the system (1)-(2), $r \leq n$. From equation (13), let $\omega_1 = y$, $\omega_2 = \dot{y}$, \dots , $\omega_r = y^{(r-1)}$, then the equation

(13) becomes $\dot{\omega} = B\omega$, with $B = \begin{pmatrix} 0 & 1 & \dots & 0 \\ \vdots & \vdots & \ddots & \vdots \\ 0 & 0 & \dots & 1 \\ \frac{-a_0}{a_r} & \frac{-a_1}{a_r} & \dots & \frac{-a_{(r-1)}}{a_r} \end{pmatrix}$. If all the roots of the

polynomial

$$p(\lambda) = a_r\lambda^r + a_{r-1}\lambda^{r-1} + \dots + a_1\lambda + a_0 \quad (14)$$

have negative real part, then a solution of differential equation (13) tends to zero as $t \rightarrow \infty$. Constants $a_i, i = 0, 1, \dots, r$ can be chosen such that all the roots of the polynomial (14) have negative real part.

Define a function

$$G(z_1, \dot{z}_1, \dots, z_1^{(r)}) = \left(\sum_{j=0}^r a_j z_1^{(j)} \right)^2, \quad r \leq n. \quad (15)$$

The main task is to design the control $u(t)$ such that the function G becomes minimum. If $r < n$, then the function G (15) contains the internal dynamic solution variable. Therefore, if the zero dynamic of the system (1) with respect to the state $y = z_1$ is not asymptotically stable, then the function G (15) becomes unbounded. Furthermore, to get dynamic feedback control, assume as follows.

Assumption 3.1 *The zero dynamic of the system (1) with respect to the state $y = z_1$ is asymptotically stable.*

From equation (12), the dynamic feedback control

$$\dot{u} = -2a_r \left(\sum_{j=0}^r a_j z_1^{(j)} \right) \frac{\partial z_1^{(r)}}{\partial u}. \quad (16)$$

Consider the extended system

$$\dot{x} = f_1(x) + f_2(x)u, \quad (17)$$

$$\dot{u} = -2a_r \left(\sum_{j=0}^r a_j z_1^{(j)} \right) \frac{\partial z_1^{(r)}}{\partial u}. \quad (18)$$

The derivative of function G (15) along the trajectory of the system (17)-(18) is given by

$$\begin{aligned} \dot{G}(z_1, \dot{z}_1, \dots, z_1^{(r)}) &= 2 \left(\sum_{j=0}^r a_j z_1^{(j)} \right) \left(\sum_{j=0}^{r-1} a_j z_1^{(j+1)} \right) \\ &+ 2a_r \left(\sum_{j=0}^r a_j z_1^{(j)} \right) \left(\frac{\partial f(z, \eta)}{\partial t} + \frac{\partial g(z, \eta)}{\partial t} u \right) - \left(\frac{\partial G}{\partial u} \right)^2. \end{aligned} \quad (19)$$

From equation (19), the value of the derivative of function G (15) along the trajectory of the system (17)-(18) can not be guaranteed to be less than zero for $0 \leq t$. For this, the dynamic feedback control in equation (16) will be modified by adding an input ν . Then the extended system (17)-(18) becomes

$$\dot{x} = f_1(x) + f_2(x)u, \quad (20)$$

$$\dot{u} = -2a_r \left(\sum_{j=0}^r a_j z_1^{(j)} \right) \frac{\partial z_1^{(r)}}{\partial u} + \nu. \quad (21)$$

In the same way, the derivative of function G (16) along the trajectory of the system (20)-(21) is given by

$$\begin{aligned} \dot{G}(z_1, \dot{z}_1, \dots, z_1^{(r)}) &= 2\left(\sum_{j=0}^r a_j z_1^{(j)}\right)\left(\sum_{j=0}^{r-1} a_j z_1^{(j+1)}\right) \\ &+ 2a_r\left(\sum_{j=0}^r a_j z_1^{(j)}\right)\left(\frac{\partial f(z, \eta)}{\partial t} + \frac{\partial g(z, \eta)}{\partial t}u\right) - \left(\frac{\partial G}{\partial u}\right)^2 + \frac{\partial G}{\partial u}\nu. \end{aligned} \tag{22}$$

Suppose equation (22) is written as follows:

$$\dot{G}(z_1, \dot{z}_1, \dots, z_1^{(r)}) = \phi(z_1, \dot{z}_1, \dots, z_1^{(r)}) + \frac{\partial G}{\partial u}\nu - \left(\frac{\partial G}{\partial u}\right)^2, \tag{23}$$

where

$$\begin{aligned} \phi(z_1, \dot{z}_1, \dots, z_1^{(r)}) &= 2\left(\sum_{j=0}^r a_j z_1^{(j)}\right)\left(\sum_{j=0}^{r-1} a_j z_1^{(j+1)}\right) \\ &+ 2a_r\left(\sum_{j=0}^r a_j z_1^{(j)}\right)\left(\frac{\partial f(z, \eta)}{\partial t} + \frac{\partial g(z, \eta)}{\partial t}u\right). \end{aligned} \tag{24}$$

If we take

$$\nu = \frac{1}{\frac{\partial G}{\partial u}} \left(-\phi(z_1, \dot{z}_1, \dots, z_1^{(r)})\right), \tag{25}$$

then

$$\dot{G}(z_1, \dot{z}_1, \dots, z_1^{(r)}) = -\left(\frac{\partial G}{\partial u}\right)^2, \tag{26}$$

with $\frac{\partial G}{\partial u} \neq 0$.

Consider the function G (15) and its time derivative (26). Adding the artificial input ν into dynamic controller (16) is used to guarantee the function G (15) will decrease until $\left(\sum_{j=0}^r a_j z_1^{(j)}\right)$ becomes zero. Furthermore, if $\frac{\partial G}{\partial u} = 0$, then we have $2a_r\left(\sum_{j=0}^r a_j z_1^{(j)}\right)\frac{\partial z_1^{(r)}}{\partial u} = 0$. Therefore $\left(\sum_{j=0}^r a_j z_1^{(j)}\right)$ becomes zero if $\frac{\partial z_1^{(r)}}{\partial u} \neq 0$. In this case, the relative degree of the system (1)-(2) is well defined.

Theorem 3.1 Consider system (1)-(2). Let the relative degree of the system (1)-(2) be r , $r \leq n$, with the relative degree of the system (1)-(2) being well defined. Especially if $r < n$ satisfies Assumptions 1. Choose constants a_i such that all the roots of the polynomial

$$p(\lambda) = a_r\lambda^r + a_{r-1}\lambda^{r-1} + \dots + a_1\lambda + a_0 \tag{27}$$

have negative real part. Then, when using the dynamic feedback control

$$\dot{u} = -2a_r\left(\sum_{j=0}^r a_j z_1^{(j)}\right)\frac{\partial z_1^{(r)}}{\partial u} + \nu, \tag{28}$$

with ν as in (25), $y = z_1$ tends to zero as $t \rightarrow \infty$. Furthermore, the system (1) has an asymptotically stable equilibrium at $x = 0$.

Proof. Let the relative degree of the system (1)-(2) be r , $r < n$ satisfies Assumption 1, then the function G becomes bounded if $\frac{\partial G}{\partial u} \neq 0$. From equation (26), then $\dot{G}(z_1, \dot{z}_1, \dots, z_1^{(r)}) < 0$, with $(\sum_{j=0}^r a_j z_1^{(j)}) \neq 0$. Let $(\sum_{j=0}^r a_j z_1^{(j)}) = 0$. From equation (26), $\dot{G}(z_1, \dot{z}_1, \dots, z_1^{(r)}) = 0$. Thus, the function G (15) becomes minimum, where the minimum value is zero. Therefore, if $G(z_1, \dot{z}_1, \dots, z_1^{(r)}) = 0$, then $(\sum_{j=0}^r a_j z_1^{(j)}) = 0$. Furthermore, $\frac{\partial G}{\partial u} = 0$. Because the relative degree of the system (1)-(2) is well defined, then $\frac{\partial z_1^{(r)}}{\partial u} \neq 0, \forall t$. Then $(\sum_{j=0}^r a_j z_1^{(j)}) = 0$. Thus, if we choose $a_j, j = 0, 1, \dots, r$ such that all the roots of polynomial (27) have negative real part, then $y = z_1$ goes to zero as $t \rightarrow \infty$. Furthermore, x goes to zero as $t \rightarrow \infty$. Thus the system (1) has an asymptotically stable equilibrium at $x = 0$.

Example 3.1 Consider the nonlinear system

$$\begin{aligned} \dot{x}_1 &= x_2 + 2x_1^2, \\ \dot{x}_2 &= x_3 + u, \\ \dot{x}_3 &= x_1 + x_3. \end{aligned} \quad (29)$$

If we choose the state $y = x_3$, then the relative degree of the system (29) with respect to x_3 is 3. Thus the system transformation with respect to the state x_3 is

$$\begin{aligned} \dot{z}_1 &= z_2, \\ \dot{z}_2 &= z_3, \\ \dot{z}_3 &= a(z) + u, \end{aligned}$$

where $z_1 = x_3$, $a(z) = z_1 + z_2 + (2(z_2 - z_1) + 1)(z_3 - z_2 - 2)(z_2 - z_1)^2 + 2(z_2 - z_1)^2$. Define a function as follows:

$$G(z_1, \dot{z}_1, \ddot{z}_1, z_1^{(3)}) = \left(\sum_{j=0}^3 a_j (z_1)^{(j)} \right)^2. \quad (30)$$

With the above equation, the dynamic feedback control is

$$\dot{u} = -2a_3 \left(\sum_{j=0}^3 a_j (z_1)^{(j)} \right) + v, \quad (31)$$

with v as in equation (25).

Simulation results are shown in Figs.1a) and 1b) for constants $a_0 = 15$, $a_1 = 23$, $a_2 = 4$, $a_3 = 1$. The initial value $x_1(0) = -1$, $x_2(0) = 1, 5$, $x_3(0) = -1.5$, $u(0) = 10$. In Fig.1a), with the application of the control as in equation (31), the system (29) is asymptotically stable at the equilibrium point $x = (0, 0, 0)$. In Fig.1b), the response curve of the control input is presented.

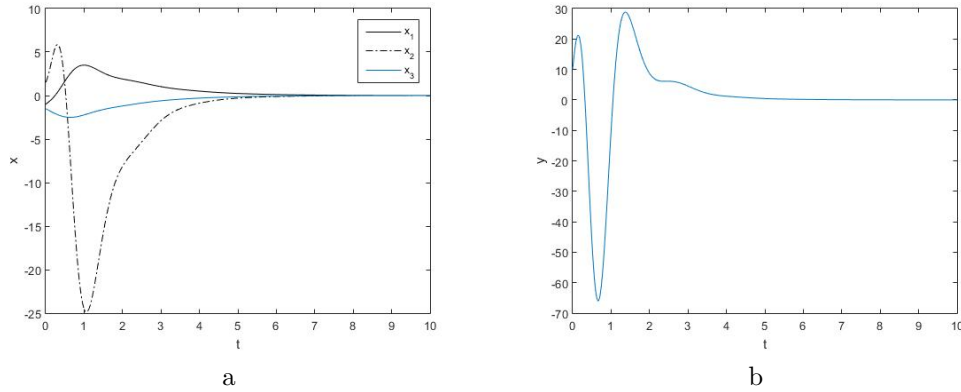


Figure 1: a) the simulation result for Example 3.1, b) the response curve of the input.

Example 3.2 Consider the nonlinear system

$$\begin{aligned}
 \dot{x}_1 &= -x_1 + x_2, \\
 \dot{x}_2 &= 3x_2 + x_1^3 + (2 + \sin^2(x_4)) u, \\
 \dot{x}_3 &= x_1 - 2x_3, \\
 \dot{x}_4 &= -x_4 + x_3^2.
 \end{aligned} \tag{32}$$

If we choose the state $y = x_4$, then the relative degree of the system (29) with respect to x_3 is 4. Thus the system transformation with respect to the state x_3 is

$$\begin{aligned}
 \dot{z}_1 &= z_2, \\
 \dot{z}_2 &= z_3, \\
 \dot{z}_3 &= z_4, \\
 \dot{z}_4 &= a(z) + b(z)u,
 \end{aligned} \tag{33}$$

where $z_1 = x_4$, $b(z) = 2x_3 (2 + \sin^2(x_4))$.

From the system transformation (33), we see that the relative degree of the system (33) with respect to the state $y = x_4$ is not well defined. So the input control as in equation (28) cannot be used to make the state $y = x_4 \rightarrow 0, t \rightarrow \infty$. In this case, the system (32) can not be achieved. The problem is how to choose such a state that the transformation of the system with respect to that state has an asymptotically stable zero dynamic.

Choose the state $y = x_3$. Then the system transformation with respect to the state x_3 is

$$\begin{aligned}
 \dot{z}_1 &= z_2, \\
 \dot{z}_2 &= z_3, \\
 \dot{z}_3 &= a(z, \eta) + b(z, \eta), \\
 \dot{\eta} &= -\eta + x_1^3,
 \end{aligned}$$

where $z_1 = x_3$, $\eta = x_4$, $a(z, \eta) = 6z_1 + 7z_2 + (2z_1 + z_2)^3$, $z_2 = x_1 - 2x_3$, $b(z, \eta) = (2 + \sin^2(\eta))$. So the zero dynamic of the system (29) with respect to the output x_3 is asymptotically stable, with the relative degree of the system being well defined.

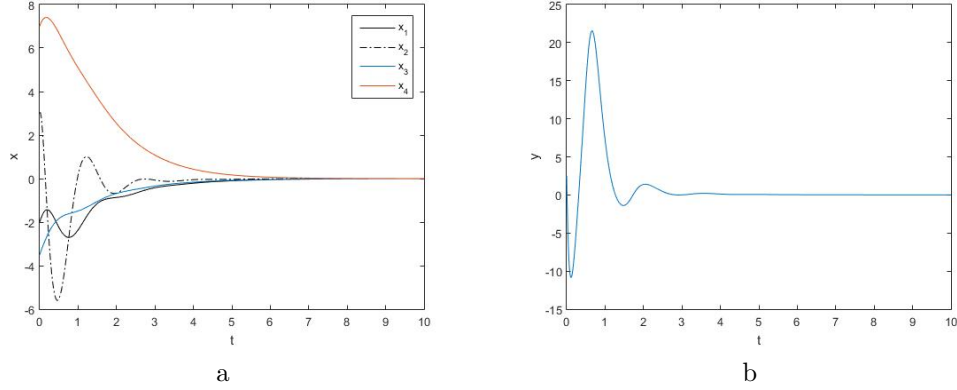


Figure 2: a) the simulation result for Example 3.2, b) the response curve of the input.

Define a function as follows:

$$G(z_1, \dot{z}_1, \ddot{z}_1, z_1^{(3)}) = \left(\sum_{j=0}^3 a_j(z_1)^{(j)} \right)^2. \quad (34)$$

With the above equation, the dynamic feedback control is

$$\dot{u} = (-4 - \sin^2(\eta)) a_3 \left(\sum_{j=0}^3 a_j(z_1)^{(j)} \right) + v, \quad (35)$$

where $v = \frac{1}{2a_3(a_0z_1 + a_1\dot{z}_1 + \dot{z}_2 + a_3\dot{z}_3)(2 + \sin^2(\eta))} (k(z_1, \dot{z}_1, \dot{z}_2, \dot{z}_3))$, with

$$\begin{aligned} (k(z_1, \dot{z}_1, \dot{z}_2, \dot{z}_3)) &= 2 \left(\sum_{j=0}^3 a_j(z_1)^{(j)} \right) \left(\sum_{j=0}^2 a_j(z_1)^{(j+1)} \right) \\ &+ 2a_3 \left(\sum_{j=0}^3 a_j(z_1)^{(j)} \right) \left(\frac{\partial a(z, \eta)}{\partial t} + \frac{\partial b(z, \eta)}{\partial t} u \right). \end{aligned}$$

Simulation results are shown in Figs.2a) and 2b) for constants $a_0 = 15$, $a_1 = 13$, $a_2 = 9$, $a_3 = 1$. Initial value $x_1(0) = -2$, $x_2(0) = 3$, $x_3(0) = -3.5$, $x_4(0) = -7$, $u(0) = 2.5$. In Fig.2a), with the application of the control as in equation (35), the system (32) is asymptotically stable at the equilibrium point $x = (0, 0, 0, 0)$. In Fig.2b), the response curve of the control input is shown.

4 Conclusion

In this paper, we have investigated the asymptotic stability for a class of nonlinear control systems, with the relative degree of the system being well defined. The dynamic feedback control has been designed for asymptotic stability problems. The design of the dynamic feedback control is based on the modification of the trajectory following method. To apply the modification of the trajectory following method, the system will

be transformed through the input state linearization. If the relative degree of the system is smaller than the dimensions of the system, then the requirement to design a dynamic feedback control is that the zero dynamic of the system must be asymptotically stable.

From the results obtained, the modification of the trajectory following method can be an alternative control design for the asymptotic stability, even though its unforced system is not asymptotically stable.

Acknowledgment

The research is supported by PDU-LPPM UNHAS Program 2021.

References

- [1] D. Cheng. Stabilization of a Class of Nonlinear Non-minimum Phase Systems. *Asian Journal of Control* **2** (2) (1996) 132–139.
- [2] Z. Ding. Backstepping Stabilization of Nonlinear Systems with a Non-minimum Phase Zero In: *Proceeding of the 40th IEEE Conference on Decision and Control.*, 2001, 85–87.
- [3] P. Chen, X.Ye and H. Qin. Stabilization of a Class of Non-Minimum Phase Nonlinear Systems by Dynamic Output Feedback. In: *Proceeding of 8th International Conference on Control, Automation, Robotics and Vision.* China, 2004, 1206–1211.
- [4] L. Diao and M. Guay. Output Feedback Stabilization of Uncertain Non-Minimum Phase Nonlinear Systems. In: *American Control Conf.*, 2004, 3671–3676.
- [5] Erkan Kayacan. Sliding Mode Learning Control of Uncertain Nonlinear Systems with Lyapunov Stability Analysis. *Transactions of the Institute of Measurement and Control* **41** (6) (2019) 1750–1760.
- [6] Riccardo Marino and Patrizio Tomei. A Class of Globally Output Feedback Stabilizable Nonlinear Nonminimum Phase Systems. *IEEE Trans. on Automatic Control* **50** (12) (2005) 2097–2101.
- [7] Z. Li, Z. Chen and Z.Dan Yuan. The Stability Analysis and Control of a Class of Non-Minimum Phase Nonlinear Systems. *International Journal of Nonlinear Science* **3** (2) (2007) 103–110.
- [8] N. Wang, W. Xu and F. Chen. Adaptive global output feedback stabilisation of some non-minimum phase nonlinear uncertain systems. *IET Control Theory* **2** (2) (2008) 117–125.
- [9] J.Naiborhu, Firman and K. Mu'tamar. Particle Swarm Optimization in the Exact Linearization Technique for Output Tracking of Non-Minimum Phase Nonlinear Systems. *Applied Mathematical Science* **7** (1) (2013) 5427–5442.
- [10] Firman, J. Naiborhu, Roberd Saragih and W.I. Supto. Output Tracking of Some Class Non-Minimum Phase Nonlinear Uncertain Systems. *Nonlinear Dynamics and Systems Theory* **7** (4) (2017) 347–356.
- [11] Firman, S. Toaha and M. Nur. Asymptotic Stability of Some Class of Affine Nonlinear Control Systems through Partial Feedback Linearization. *Nonlinear Dynamics and Systems Theory* **21** (3) (2021) 238–245.
- [12] J. Naiborhu and K. Shimizu. Direct Gradient Descent Control for Global Stabilization of General Nonlinear Control System. *IEEE Trans. Fundamental* **E83-A** (3) (2000) 516–523.
- [13] A. Isidori. *Nonlinear Control Systems: An Introduction.* Springer, Berlin, Heidelberg, 1989.
- [14] T. L. Vincent and W. J. Grantham. Trajectory Following Methods in Control System Design *J. of Global Optimization* **23** (2002) 267–282.



Direct Torque Control of Three-Phase Induction Motor Powered by Three-Level Indirect Matrix Converter

Ameur Khaldi^{1*}, El Madjid Berkouk¹, Mohand Oulhadj Mahmoudi¹ and
Abdellah Kouzou²

¹ *Process Control Laboratory, National Polytechnic School, Algiers, Algeria.*

² *Laboratory of Applied Automation and Industrial Diagnosis, Faculty of Sciences and
Technology, Djelfa University, Algeria.*

Received: October 6, 2021; Revised: March 29, 2022

Abstract: In this paper, the three-phase induction machine (IM) fed by a three-level indirect matrix converter (IMC3) is proposed and investigated. Indeed, the IMC3 converter consists of a current rectifier connected to a three-level neutral-point-clamped voltage source inverter (NPC-VSI) without a bulky DC link capacitor interface. The rectifier ensures the bidirectional power transfer, where it is controlled by the space vector modulation (SVM) with the aim to obtain nearly a unity input power factor and to improve the input current waveform by the minimization of the harmonics content. On the other hand, the direct torque control (DTC) strategy is used to ensure the control of the three-phase IM, where the appropriate voltage vectors applied on the IM are generated via the control of the NPC-VSI. This combination can benefit from the advantages of the DTC and the IMC3 at the same time, allowing to improve the dynamic performances of the controlled three-phase IM compared to conventional topologies. For the validation of the advantages brought by this combination of the proposed topology of the used converter and the control strategy, simulations tests have been carried out.

Keywords: *direct torque control; induction machine; three-level inverter; space vector modulation; indirect matrix converter.*

Mathematics Subject Classification (2010): 70K70, 70K75, 34H05, 93B52, 93C10.

* Corresponding author: <mailto:khaldi.ameur@gmail.com>

1 Introduction

In the AC drive system, there are several converter topologies. The first family provides AC-DC conversion followed by DC - AC conversion. The main drawback of this converter is the use of a large capacitor on the DC link which has a limited lifetime when compared to the power devices, and increases the volume of the used converter. The second family ensures a direct conversion alternating-alternating (AC/AC). This direct conversion can be achieved either by cycloconverters or by matrix converters. The matrix converter is a recent topology of the frequency converters. This makes it possible to obtain an output voltage with variable amplitude and frequency from a fixed power supply voltage [1]. This can be achieved by the bidirectional current and voltage power switches, which are used in this kind of converters. Indeed, the matrix converter has many advantages such as

- A wide range of output frequency.
- The power factor at the output can vary freely according to the operating point of the load.
- The power factor at the input can be nearly unitary, and it can be imposed by the control.
- The operation in the four quadrants of the voltage-current plane.

However, it has some disadvantages such as

- The switching of current is more difficult due to the absence of the freewheeling diodes.
- The ratio of output-input voltage is reduced to 0.8666.

There are two topologies of matrix converters: the direct matrix converter (DMC) and indirect matrix converter (IMC).

The direct matrix converter (DMC) was first introduced by Gyugyi [2]. It connects directly three inputs to three output phases via nine bidirectional switches where basically the space vector modulation is used to ensure its control [3]. The conventional concept of space vector modulation (SVM), which was used for the control of inverter topologies, has been extended to ensure the control of the matrix converters with the aim to obtain improved input and output currents waveforms of the DMC [4].

In [5], the direct matrix converter is used with the direct torque control where a new switching table has been developed for this control taking into account the input displacement angle as a third control variable. On the other hand, the indirect matrix converter (IMC) scheme was firstly introduced by Huber and Borojevic [6]. It consists of a current rectifier connected to a voltage source inverter without intermediate bulky circuit [7]. The paper [8] investigates the application of the conventional DTC strategy for the induction machine based on the IMC. The classical DTC is based on the control of the inverter stage, where on the rectifier stage it is used to produce the DC bus voltage at the input side of the DC-AC stage, at the same time, it can be also controlled to ensure improved input current waveform and input power factor.

Indeed, to improve the quality of output voltage, the three-level indirect matrix converter (IMC3) was suggested and investigated by the authors in [9]. This topology is composed of a rectifier stage incorporated with a three-level-neutral point clamped voltage source inverter that has the ability to generate three-level voltages at the outputs.

In order to use the NPC VSI with IMC3, the DC voltage provided by the rectifier V_{pn} is subdivided into two voltage levels V_{po} and V_{on} , and the neutral point (o) is connected to the star connected input filter capacitor as shown in Figure 1. To ensure balanced input capacitor voltages, the nearest three virtual space vector modulation (NTV SVM)

approach is used to control the DC-AC stage. This method requires that the sum of the three output phase currents equals zero at any sampling time.

In this paper, the application of a direct torque control based on the IMC3 to ensure the control of the three-phase induction motor is analyzed. It is well known that in the DTC, the generation of the control signals of the voltage source inverter switches depends on the output of the hysteresis comparators and the position of stator flux, which requires high frequency switching in the case of conventional two-level inverters. At the same time, when the conventional two-level inverter is used, the switches are subject to high voltage stress or high current when used in high voltage or high power application, respectively. However, the recent multilevel converter topologies (IMC3) seem to be well suitable for high voltage and high power applications, due to the segmentation of voltages and currents within the relatively high number of switches, hence they allow the use of fast semiconductors (eg. IGBT) where the commutation can be ensured without any risk or impact on the operational safety of the whole system. Based on these main advantages offered by the IMC3 topology and the direct torque control technique, the present paper investigates the use of the DTC with the IMC3 to ensure the control of the three-phase IM. Indeed, the high number of available voltage vectors resulting from the IMC3 and the use of the five-level torque controllers enhance considerably the output signal quality and the drive performances. It can be said initially that this combination of the DTC and IMC3 makes it possible to minimize the harmonics content of the output voltage and current, which have an important effect on the dynamic control of the IM.

The present paper is organized as follows. Section 2 introduces the modeling of induction machine, whereas Section 3 presents the DTC principle. The three-level neutral-point-clamped voltage source inverter is explained in Section 4. In Section 5, the DTC based on the IMC3 is presented, whereas simulation results are presented in the last section for the validation of the proposed control strategy. Finally, a conclusion is presented at the end of the paper.

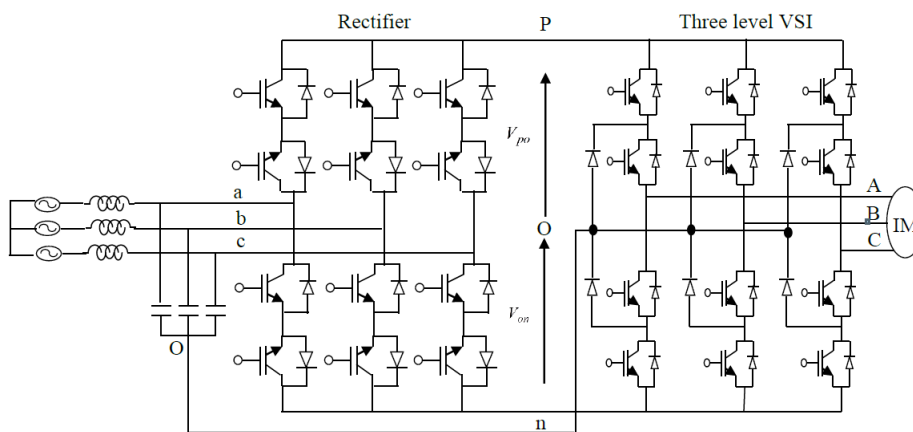


Figure 1: Three-level indirect matrix converter.

2 Modeling of Induction Machine

The induction machine consists of a stator which is connected to the power supply or a variable-speed drive and a short circuited rotor [10]. The model of the induction motor is presented in $(\alpha\beta)$ as follows:

$$V_s = R_s I_s + \frac{d\varphi_s}{dt}, \quad (1)$$

$$V_r = R_r I_r + \frac{d\varphi_r}{dt}. \quad (2)$$

V_s is the stator voltage and V_r is the rotor voltage, I_s is the stator current and I_r is the rotor current. Here

$$\varphi_s = L_s I_s + L_m I_r, \quad (3)$$

$$\varphi_r = L_r I_r + L_m I_s. \quad (4)$$

φ_s is the stator flux and φ_r is the rotor flux, L_s, L_r are the stator and rotor self-inductances, L_m is the mutual inductance.

The electromagnetic torque equation developed by the motor is expressed as follows:

$$T_{em} = \frac{3}{2} p \frac{L_m}{\sigma L_s L_r} \varphi_s \varphi_r \sin \theta, \quad (5)$$

σ is the leakage factor, p is the number of pole pairs and θ is the torque angle.

The equation of motion, connecting the electrical and mechanical parts, is written as follows:

$$j \frac{d\Omega}{dt} = T_{em} - T_r(\Omega). \quad (6)$$

T_{em} and T_r are the electromagnetic torque and the load torque, j is the rotor inertia.

3 Direct Torque Control Principle

The direct torque control (DTC) technique was proposed by Isao Takahashi in 1986 [11]. It consists of a pair of hysteresis controllers, a flux and torque estimators, and a voltage vector selection table. The basic advantages of the DTC scheme are presented as follows:

- High dynamic.
- Robustness.
- Reduced response time.
- Absence of park transformation.

The DTC has also some disadvantages, namely, the control of the torque and the flux at low speed is difficult, the switching frequency is not constant. The last one produces higher current and torque ripple and, consequently, higher machine losses, more noises and mechanical stress, which may reduce the lifespan of the machine. It is well known that the direct torque control (DTC) of an induction machine is based on the "direct" determination of the sequence of the control signal applied to the switches of the used voltage source inverter. This choice is generally based on the use of hysteresis regulators whose function is to control the amplitude of the stator flux and the electromagnetic torque. In Figure 2(a) and Figure 2(b) the schematic circuit of the conventional three-phase two-level voltage source inverter and the voltage vectors corresponding to the eight different possible switching configurations are presented, where two vectors determine the zero voltage vectors V_0 and V_7 .

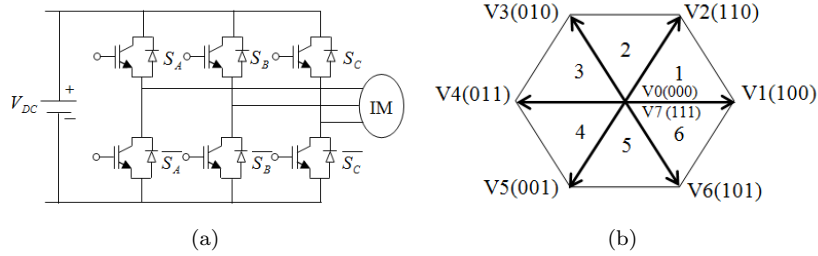


Figure 2: (a) Schematic circuit of voltage source inverter, (b) Switching configurations of voltage vectors.

3.1 Stator flux control

The stator voltage in the stationary reference frame ($\alpha\beta$) of the three-phase IM can be obtained as follows:

$$V_s = R_s I_s + \frac{d\varphi_s}{dt}. \quad (7)$$

Hence, the stator flux can be expressed as

$$\varphi_s = \varphi_{s0} + \int_0^t (V_s - R_s I_s) dt. \quad (8)$$

Neglecting the voltage drop due to the stator resistance, the stator flux can be written as follows:

$$\varphi_s = \varphi_{s0} + \int_0^t (V_s) dt. \quad (9)$$

It can be considered that during a sampling period T_s , which is usually infinitesimal, the voltage vector applied to the IM remains constant, therefore

$$\varphi_s(k+1) = \varphi_s(k) + V_s T_s \rightarrow \Delta\varphi_s \simeq V_s T_s. \quad (10)$$

T_s : Sampling period,

$\varphi_s(k+1)$: Stator flux vector at the next sampling period $(k+1)T_s$,

$\varphi_s(k)$: Stator flux vector at current sampling period kT_s ,

$\Delta\varphi_s$: Flux variation vector ($\varphi_s(k+1) - \varphi_s(k)$).

While the sampling period is fixed, $\Delta\varphi_s$ is proportional to the voltage vector applied to the motor.

From the equation (10), it is clear that the vector flux φ_s can be perfectly controlled by the voltage vector V_s .

3.2 Torque control

The torque equation is expressed as follows:

$$T_{em} = \frac{3}{2} p \frac{L_m}{\sigma L_s L_r} \varphi_s \varphi_r \sin \theta, \quad (11)$$

where θ is the torque angle which represents the shift angle between the flux vectors φ_s and φ_r (relative position of flux vectors).

It is obvious from equation (11) that the torque depends on the flux vectors φ_s and φ_r and on their relative position θ . However, the amplitude of φ_s is kept limited in the hysteresis band around its reference value and the amplitude of φ_r is also approximately constant. Consequently, the electromagnetic torque depends only on the angle (θ), which means that T_{em} increases with the increase of θ , and T_{em} decreases when θ decreases. The error between the reference flux and the estimated flux is introduced into the hysteresis controller which generates a variable C_φ . When $C_\varphi = 1$, it means that the amplitude of the flux should be increased, whereas when $C_\varphi = -1$, it means that the amplitude of the flux should be decreased. On the other hand, the error between the reference torque and the estimated torque is processed by a three-level hysteresis controller which generates the variable C_T which may take three values 1,-1 and 0. When $C_T = 1$, it means that the amplitude should be increased, and when $C_T = -1$, it means that it should be decreased. If $C_T = 0$, then it should be kept constant. Table 1. shows the different voltage vectors to be applied in order to maintain the stator flux and the electromagnetic torque inside their hysteresis bands.

C_φ	1	1	1	-1	-1	-1
C_T	1	0	-1	1	0	-1
$S(1)$	V_2	V_7	V_6	V_3	V_0	V_5
$S(2)$	V_3	V_0	V_1	V_4	V_7	V_6
$S(3)$	V_4	V_7	V_2	V_5	V_0	V_1
$S(4)$	V_5	V_0	V_3	V_6	V_7	V_2
$S(5)$	V_6	V_7	V_4	V_1	V_0	V_3
$S(6)$	V_1	V_0	V_5	V_2	V_7	V_4

Table 1: The basic DTC switching table using VSI.

As an example, if the stator flux vector is in the first sector, the voltage vectors V_2 and V_6 can be applied to increase the flux, whereas, the vectors V_3 and V_5 can be selected to decrease the flux. On the other hand, within the same sector, the vectors V_2 and V_3 can be used to increase the torque and the vectors V_5 and V_6 can be applied to decrease the torque. A general block diagram of the DTC scheme is presented in Figure 3.

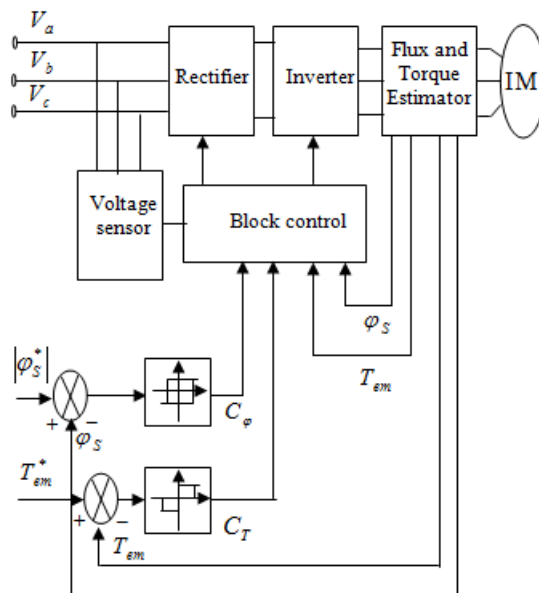


Figure 3: Block diagram of the DTC.

4 Three-Level Neutral-Point-Clamped Voltage Source Inverter

The neutral-point-clamped (NPC) inverter has many advantages [12, 13]. The voltage across each semiconductor is halved, which reduces the voltage stress, the harmonic content of the output voltages is diminished compared to the conventional two-level inverter. However, the capacitor voltage unbalance at the input side of the inverter increases the voltage stresses on the semiconductors and leads to the distortion of the output voltage [14, 15]. Furthermore, they may be subject to the voltage unbalance, which causes the unbalance of the three-phase output voltages. In this topology, in each phase/leg, there are 4 switching devices and 6 diodes that allow performing a combination of 27 switching states (Figure 4(a)).

It is obvious that the switching states can be presented by space voltage vectors. This representation is illustrated in Figure 4(b).

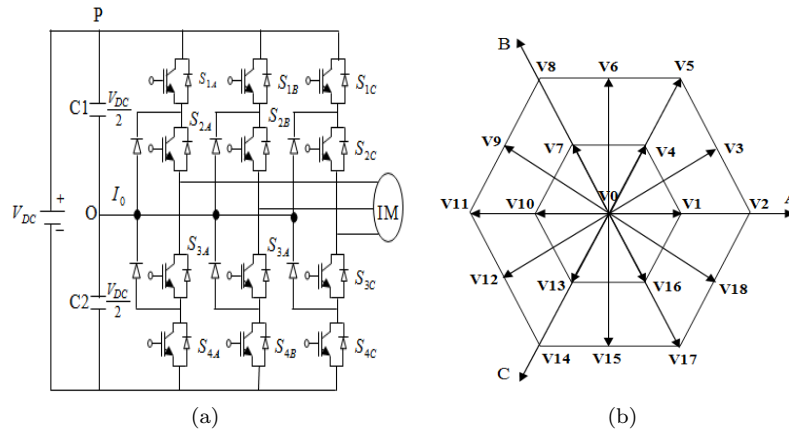


Figure 4: (a) Three-level neutral-point-clamped voltage source inverter, (b) Space vector diagram of three-level inverter.

According to the possible switching states that may be achieved for each leg following the combination presented in Table 2, it is clear that there are three possible voltage levels: $\frac{V_{DC}}{2}$, 0 , $-\frac{V_{DC}}{2}$. These values justify the ability of the presented topology to generate three-level outputs voltage. The space voltage vectors can be divided into four groups:

S_{1x}	S_{2x}	S_{3x}	S_{4x}	$V_{x0} : x \in \{A, B, C\}$	Switching states
ON	ON	OFF	OFF	$\frac{V_{DC}}{2}$	P
OFF	ON	ON	OFF	0	0
OFF	OFF	ON	ON	$-\frac{V_{DC}}{2}$	N

Table 2: The switch combination of three-level NPC VSI.

the zero vectors group, the small vectors group, the medium vectors group and the large vectors group as shown in Figure 4(b) [16].

5 DTC Based on Three-Level Indirect Matrix Converter

The three-level indirect matrix converter consists of a current rectifier connected to a three-level neutral-point-clamped voltage source inverter. The rectification stage has nine allowed combinations, it is formed by a six bidirectional switches so that the three-level indirect matrix converter can operate in the four quadrants. In this stage, the positive input voltage is connected to the p-terminal and the negative input voltage is connected to the n-terminal of the DC bus to generate the DC link voltage at the input side of the inverter stage. The NPC-VSI has nineteen voltage vectors describing 27 possible switching states, where three switching states among them produce the zero vector. This zero vector allows avoiding the DC bus short circuit and the open circuits in the case of inductive load which is the case of the IM. The other vectors are divided into three groups such as the large vectors (six vectors corresponding to six switching

states), medium vectors (six vectors corresponding to six switching states) and small vectors (six double vectors corresponding to twelve switching states). All of these vectors (large, medium, small and zero) are exploited to improve the control of the three-phase IM performances. As aforementioned, in this paper the advantages of the DTC and the IMC3 are combined to improve the performances of the control of the three-phase IM such as the response time, the precision of the developed torque and allowing the operation in the four quadrants of the torque-speed plane. Thus, a switching table is issued based on this combination which allows the generation of the appropriate vectors to be applied to the induction machine via the NPC-VSI [17].

5.1 The rectifier side control

In the rectification stage, only the two largest line-to-line input voltages in every sector are used. For example, in the first sector, the two maximum voltages u_{ac} and u_{ab} are considered as the supply for the inverter stage. The rectifier stage is controlled by a traditional space vector modulation. This method is based on [18]:

- the determination of the sector where the current or voltage reference is located;
- the application of the nearest vectors;
- the calculation of the corresponding duty cycles.

The input voltage vector can be represented as follows:

$$V_i = \frac{2}{3}(V_a + aV_b + a^2V_c), \quad (12)$$

where $a = e^{j\frac{2\pi}{3}}$, V_i is the input voltage vector, V_a, V_b and V_c are the three phase-input voltages. The reference input current space vector can be represented as follows:

$$\bar{I}_{in} = I_{im}e^{(j\omega_i - \varphi_i)} = I_{im}\angle\theta_i, \quad (13)$$

I_{im} is the magnitude of the reference vector, ω_i is the angle of the input voltages, φ_i is the displacement angle between the fundamental of input current phase and the corresponding line-to-neutral voltage, $\theta_i = \omega_i - \varphi_i$ is the direction of reference vector.

There are six active current space vectors, as shown in Figure 5(a). Each one represents the connection of the input phase voltages to the terminals of the DC-link. For example, the current $I_5 = (c, b)$ vector represents the connection of the input phase voltage V_c to the p-terminal and V_b to the n-terminal. The reference current vector can be synthesized with the two adjacent vectors (I_v, I_u) as shown in Figure 5(b).

The corresponding duty cycles are

$$d_u = \frac{T_u}{T_s} = m_R \sin\left(\frac{\pi}{3} - \theta_i\right), \quad (14)$$

$$d_v = \frac{T_v}{T_s} = m_R \sin(\theta_i), \quad (15)$$

$$d_0 = \frac{T_0}{T_s} = 1 - d_u - d_v. \quad (16)$$

The zero current vector cannot be used, so the duty cycles of rectification stage are adjusted as follows:

$$d_u^R = \frac{d_u}{d_u + d_v}, \quad (17)$$

$$d_v^R = \frac{d_v}{d_v + d_u}. \quad (18)$$

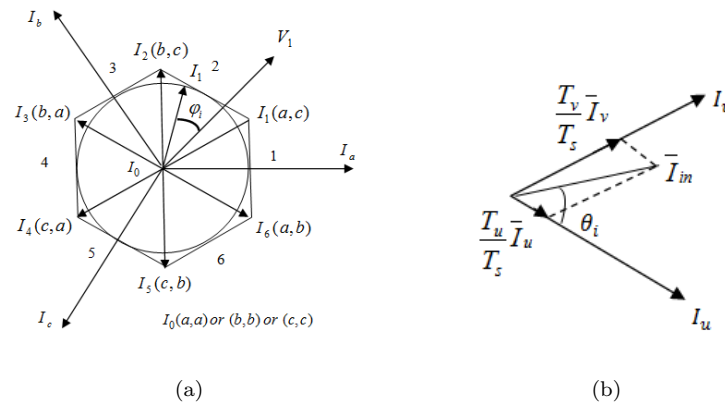


Figure 5: (a) Input voltage and current vectors, (b) Generation of the reference input current.

5.2 The three-level inverter side control

The three-level inverter of the IMC3 ensures more control flexibility by offering several choices for the selection of the voltage vector under the direct torque control. Indeed, a switching table of the control structure makes it possible to select the appropriate voltage vector at each sampling instant according to the state of the flux and torque comparators and the sector where the stator flux vector is located [19–22]. The chosen vector should satisfy the requirement of the torque and the flux, and limits ΔV voltage to $\frac{V_{DC}}{2}$.

For instance, suppose that the stator flux is located in the first sector, and the currently used voltage vector is V_2 . To increase the torque and the flux, V_5 should be selected. In this case, a high $\frac{\Delta V}{dt}$ is applied on the semiconductor of the phase B, which should be avoided. However, this problem can be resolved by inserting a medium voltage vectors, which leads to reducing considerably the voltage stress across these devices. The position of the stator flux can be calculated as follows:

$$\theta_s = \arctan \frac{\varphi_{\beta s}}{\varphi_{\alpha s}}, \tag{19}$$

$\varphi_{\alpha s}$ and $\varphi_{\beta s}$ are the components of the stator flux in $\alpha\beta$ reference axes.

The reference torque can be obtained at the output of a PI which receives at its input the speed which presents the difference between the reference speed and the machine rotor speed. This reference torque is compared with the estimated value, and the error is processed using five-level hysteresis comparator which allows minimizing the torque ripples and improving the dynamic behavior of the electromagnetic torque developed by the machine.

The error ($\varepsilon_T = T_{em}^* - T_{em}$) belongs to one of the five regions fixed by the following constraints:

- $C_T = +2$ for ($\varepsilon_{Tmax2} < \varepsilon_T$) high increase,
- $C_T = +1$ for ($\varepsilon_{Tmax1} < \varepsilon_T < \varepsilon_{Tmax2}$) small increase,
- $C_T = 0$ for ($\varepsilon_{Tmin1} < \varepsilon_T < \varepsilon_{Tmax1}$) maintaining,
- $C_T = -1$ for ($\varepsilon_{Tmin2} < \varepsilon_T < \varepsilon_{Tmin1}$) small decrease,
- $C_T = -2$ for ($\varepsilon_T < \varepsilon_{Tmin2}$) high decrease,

$$\varepsilon_{T_{max2}} = 0.1, \varepsilon_{T_{min2}} = -0.1, \varepsilon_{T_{max1}} = 0.04, \varepsilon_{T_{min1}} = -0.04.$$

The estimated flux is compared with its reference value and the error is introduced to a three-level hysteresis controller. The error ($\varepsilon_\varphi = \varphi_s^* - \varphi_s$) is located in one of three regions defined by the following constraints:

$$\begin{aligned} C_\varphi &= +1 \text{ for } \varepsilon_\varphi > \varepsilon_{\varphi_{max}}, \\ C_\varphi &= 0 \text{ for } \varepsilon_{\varphi_{min}} > \varepsilon_\varphi > \varepsilon_{\varphi_{max}}, \\ C_\varphi &= -1 \text{ for } \varepsilon_\varphi < \varepsilon_{\varphi_{min}}, \\ \varepsilon_{\varphi_{max}} &= 0.001, \varepsilon_{\varphi_{min}} = -0.001. \end{aligned}$$

The three-level torque controller and the five-level flux controller are shown in Figure 6(a) and Figure 6(b) According to the flux and torque errors and the position of the

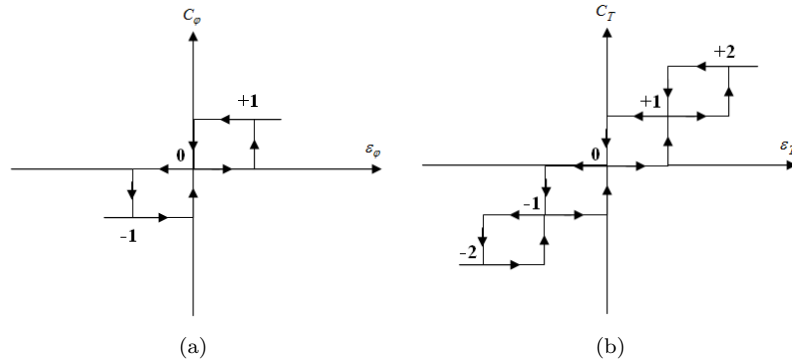


Figure 6: (a) Flux hysteresis comparator, (b) Torque hysteresis comparator.

stator flux, an appropriate voltage vector from the 19 vectors generated by the NPC inverter is selected to maintain the flux and torque within the limits of hysteresis bands. Assume that the stator flux is located in the first sector to increase the flux.

For a large increase of the torque, the vector V_5 is used to diminish the torque and the flux errors. During one T_s , φ_s advances by the angle (δ_1) from its last position and therefore, the corresponding angular speed (ω_{s1}) is expressed as follows (Figure 7(a)) :

$\omega_{s1} = \frac{\delta_1}{T_s}$. Consequently, the new formed angle between the stator and rotor flux becomes equal to $\theta + \delta_1$, which results in a large increase of the torque compared to its last value, whereas the rotor flux continues rotating by (ω_{s1}). For a small increase of the torque, the vector V_3 is applied. The stator flux advances by angle δ_2 , regarding that $\delta_2 < \delta_1$. The angular speed (ω_{s2}) is given as follows (Figure 7(b)): $\omega_{s2} = \frac{\delta_2}{T_s} < \omega_{s1}$.

The rotation speed of the stator flux is reduced compared to its previous value. This leads to reducing the angle between φ_s and φ_r , which therefore leads to a small increase of the torque [23–27]. A voltage vector is generated (Table 3) depending on the position of the stator flux and the output of the two comparators.

6 Simulation Results

For the validation of the application of the proposed control on the three-level indirect matrix converter topology driving a three-phase induction motor, two simulation tests

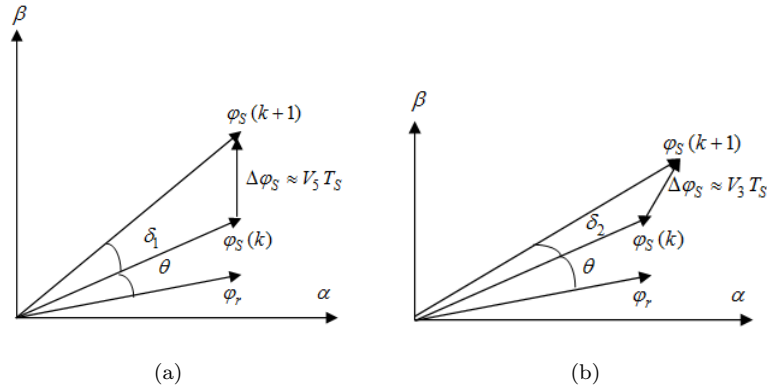


Figure 7: (a),(b) Evolution of the flux vector in the $\alpha\beta$ plane.

C_φ	C_T	$S(1)$	$S(2)$	$S(3)$	$S(4)$	$S(5)$	$S(6)$
+1	+2	V_5	V_8	V_{11}	V_{14}	V_{17}	V_2
+1	+1	V_3	V_6	V_9	V_{12}	V_{15}	V_{18}
+1	0	V_0	V_0	V_0	V_0	V_0	V_0
+1	-1	V_{18}	V_3	V_6	V_9	V_{12}	V_{15}
+1	-2	V_{17}	V_2	V_5	V_8	V_{11}	V_{14}
0	+2	V_4	V_7	V_{10}	V_{13}	V_{16}	V_1
0	+1	V_4	V_7	V_{10}	V_{13}	V_{16}	V_1
0	0	V_0	V_0	V_0	V_0	V_0	V_0
0	-1	V_0	V_0	V_0	V_0	V_0	V_0
0	-2	V_{13}	V_{16}	V_1	V_4	V_7	V_{10}
-1	+2	V_8	V_{11}	V_{14}	V_{17}	V_2	V_5
-1	+1	V_9	V_{12}	V_{15}	V_{18}	V_3	V_6
-1	0	V_0	V_0	V_0	V_0	V_0	V_0
-1	-1	V_{12}	V_{15}	V_{18}	V_3	V_6	V_9
-1	-2	V_{14}	V_{17}	V_2	V_5	V_8	V_{11}

Table 3: The basic DTC switching table using VSI.

have been carried out under normal speed with sudden rotation reversal and under low speed with sudden rotation reversal. The input of the matrix converter is connected to three-phase 220V, 50HZ power supply and the induction motor to be controlled is of power 1.5kW and its parameters are presented in Table 4.

6.1 Scenario 1

In this scenario, the profile of the reference speed is presented in Figure 8(a), where the speed is the same for the forward and backward rotation with a value of 100 rad/s and -100 rad/s, respectively. It can be seen clearly that the motor follows the reference profile precisely without any kind of overshoot after short transient durations along the start-up and the sudden rotations reversal, which last 0.32s and 0.40s, respectively, as

Rated power	1.5 kw
Rated current	3.7 A
Rated speed	1420 r/m
Rated Torque	10 N.m
Number of pole pairs	2
Stator resistance	4.85 Ω
Rotor resistance	3.805 Ω
Stator self inductance	0.274 H
Rotor self inductance	0.274 H
Mutual inductance	0.285 H
Rotor inertia	0.031kg.m ²
Friction coefficient	0.001136N.m.s/rd

Table 4: The induction machine parameters.

shown in Figure 8(a). Indeed, the mismatch between the reference speed and the motor rotor speed at steady state is nearly neglected, which proves that the applied control on the studied topology fulfills the requirements of the speed imposed at relatively normal speed values. On the other hand, to check the robustness of the speed control under torque load changes, a load torque is applied into two intervals of $t \in [0.6s, 0.9s]$ and $t \in [2s, 2.2s]$ with a value of 5N.m and -5N.m, respectively. It can be seen clearly that the changes of the load torque have no impact on the speed where it remains equal to the reference speed, which proves the robustness of the applied control on the studied topology in terms of load torque variation within the rated values of the motor.

Figure 8(b) represents the dynamic response of the electromagnetic torque developed by the motor T_{em} to ensure the dynamics of the motor imposed by the speed profile and the applied load torque. It can be noted that during the startup step at no load, the motor operates at the acceleration mode to reach the imposed reference speed, and therefore, T_{em} should behave accordingly where it takes the value of 10N.m to ensure a fast passage of such mode, whereas when the rotor speed reaches the reference speed at $t = 0.32s$, T_{em} falls to the value of 0.11N.m, which is equal to the value of torque resulting from the motor friction. When the load torque $T_L = 5N.m$ is applied to the induction machine shaft during the time interval $t \in [0.6s, 0.9s]$, the T_{em} is changed accordingly to be equal to the load torque. The zoom window taken at this time interval proves clearly the high dynamics of T_{em} as shown in Figure 8(b), where its average value is slightly greater than the load torque, this is due to the fact that the resulting friction torque aforementioned is added to the load torque. The same dynamics behavior of the T_{em} can be observed in the zoom window within the time interval $t \in [2s, 2.2s]$ when the motor is running in the backward direction with the same speed of -100 rad/s and the load torque $T_L = -5N.m$ as shown in Figure 8(b). It is worthy to clarify the high dynamics of the used control during the rotation reversal of the machine at time 1.3s, where the electromagnetic torque increases promptly to -10N.m in the inverse direction to ensure the inversion of the rotor speed which is achieved nearly within 0.4s passing through the deceleration mode during $t \in [1.2s, 1.4s]$ and the acceleration mode in the backward direction during $t \in [1.4s, 1.6s]$. As the rotor speed of the machine reaches the reference speed -100 rad/s, the electromagnetic torque is set back to be equal to

the resulting machine friction torque as shown in Figure 8(b). Based on the whole observation of Figures 8(a) and 8(b), it can be said that the used control with the used inverter topology allow ensuring a high dynamics performance control of the machine with an accurate tracking of the reference speed and the load torque variations.

Figure 8(c) shows the stator flux which tracks the reference flux with a neglected deviation of 0.1% , where it keeps its value constant with a very neglected ripples along the variation of the speed and the load torque as it can be seen in the zoom windows taken at different intervals. Whereas the flux in the $(\alpha\beta)$ frame is shown in Figure 8(d), it presents a circle with a very tiny thickness.

The stator currents in the three phases are shown in Figure 8(e). Without taking into account the very short transient periods at different stage of start-up and speed reversal, it can be observed clearly within the zoom windows that the current is balanced under no-load and load torque application in both speed directions, where the measured currents are 1.48 A and 2.26 A, respectively. On the other hand, despite the output voltages of the matrix converter which are applied to the terminals of the machine, the currents absorbed by the machine possess sine waveform with neglected ripples as shown clearly within the zoom windows of Figure 8(e).

Figure 8(f) shows the DC-link voltage. It is obvious that it presents important fluctuations around its average value of 475 V. The zoom windows taken at four regions with a width corresponding to the power supply period of 0.02 s, demonstrate that the DC-link voltage fluctuates with a frequency which equals six times the frequency of the input voltage and its amplitude is limited within the range of 540 V and 310 V.

Figure 8(g) shows the IMC3 input current of phase “a”, where it can be noted in each zoomed window at different intervals of time that this current is rich in harmonics and can be a source of pollution to the power supply. Therefore, a passive LC low pass filter is inserted between the source and the IMC3 input to reduce the harmonics content and to overcome this major problem. The resulting current at the power supply side of phase “a” is depicted in Figure 8(h), it can be seen clearly within the zoomed window in this figure that the power supply current has nearly a sine waveform, furthermore, the shift phase with the power supply voltage is zero, which means a nearly power factor is ensured. Therein, the zoomed window is within the interval of time $[1.2s, 1.8s]$ that presents the step of speed reverse, where the motor works into quadrant II and quadrant III. Indeed, in the quadrant II, the mode of operation is referred to the breaking of the motor to reach the zero speed, which means that the power absorbed from the source decreases and transfer of power is directed from the motor to the DC-link. Whereas, when the motor starts changing its speed, it works in the quadrant III and the power is transferred from the power supply to the motor, hence the current increases till it reaches the required value which is corresponding to the steady state speed. Based on the obtained simulation results, it can be concluded that the proposed control with the proposed topology of the IMC3 can ensure sufficient dynamics for the control of the speed of the motor under different aforementioned operation modes. It is also worthy to mention that the use of the multi-level IMC allows obtaining better flexibility of the control and avoiding the bulky topology of the conventional two-stage three-level inverter and its intermediate DC-link.

6.2 Scenario 2

In this scenario, the profile of the reference speed is presented in Figure 9(a). The motor operates along three modes. The first mode is the forward mode at low speed

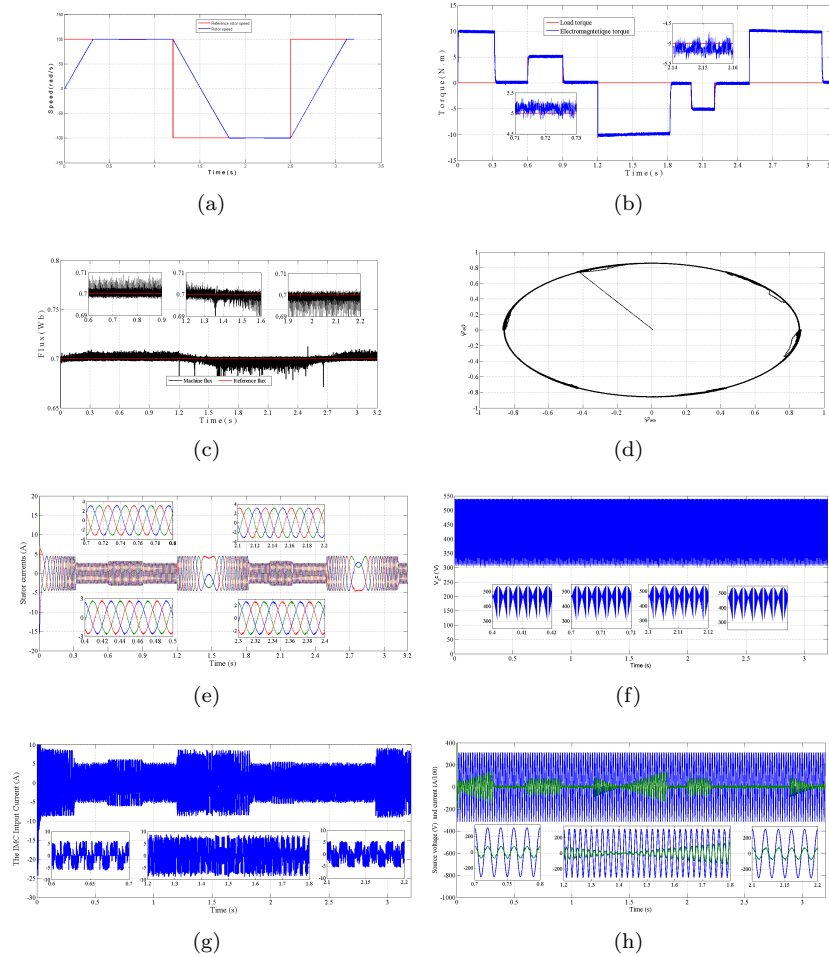


Figure 8: (a) The rotor speed of the controlled machine and the imposed reference speed, (b) The electromagnetic torque of the motor and the applied load torque, (c) The stator flux and the reference flux, (d) The stator flux in the $(\alpha\beta)$ frame, (e) The stator currents, (f) The virtual DC-link between the rectifier stage and the three-level inverter stage in the used indirect matrix converter, (g) The input current of the IMC at phase “a”, (h) The current and the voltage of phase “a” at the source side.

$t \in [0s, 1.2s]$, where the motor starts up from zero speed to reach its steady value of 30 rad/s. The second mode is the backward mode at low speed $t \in [1.2s, 2.5s]$, where the rotor speed is reversed to reach the steady value of -30 rad/s. The last mode is the forward mode at high speed $t \in [2.5s, 4s]$, where the rotor speed is reversed once more to reach the speed value of 100 rad/s. It can be noted clearly within the three steps of speed changes that the motor follows the reference profile precisely without any kind of overshoot after short transient durations along the start-up and the two sudden rotation reversals, which last 0.1s, 0.2s and 0.5s, respectively, as shown in Figure 9(a). On the other hand, a load torque is applied within two intervals of $t \in [0.6s, 0.9s]$ and

$t \in [2s, 2.2s]$ with a value of 5N.m and -5N.m, respectively, as shown in Figure 9(b). It can be noted that during the startup step at no load in the first mode and during the speed reversal in the third mode, the T_{em} takes the value of 10N.m to ensure a fast passage to the steady speed, whereas when the rotor speed reaches the reference speed, T_{em} falls to the value of the 0.034N.m, which is equal to the value of torque resulting from the motor friction. On the contrary, when the motor runs at steady speed in the two first modes, T_{em} is equal to the applied load torque during the time interval $t \in [0.6s, 0.9s]$ and $t \in [2s, 2.2s]$ as shown in Figure 9(b). It is also observed that the electromagnetic torque increases according to the speeds changes to ensure the rapid tracking of the reference speed as shown in the different transition steps of the speed reference. Figure 9(c) shows the stator flux, where it is equal to the reference flux 0.7Wb with limited ripples. It can be seen clearly that when the speed is high, more ripples are observed, which is related to the increase of harmonics components magnitudes within the tolerable range. On the other hand, the motor currents change according to the transition steps and the applied load. It behaves similarly as in the first scenario, however the increase of current during the transition steps is less, as shown in Figure 9(d). The virtual DC-link voltage also behaves in the same way as in the first scenario with the same characteristics as shown in Figure 9(e). The source currents from the input side of the IMC3 before the filter have nearly a sine waveform and are in phase with the power supply voltage as it can be noticed for the phase “a” in Figure 9(f).

It can be concluded that the application of the DTC with the topology of three-level IMC can ensure improved performance dynamics for the control of the induction machine within a wide range of speed variation.

Based on the obtained results from the both investigated scenarios, it can be said that the presented topology of the three-level matrix converter presents better performance compared to the conventional two-level inverters, which are commonly used in many industrial applications. Indeed, the dynamic responses of the induction motor towards the variation of the load at nominal and low speed prove the improved reliability and the accuracy of the applied control technique with the aforementioned converter topology for ensuring the dynamic behavior of the induction motor. On the other hand, the used converter allows to provide a current with low harmonics content, which means low ripples in the developed torque, and hence less mechanical stresses are applied on the motor. At the same time, it is always possible to perform the control of the converter to meet the requirements of the quality of the input current, which is a major drawback within the conventional converter topologies, where the absorbed harmonics from the power source are minimized and their effect is limited. It is worthy to mention that based on the carried control, the input power factor is nearly equal to the unit, which means high efficiency of the whole system can be achieved.

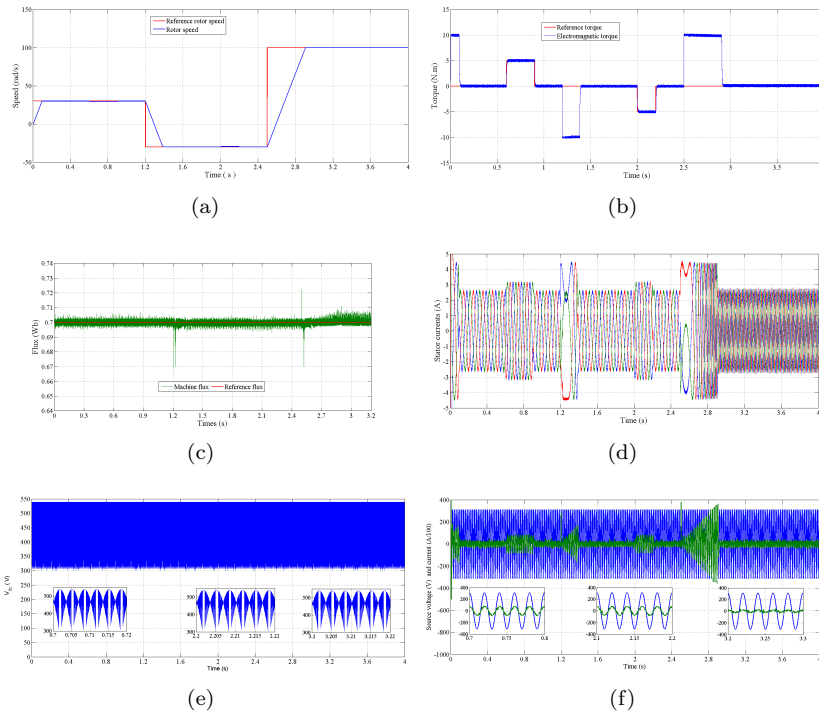


Figure 9: (a) The rotor speed of the controlled machine and the imposed reference speed, (b) The electromagnetic torque of the motor and the applied load torque, (c) The stator flux and the reference flux, (d) The stator currents, (e) The virtual DC-link between the rectifier stage and the three-level inverter stage in the used indirect matrix converter, (f) current and the voltage of phase “a” at the source side.

7 Conclusion

In this paper, the direct torque control (DTC) technique is applied for the control of a three-phase induction machine within a wide speed range variation based on the use of a three-level indirect matrix converter (IMC3). The main aim of using the IMC3 under DTC technique is to ensure improved advantages compared to the conventional conversion topologies such as ensuring small size, eliminating the bulky DC-link, improving the output form, controlling the input current wave for controlling the input power factor, reducing the rate of $\frac{dV}{dt}$ at the used switches, and ensuring a fast and accurate torque response. Indeed, due to the large number of voltage vectors that can be generated by IMC3, the use of the IMC3 allows elaborating a switching table for the selection of the appropriate vectors to be applied to the induction machine to ensure the regulation of the stator flux and the electromagnetic torque with high performance, to improve the output current waveform to guarantee nearly sine waveform of the input current with unity power factor and to operate within a wide range of speed variation without deficiency. Based on the obtained simulation results, it can be said the application of the three-level indirect matrix converter for driving the three-phase induction motor can provide improved dynamic and static performances under an appropriate control technique such as

the DTC, in terms of dynamic responses, quality of input and output currents, range of speed variation, less ripples of torque, which lead to less vibrations and less mechanical constraints, less size and less costs.

References

- [1] L. Neft and C. D. Shauder. Theory and design of a 30-hp matrix converter. In: *Conference Record. IEEE Industry Applications Society Annual Meeting* (October 1988) 934–939.
- [2] B. Gyugyi and Pelly. *Static Power Frequency Changer Theory. Performance and Application*. New York, Wiley–Interscience, 1976.
- [3] D. Casadei, G. Grandi, G. Serra, and A. Tani. Space vector control of matrix converters with unity input power factor and sinusoidal input/ output waveforms. In: *European Conference on Power Electronics and Applications. IET* (1993) 170–175.
- [4] L. Huber and D. Borojevic. Space vector modulator for forced commutated cycloconverters. In: *Conference Record of the IEEE Industry Applications Society Annual Meeting*, (October 1989) 871–876.
- [5] D. Casadei, G. Serra and A. Tani. The Use of Matrix Converters in Direct Torque Control of Induction Machines. *IEEE Transactions on Industrial Electronics* **48** (6) (2001) 1057–1064.
- [6] L. Huber and D. Borojevic. Space Vector Modulated Three Phase To Three Phase Matrix Converter With Input Power Factor Correction. *IEEE Transactions on Industry Applications* **31** (6) (1995) 1234–1246.
- [7] L. Huber, D. Borojevic. Space vector modulation with unity input power factor for forced commutated cycloconverters. In: *Conference Record of the IEEE Industry Applications Society Annual Meeting*, (1991) 1032–1041.
- [8] X. Chen and M. Kazerani. A New Direct Torque Control Strategy for Induction Machine Based on Indirect Matrix Converter. *IEEE International Symposium on Industrial Electronics* **3** (2006) 2479–2484.
- [9] MY. Lee, P. Wheeler and C. Klumpner. *new modulation method for the three-level-output-stage matrix converter. IEEE Power Conversion Conference* (2007) 776–783.
- [10] G. R. Slemon. Modeling of induction machines for electric drives. *IEEE Trans. Ind. Appl.* **25** (6) (1989) 1126–1131.
- [11] I. Takahashi and T. Noguchi. A new quick-response and high-efficiency control strategy of an induction motor. *IEEE Trans Ind Appl.* (1986) 820–827.
- [12] N. Celanovic and D. Boroyevich. A comprehensive study of neutral-point voltage balancing problem in three level neutral-point-clamped voltage source PWM inverters. *IEEE Applied Power Electronics Conference* (1999).
- [13] C. Yiqiang, M. Bakari, W. Zbigniew and O. Boontek. Regulating and equalizing DC capacitance voltages in multilevel statcom. *IEEE Trans. on Power Delivery* (1997) 901–907.
- [14] Jih-Sheng Lai and Fang Zheng Peng. Multilevel converters-a new breed of power converters. *IEEE Trans. Ind. Appl.* (1996) 509–517.
- [15] A. Nabae, I. Takahashi and H. Akagi. A new neutral-point clamped PWM inverter. *IEEE Trans. Ind. Appl.* (1981) 518–523.
- [16] C. Ui-Min and L. Kyo-Beum. Space vector modulation strategy for neutral-point voltage balancing in three-level inverter systems. *IET Power Electronics* (2013) 1390–1398.

- [17] B. Chikondra, M. R. Utkal and B. K. Ranjan . Fault-tolerant dtc technique for five-phase three-level npc inverter-fed induction motor drive with an open-phase fault. *IEEE Energy Conversion Congress and Exposition (ECCE)*. IEEE (2019).
- [18] H. S. Purnama, HendrilSatrian, T. Sutikno and M. Facta. Modulation Strategies for Indirect Matrix Converter: Complexity, Quality and Performance. *5th International Conference on Electrical Engineering, Computer Science and Informatics (EECSI)*. IEEE (2018).
- [19] I. Messsaif, E. M. Berkouk and N. Saadia. Ripple reduction in DTC drives by using a three-level NPC VSI. *IEEE Trans. Ind. Appl.* (2007) 1179—1182.
- [20] R. Zaimedidine, E. M. Berkouk, L. Refoufi and M. Bousalah. scheme of EDTC control using a three-level voltage source inverter for an induction motor. *The IEEE International Symposium on Industrial Electronics*. Vigo, Spain, 2007, 2250–2255.
- [21] M. Bermudez, I. G. Prieto, F. Barrero, H. Guzman, M. J. Duran and X. Kestelyn. Open-phase fault-tolerant direct torque control technique for five-phase induction motor drives. *IEEE Tran. on Ind. Electron.* **64** (2) (2017) 902–911.
- [22] B. Ch, U. R. Muduli and R. K. Behera. Performance comparison of five-phase three-level npc to five-phase two-level voltage source inverter. In: *IEEE International Conference on Power Electronics, Drives and Energy Systems (PEDES)*, (December 2018) 1–6.
- [23] S. Payami, R. K. Behera and A. Iqbal. Dtc of three-level npcinverterfed five-phase induction motor drive with novel neutral point voltage balancing scheme. *IEEE Trans. on Power Electronics* **33** (2) (2018) 1487—1500.
- [24] J. K. Pandit, M. V. Aware, R. V. Nemade and E. Levi. Direct Torque Control Scheme for a Six-Phase Induction Motor With Reduced Torque Ripple. *IEEE Trans. on Power Electronics* **32** (9) (2016) 7118–7129.
- [25] I. M. Alsofyani and N. R. N. Idris. Simple Flux Regulation for Improving State Estimation at Very Low and Zero Speed of a Speed Sensorless Direct Torque Control of an Induction Motor. *IEEE Trans. on Power Electronics* **31** (4) (2015) 3027–3035.
- [26] B. Chikondra, U. R. Muduli and R. Kumar Behera. Fault-Tolerant DTC Technique for Five-phase Three-Level NPC Inverter-fed Induction Motor Drive with an Open-Phase Fault. *IEEE Energy Conversion Congress and Exposition (ECCE)* (2019) 5281–5287.
- [27] P. Naganathan, S. Srinivas, and H. Ittamveettil. Five-level torque controller-based DTC method for a cascaded three-level inverter fed induction motor drive. *IET Power Electronics* (2017) 1223—1230.



On the Existence of Periodic Solutions of a Degenerate Parabolic Reaction-Diffusion Model

Amer Mesbahi¹ and Salim Mesbahi^{2*}

¹ LIM Laboratory, Department of Mathematics and Computer Science, Faculty of Sciences and Technology, Mohamed-Cherif Messaidia University, Souk Ahras, Algeria.

² LMFN Laboratory, Department of Mathematics, Faculty of Sciences, Ferhat Abbas University, Setif, Algeria.

Received: July 30, 2021; Revised: February 23, 2022

Abstract: The aim of this paper is to study a degenerate parabolic reaction-diffusion model with nonlinear boundary conditions. Its specificity lies in the introduction of degenerate diffusion. We prove the existence of maximal and minimal periodic solutions, including the uniqueness of the solution. This model appears in the modeling of many periodic diffusion phenomena in various sciences. Our approach towards our goal is through the method of upper and lower solutions.

Keywords: reaction-diffusion systems; degenerate parabolic systems; nonlinear dynamics; upper and lower solutions.

Mathematics Subject Classification (2010): 35K57, 35K65, 93A30, 70K42.

1 Introduction

Many problems arise in biology, chemistry, applied science and engineering in the form of periodic reaction-diffusion models. This has been observed in recent scientific studies. Different models can be found in Murray [12,13]. As for the mathematical methods used, some of them are found in the works of Alaa and Mesbahi et al. [2,3,10,11,17], and also in Pao [16].

In recent years, special attention has been paid to degenerate reaction-diffusion systems with specific diffusion coefficients and reaction functions, either in the elliptical or parabolic case, as it is in our work. This is due to their wide applications in various sciences. Our work will be in this context; we will prove the existence of periodic maximal

* Corresponding author: <mailto:salimbra@gmail.com>

and minimal solutions for a class of degenerate quasilinear parabolic reaction-diffusion systems, including the uniqueness of the positive solution.

Degenerate reaction-diffusion systems appear naturally in the mathematical modeling of a wide variety of diffusion phenomena, not only in the natural sciences but also in engineering, chemistry and economics, as, for example, the dynamics of gas, population dynamics, dynamic systems, fusion process, certain biological models, valuation of assets in economy, composite media. We find many models and applications in Abuweden [1], Alaa *et al.* [3], Anderson [4], Bouzelmate and Gmira [5], Carrillo [6], Holden *et al.* [8], Saffidine and Mesbahi [17], and Zhang and Lin [18], where we also find well-known techniques and methods which are frequently used to study such a problem.

These systems are of great importance from the point of view of applications and also from the point of view of analysis, as they require the design of new technologies and the development of known techniques to study them. Therefore, this topic is of great and growing importance in science and engineering.

The introduction of degenerate diffusion leads to difficulties in the mathematical analysis of the model. For this, we will use a successful technique described by Pao based on the method of upper and lower solutions and its associated monotone iterations. The basic idea of this method is that when using an upper solution or a lower solution as the initial iteration in a suitable iterative process, the resulting sequence of iterations is monotone and converges to a solution of the problem. For more details on this technique, see Pao's works [14–16]. We will therefore pay special attention to a model that has several applications which all have in common that they are modeled by the following nonlinear degenerate parabolic reaction-diffusion system:

$$\begin{cases} (u_j)_t - d_j \operatorname{div} (D_j(u_j) \nabla u_j) = f_j(t, x, \mathbf{u}) & \text{in } \Gamma, \\ D_j(u_j) \frac{\partial u_j}{\partial \eta} = \beta_j(t, x) u_j + \varphi_j(t, x, \mathbf{u}) & \text{on } \Sigma, \\ u_j(0, x) = u_j(T, x) & \text{in } \Omega, \\ \text{for all } 1 \leq j \leq m, \end{cases} \quad (1)$$

where $\mathbf{u} = \mathbf{u}(t, x) = (u_1(t, x), \dots, u_m(t, x))$, Ω is a bounded domain subset of \mathbb{R}^n ($n \geq 1$) with the smooth boundary $\partial\Omega$, $\Gamma = \mathbb{R}^+ \times \Omega$, $\bar{\Gamma} = \mathbb{R}^+ \times \bar{\Omega}$, $\Sigma = \mathbb{R}^+ \times \partial\Omega$, η denotes the unit normal vector to the boundary $\partial\Omega$, $\frac{\partial}{\partial \eta}$ denotes the outward normal derivative on $\partial\Omega$. For each $1 \leq j \leq m$, $d_j > 0$ and D_j , f_j , φ_j , β_j are prescribed functions satisfying the conditions in hypothesis (H), which we will mention in the next section.

The rest of this paper is organized as follows. In the next section, we present the assumptions under which we will study our problem. Next, we give some results regarding the approximate problem. In the fourth section, we state our main result and also present its proof in detail. The penultimate section is devoted to an application of the obtained result. Finally, we conclude with some remarks and perspectives.

2 Assumptions and Notations

In all that follows, we denote $\tilde{\mathbf{u}} \equiv (\tilde{u}_1, \dots, \tilde{u}_m)$, $\hat{\mathbf{u}} \equiv (\hat{u}_1, \dots, \hat{u}_m)$. The inequality $\hat{\mathbf{u}} \leq \tilde{\mathbf{u}}$ means that $\hat{u}_j \leq \tilde{u}_j$ for all $1 \leq j \leq m$. Below, we will denote \mathbf{E} to one of the sets Γ , $\bar{\Gamma}$, Σ or Ω , $\mathbf{C}^\ell(\mathbf{E})$ to the space of all continuous functions whose partial derivatives up to the m -th order are continuous in \mathbf{E} , $\mathbf{C}^{\ell+\alpha}(\mathbf{E})$ to the space of functions in $\mathbf{C}^\ell(\mathbf{E})$ that

are Hölder continuous in \mathbf{E} with exponent $\alpha \in (0, 1)$. Let, also, $\mathbf{C}^{\ell,m}(\mathbf{E})$ be the space of functions whose ℓ -times derivatives in t and m -times derivatives in x are continuous in \mathbf{E} . In particular, the space $\mathbf{C}^{1,2}(\mathbf{E})$ consists of all functions that are once continuously differentiable in t and twice continuously differentiable in x for $(t, x) \in \mathbf{E}$. When $\ell = 0$, we denote by $\mathbf{C}(\mathbf{E})$ the set of continuous functions in \mathbf{E} .

Now, we have to clarify in which sense we want to solve our problem.

Definition 2.1 A pair of vector functions $\tilde{\mathbf{u}} \equiv (\tilde{u}_1, \dots, \tilde{u}_m)$, $\hat{\mathbf{u}} \equiv (\hat{u}_1, \dots, \hat{u}_m)$ in $\mathbf{C}(\bar{\Gamma}) \cap \mathbf{C}^{1,2}(\Gamma)$ are called ordered upper and lower solutions of (1) if $\hat{\mathbf{u}} \leq \tilde{\mathbf{u}}$ and if $\hat{\mathbf{u}}$ satisfies the relations

$$\begin{cases} (\hat{u}_j)_t - d_j \operatorname{div}(D_i(\hat{u}_j) \nabla \hat{u}_j) \leq f_j(t, x, \hat{\mathbf{u}}) & \text{in } \Gamma, \\ D_j(\hat{u}_j) \frac{\partial \hat{u}_j}{\partial \eta} \leq \beta_j(t, x) \hat{u}_j + \varphi_j(t, x, \hat{\mathbf{u}}) & \text{on } \Sigma, \\ \hat{u}_j(0, x) \leq \hat{u}_j(T, x) & \text{in } \Omega, \end{cases} \quad (2)$$

for all $1 \leq j \leq m$, and $\tilde{\mathbf{u}}$ satisfies (2) with inequalities reversed.

Now, we make the following assumption:

(H) For each $1 \leq j \leq m$, the following conditions hold:

- (i) $f_j(t, x, \cdot) \in \mathbf{C}^{\frac{\alpha}{2}, \alpha}(\bar{\Gamma})$, $0 \leq \beta_j \in \mathbf{C}^1(\Sigma)$, $\varphi_j(t, x, \cdot) \in \mathbf{C}^{1+\frac{\alpha}{2}, 2+\alpha}(\Sigma)$, and they are all T -periodic in t .
- (ii) $D_j(u_j) \in \mathbf{C}^{1+\alpha}(\mathbf{Q}_j)$, $D_j(u_j) > 0$ for $u_j > 0$ and $D_j(0) \geq 0$.
- (iii) $f_j(\cdot, \mathbf{u})$, $\varphi_j(\cdot, \mathbf{u}) \in \mathbf{C}^1(\mathbf{Q})$ such that

$$\begin{aligned} \frac{\partial f_j}{\partial u_i}(\cdot, \mathbf{u}) &\geq 0, \quad \frac{\partial \varphi_j}{\partial u_j}(\cdot, \mathbf{u}) = 0, \\ \frac{\partial \varphi_j}{\partial u_i}(\cdot, \mathbf{u}) &\geq 0 \text{ for all } j \neq i, \mathbf{u} \in \mathbf{Q}. \end{aligned}$$

In the above hypothesis, the subsets \mathbf{Q}_j and \mathbf{Q} are given by the sectors between a pair of upper and lower solutions.

Remark 2.1 In the above hypothesis, we allow $D_j(u_j) > 0$ for $u_j > 0$ and $D_j(0) \geq 0$. This is why we say that system (1) is degenerate, this is our main point of research. For more information on degenerate parabolic problems, see DiBenedetto [7].

3 Approximating Scheme

To simplify our study, we perform the following change of variables:

$$w_j = I_j(u_j) = \int_0^{u_j} D_j(s) ds \text{ for } u_j \geq 0, 1 \leq j \leq m.$$

Note that this is a continuous change, where $I_j'(u_j) = D_j(u_j)$, and therefore its inverse $u_j = q_j(w_j)$ exists and is an increasing function of $w_j > 0$ for all $1 \leq j \leq m$. We have

$$(w_j)_t = D_j(u_j)(u_j)_t, \quad \nabla w_j = D_j(u_j) \nabla u_j, \quad \frac{\partial w_j}{\partial \eta} = D_j(u_j) \frac{\partial u_j}{\partial \eta},$$

then system (1) is equivalent to the following:

$$\left\{ \begin{array}{ll} (D_j(u_j))^{-1}(w_j)_t - d_j \Delta w_j = f_j(t, x, \mathbf{u}) & \text{in } \Gamma, \\ \frac{\partial w_j}{\partial \eta} = \beta_j(t, x) \cdot q_j(w_j) + \varphi_j(t, x, \mathbf{u}) & \text{on } \Sigma, \\ w_j(0, x) = w_j(T, x) & \text{in } \Omega, \\ u_j = q_j(w_j) & \text{in } \bar{\Gamma}, \\ \text{for all } 1 \leq j \leq m. \end{array} \right. \quad (3)$$

Let $\tilde{w}_j = I_j(\tilde{u}_j)$, $\hat{w}_j = I_j(\hat{u}_j)$, $\tilde{\mathbf{w}} = (\tilde{w}_1, \dots, \tilde{w}_m)$ and $\hat{\mathbf{w}} = (\hat{w}_1, \dots, \hat{w}_m)$. It is easy to verify that $(\tilde{\mathbf{u}}, \tilde{\mathbf{w}})$ and $(\hat{\mathbf{u}}, \hat{\mathbf{w}})$ are ordered upper and lower solutions of (3). We set

$$\begin{aligned} \mathbf{Q}_j &= \{u_j \in C(\bar{\Gamma}) : \hat{u}_j \leq u_j \leq \tilde{u}_j\}, \quad 1 \leq j \leq m, \\ \mathbf{Q} &= \{\mathbf{u} \in C(\bar{\Omega}) : \hat{\mathbf{u}} \leq \mathbf{u} \leq \tilde{\mathbf{u}}\}, \\ \mathbf{Q}_j \times \mathbf{Q} &= \{(\mathbf{u}, \mathbf{w}) \in C(\bar{\Omega}) \times C(\bar{\Omega}) : (\hat{\mathbf{u}}, \hat{\mathbf{w}}) \leq (\mathbf{u}, \mathbf{w}) \leq (\tilde{\mathbf{u}}, \tilde{\mathbf{w}})\}. \end{aligned}$$

Now, we define the modified functions $\bar{D}_j(u_j)$, $1 \leq j \leq m$, by

$$\bar{D}_j(u_j) = \begin{cases} D_j(u_j) + (u_j - \tilde{u}_j), & \text{if } u_j > \tilde{u}_j, \\ D_j(u_j), & \text{if } \hat{u}_j \leq u_j \leq \tilde{u}_j, \\ D_j(u_j) + (\hat{u}_j - u_j), & \text{if } u_j < \hat{u}_j. \end{cases}$$

It is clear that $\bar{D}_j(0) > 0$ if either $D_j(0) > 0$ and $\hat{u}_j \geq 0$ or $D_j(0) = 0$ and $\hat{u}_j \geq \delta_j > 0$. This implies the existence of nonnegative functions $\lambda_j^{(1)}, \lambda_j^{(2)} \in C^\alpha(\bar{\Gamma})$ such that

$$\lambda_j^{(1)} \bar{D}_j(u_j) + \frac{\partial f_j}{\partial u_j}(\cdot, \mathbf{u}) \geq 0, \quad \lambda_j^{(2)} \bar{D}_j(u_j) + \beta_j \geq 0 \quad \text{for } \mathbf{u} \in \mathbf{Q}. \quad (4)$$

System (3) directly implies

$$\left\{ \begin{array}{ll} (D_j(u_j))^{-1}(w_j)_t - (d_j \Delta w_j - \lambda_j^{(1)} w_j) = f_j(t, x, \mathbf{u}) + \lambda_j^{(1)} w_j & \text{in } \Gamma, \\ \frac{\partial w_j}{\partial \eta} + \lambda_j^{(2)} w_j = \beta_j(t, x) q_j(w_j) + \varphi_j(t, x, \mathbf{u}) + \lambda_j^{(2)} w_j & \text{on } \Sigma, \\ w_j(0, x) = w_j(T, x) & \text{in } \Omega, \\ u_j = q_j(w_j) & \text{in } \bar{\Gamma}, \\ \text{for all } 1 \leq j \leq m. \end{array} \right.$$

For all $1 \leq j \leq m$, we denote

$$\begin{aligned} F_j(t, x, \mathbf{u}) &= f_j(t, x, \mathbf{u}) + \lambda_j^{(1)} w_j = f_j(t, x, \mathbf{u}) + \lambda_j^{(1)} \bar{I}_j(u_j), \\ \Psi_j(t, x, \mathbf{u}) &= \beta_j(t, x) u_j + \varphi_j(t, x, \mathbf{u}) + \lambda_j^{(2)} \bar{I}_j(u_j), \\ L_j w_j &= d_j \Delta w_j - \lambda_j^{(1)} w_j, \\ B_j w_j &= \frac{\partial w_j}{\partial \eta} + \lambda_j^{(2)} w_j, \end{aligned}$$

where

$$\bar{I}_j(u_j) = \int_0^{u_j} \bar{D}_j(s) ds, \text{ for } u_j \geq 0, 1 \leq j \leq m.$$

According to (4), $F_j(\cdot, \mathbf{u})$ and $G_j(\cdot, \mathbf{u})$ are nondecreasing, i.e.,

$$F_j(\cdot, \mathbf{v}) \leq F_j(\cdot, \mathbf{u}), \Psi_j(\cdot, \mathbf{v}) \leq \Psi_j(\cdot, \mathbf{u}), \text{ where } \hat{\mathbf{u}} \leq \mathbf{v} \leq \mathbf{u} \leq \bar{\mathbf{u}}. \tag{5}$$

Consequently, system (3) can be reformulated as follows:

$$\begin{cases} (D_j(u_j))^{-1}(w_j)_t - L_j w_j = F_j(t, x, \mathbf{u}) & \text{in } \Gamma, \\ B_j w_j = \Psi_j(t, x, \mathbf{u}) & \text{on } \Sigma, \\ w_j(0, x) = w_j(T, x) & \text{in } \Omega, \\ u_j = q_j(w_j) & \text{in } \bar{\Gamma}, \\ \text{for all } 1 \leq j \leq m. \end{cases} \tag{6}$$

It is clear that systems (1) and (6) are equivalent, therefore the existence of a periodic solution to the equivalent system(6) leads to the existence of that to system (1).

We recall the following important lemma, which will be used to construct monotone convergent sequences. In Pao and Ruan [14], we find a detailed proof of this lemma.

Lemma 3.1 *Let $\sigma(t, x) > 0$ in Γ , $C^{(2)}(t, x) \geq 0$ on Σ , and let either (i) $C^{(1)}(t, x) > 0$ in Γ or (ii) $\left(\frac{-C^{(1)}}{\sigma}\right)$ be bounded on $\bar{\Gamma}$. If $z \in C^{2,1}(\bar{\Gamma}) \cap C(\bar{\Gamma})$ and satisfies the following inequalities:*

$$\begin{cases} \sigma(t, x) z_t - \mathbf{div}(a \nabla z) + b \cdot \nabla z + C^{(1)} z \geq 0 & \text{in } \Gamma, \\ \frac{\partial z}{\partial \eta} + C^{(2)} z \geq 0 & \text{on } \Sigma, \\ z(0, x) \geq 0 & \text{in } \Omega, \end{cases}$$

then $z \geq 0$ in $\bar{\Gamma}$.

Assume that a pair of ordered upper and lower solutions $\bar{\mathbf{u}}, \hat{\mathbf{v}}$ exist and hypothesis (H) holds, using either $\mathbf{u}^{(0)} = \bar{\mathbf{u}}$ or $\mathbf{u}^{(0)} = \hat{\mathbf{u}}$ as the initial iteration, we can construct a sequence $\{\mathbf{u}^{(k)}, \mathbf{w}^{(k)}\}$ from the linear iteration process

$$\begin{cases} \left(\bar{D}_j(u_j^{(k)})\right)^{-1} (w_j^{(k)})_t - L_j w_j^{(k)} = F_j(t, x, \mathbf{u}^{(k-1)}) & \text{in } \Gamma, \\ B_j w_j^{(k)} = \Psi_j(t, x, \mathbf{u}^{(k-1)}) & \text{on } \Sigma, \\ w_j^{(k)}(0, x) = w_j^{(k-1)}(T, x) & \text{in } \Omega, \\ u_j^{(k)} = q_j(w_j^{(k-1)}) & \text{in } \bar{\Gamma} \\ \text{for all } 1 \leq j \leq m, \end{cases} \tag{7}$$

where $\mathbf{u}^{(k)} = (u_1^{(k)}, \dots, u_m^{(k)})$ and $\mathbf{w}^{(k)} = (w_1^{(k)}, \dots, w_m^{(k)})$. It is clear that this sequence is well defined, see Ladyženskaja et al. [9]. Denote the sequence by $\{\bar{\mathbf{u}}^{(k)}, \bar{\mathbf{w}}^{(k)}\}$ if $\mathbf{u}^{(0)} = \bar{\mathbf{u}}$, and by $\{\underline{\mathbf{u}}^{(k)}, \underline{\mathbf{w}}^{(k)}\}$ if $\mathbf{u}^{(0)} = \hat{\mathbf{u}}$, and refer to them as the maximal and minimal sequences, respectively.

Lemma 3.2 *The maximal and minimal sequences $\{\bar{\mathbf{u}}^{(k)}, \bar{\mathbf{w}}^{(k)}\}$, $\{\underline{\mathbf{u}}^{(k)}, \underline{\mathbf{w}}^{(k)}\}$ possess the monotone property, i.e., for $k \geq 1$,*

$$(\hat{\mathbf{u}}, \hat{\mathbf{w}}) \leq (\underline{\mathbf{u}}^{(k)}, \underline{\mathbf{w}}^{(k)}) \leq (\underline{\mathbf{u}}^{(k+1)}, \underline{\mathbf{w}}^{(k+1)}) \leq (\bar{\mathbf{u}}^{(k+1)}, \bar{\mathbf{w}}^{(k+1)}) \leq (\bar{\mathbf{u}}^{(k)}, \bar{\mathbf{w}}^{(k)}) \leq (\bar{\mathbf{u}}, \bar{\mathbf{w}}).$$

Proof. Let $z_j^{(1)} = \underline{w}_j^{(1)} - \underline{w}_j^{(0)} = \underline{w}_j^{(1)} - \hat{w}_j$, $1 \leq j \leq m$. Then by (7) and the property of a lower solution stipulated in the previous Definition 2.1, we obtain

$$\begin{cases} \left(\bar{D}_j \left(u_j^{(1)} \right) \right)^{-1} \left(z_j^{(1)} \right)_t - L_j z_j^{(1)} + \gamma_j^{(0)} z_j^{(1)} \geq 0 & \text{in } \Gamma, \\ B_j z_j^{(1)} = \Psi_j \left(\cdot, \underline{\mathbf{u}}^{(0)} \right) - B_j \hat{w}_j \geq 0 & \text{on } \Sigma, \\ z_j^{(1)}(0, x) = \underline{w}_j^{(0)}(T, x) - \underline{w}_j^{(0)}(0, x) = \hat{w}_j(T, x) - \hat{w}_j(0, x) & \text{in } \Omega, \end{cases}$$

where $\gamma_j^{(0)}$ is a bounded function on $\bar{\Gamma}$ given in the form

$$\gamma_j^{(0)} = - \frac{\bar{D}'_j \left(\xi_j^{(0)} \right)}{\left(\bar{D}_j \left(\xi_j^{(0)} \right) \right)^3} \left(\underline{w}_j^{(0)} \right)_t \quad \text{with } \underline{u}_j^{(0)} \leq \xi_j^{(0)} \equiv \xi_j^{(0)}(t, x) \leq \underline{u}_j^{(1)}.$$

By the hypothesis $\bar{D}_j(0) > 0$ or $D_j(0) = 0$ and $\hat{u}_j \geq \delta_j > 0$, the function $\left(\bar{D}_j \left(u_j^{(1)} \right) \right)^{-1}$ is also bounded in $\bar{\Gamma}$. By Lemma 3.1, we find $z_j^{(1)} \geq 0$. This proves $\underline{w}_j^{(1)} \geq \underline{w}_j^{(0)}$ and $\underline{u}_j^{(1)} \geq \underline{u}_j^{(0)}$. In the same way, but with the upper solution, we find $\bar{w}_j^{(1)} \leq \bar{w}_j^{(0)}$ and $\bar{u}_j^{(1)} \leq \bar{u}_j^{(0)}$. In the following, we prove that $\bar{u}_j^{(1)} \geq \underline{u}_j^{(1)}$. Let $z_j^{(1)} = \bar{w}_j^{(1)} - \underline{w}_j^{(1)}$, then by (5) and (7), we have

$$\begin{cases} \left(\bar{D}_j \left(u_j^{(1)} \right) \right)^{-1} \left(z_j^{(1)} \right)_t - L_j z_j^{(1)} + \gamma_j^{(0)} z_j^{(1)} = F_j \left(\cdot, \bar{\mathbf{u}}^{(0)} \right) - F_j \left(\cdot, \underline{\mathbf{u}}^{(0)} \right) & \text{in } \Gamma, \\ B_j z_j^{(1)} = \Psi_j \left(\cdot, \bar{\mathbf{u}}^{(0)} \right) - \Psi_j \left(\cdot, \underline{\mathbf{u}}^{(0)} \right) \geq 0 & \text{on } \Sigma, \\ z_j^{(1)}(0, x) = \bar{w}_j^{(1)}(0, x) - \underline{w}_j^{(1)}(0, x) = \bar{w}_j^{(0)}(T, x) - \underline{w}_j^{(0)}(T, x) \geq 0 & \text{in } \Omega. \end{cases}$$

By Lemma 3.1, we have $z_j^{(1)} \geq 0$. This is what gives

$$\underline{\mathbf{u}}^{(0)} \leq \underline{\mathbf{u}}^{(1)} \leq \bar{\mathbf{u}}^{(1)} \leq \bar{\mathbf{u}}^{(0)}.$$

By induction, we can easily have the monotone property.

According to Lemma 3.2, the pointwise limits

$$\lim_{k \rightarrow \infty} \left(\bar{\mathbf{u}}^{(k)}, \bar{\mathbf{w}}^{(k)} \right) = (\bar{\mathbf{u}}, \bar{\mathbf{w}}), \quad \lim_{k \rightarrow \infty} \left(\underline{\mathbf{u}}^{(k)}, \underline{\mathbf{w}}^{(k)} \right) = (\underline{\mathbf{u}}, \underline{\mathbf{w}}) \quad (8)$$

exist and verify the relation $(\bar{\mathbf{u}}, \bar{\mathbf{w}}) \geq (\underline{\mathbf{u}}, \underline{\mathbf{w}})$ in $\bar{\Gamma}$. It results from (8) and $\mathbf{u}^{(k)}(0, x) = \mathbf{u}^{(k)}(T, x)$ that $\bar{\mathbf{u}}(0, x) = \bar{\mathbf{u}}(T, x)$ and $\underline{\mathbf{u}}(0, x) = \underline{\mathbf{u}}(T, x)$ on $\bar{\Omega}$.

We will show that $\bar{\mathbf{u}}$ and $\underline{\mathbf{u}}$ are, respectively, the maximal and minimal periodic solutions of (1). In other words, we will prove that if \mathbf{u} is another periodic solution of (1) in $(\hat{\mathbf{u}}, \hat{\mathbf{u}})$, then $\underline{\mathbf{u}} \leq \mathbf{u} \leq \bar{\mathbf{u}}$.

4 The Main Result

Now, we can state the main result of this paper, it is the following theorem.

Theorem 4.1 *Let $\tilde{\mathbf{u}}, \hat{\mathbf{u}}$ be a pair of ordered upper and lower solutions of (1), and let hypothesis (H) hold with $D_j(0) > 0$ or $D_j(0) = 0$ and $\hat{u}_j \geq \delta > 0$. Then the sequences $\{\tilde{\mathbf{u}}^{(k)}, \tilde{\mathbf{w}}^{(k)}\}, \{\underline{\mathbf{u}}^{(k)}, \underline{\mathbf{w}}^{(k)}\}$ obtained from (7) converge monotonically from above to a maximal periodic solution $(\tilde{\mathbf{u}}, \tilde{\mathbf{w}})$ and from below to a minimal periodic solution $(\underline{\mathbf{u}}, \underline{\mathbf{w}})$ in $\mathbf{Q} \times \mathbf{Q}$, respectively, and satisfy the following inequalities for $k \geq 1$:*

$$\begin{aligned} (\hat{\mathbf{u}}, \hat{\mathbf{w}}) &\leq (\underline{\mathbf{u}}^{(k)}, \underline{\mathbf{w}}^{(k)}) \leq (\underline{\mathbf{u}}^{(k+1)}, \underline{\mathbf{w}}^{(k+1)}) \leq (\underline{\mathbf{u}}, \underline{\mathbf{w}}) \\ &\leq (\tilde{\mathbf{u}}, \tilde{\mathbf{w}}) \leq (\tilde{\mathbf{u}}^{(k+1)}, \tilde{\mathbf{w}}^{(k+1)}) \leq (\tilde{\mathbf{u}}^{(k)}, \tilde{\mathbf{w}}^{(k)}) \leq (\tilde{\mathbf{u}}, \tilde{\mathbf{w}}). \end{aligned}$$

Moreover, $\tilde{\mathbf{u}}$ and $\underline{\mathbf{u}}$ are the maximal and minimal periodic solutions of (1), respectively. If, in addition, $\tilde{\mathbf{u}}(0, x) = \underline{\mathbf{u}}(0, x)$, then $\tilde{\mathbf{u}}(t, x) = \underline{\mathbf{u}}(t, x) (\equiv \mathbf{u}^*(t, x))$ and $\mathbf{u}^*(t, x)$ is the unique solution of (1).

Proof. As in Theorem 2.1 in Pao and Ruan [14], using the standard regularity argument for the equivalent quasilinear parabolic equations and Schauder estimates, we can conclude that the limits $(\tilde{\mathbf{u}}, \tilde{\mathbf{w}})$ and $(\underline{\mathbf{u}}, \underline{\mathbf{w}})$ are the solutions of (6), and therefore $\tilde{\mathbf{u}}, \underline{\mathbf{u}}$ are the solutions of (1). We next show the periodic property of solutions $(\tilde{\mathbf{u}}, \tilde{\mathbf{w}})$ and $(\underline{\mathbf{u}}, \underline{\mathbf{w}})$. We let $z_j(t, x) = w_j(t, x) - w_j(t + T, x)$, where w_j stands for either \tilde{w}_j or \underline{w}_j for $1 \leq j \leq m$. By hypothesis (H) and the mean-value theorem, we have

$$\begin{aligned} &(D_j(u_j))^{-1}(z_j)_t - L_j(t)z_j \\ &= [(D_j(u_j(t, x)))^{-1}(w_j)_t(t, x) \\ &\quad - L_j(t)w_j(t, x)] - [(D_j(u_j(t, x)))^{-1}(w_j)_t(t + T, x) \\ &\quad - L_j(t + T)w_j(t + T, x)] \\ &= F_j(t, x, \mathbf{u}(t, x)) - F_j(t, x, \mathbf{u}(t + T, x)) \\ &\quad + (D_j(u_j(t + T, x)))^{-1}(w_j)_t(t + T, x) \\ &\quad - (D_j(u_j(t, x)))^{-1}(w_j)_t(t + T, x) \\ &= \sum_{k=1}^m \frac{\partial F_j}{\partial u_k}(t, x, \xi)z_j(t, x) + \frac{D'_j(\eta_j)}{(D_j(\eta_j))^3}(w_j)_t(t + T, x)z_j(t, x), \end{aligned}$$

which gives us

$$(D_j(u_j))^{-1}(z_j)_t - L_j(t)z_j + \gamma_j z_j = \sum_{k=1}^m \frac{\partial F_j}{\partial u_k}(t, x, \xi)z_j(t, x) \quad \text{in } \bar{\Gamma}, \tag{9}$$

where $\gamma_j = \frac{D'_j(\eta_j)}{(D_j(\eta_j))^3}(w_j)_t(t + T, x)$ is bounded in $\bar{\Gamma}$, $\xi \equiv \xi(t, x)$ is the different intermediate value in \mathbf{Q} . We can also get

$$\begin{aligned} B_j z_j &= B_j(t)w_j(t, x) - B_j(t + T)w_j(t + T, x) \\ &= \Psi_j(t, x, \mathbf{u}(t, x)) - \Psi_j(t, x, \mathbf{u}(t + T, x)) \\ &= \sum_{k=1}^m \frac{\partial \Psi_j}{\partial u_k}(t, x, \zeta)z_j(t, x) \quad \text{on } \Sigma, \end{aligned} \tag{10}$$

and

$$z_j(0, x) = w_j(0, x) - w_j(T, x) \quad \text{in } \Omega, \tag{11}$$

where $\zeta = \zeta(t, x)$ is the different intermediate value in \mathbf{Q} . Using relation (5) and Lemma 10.9.1 in Pao [16], we obtain $z_j(t, x) \geq 0$ in $\bar{\Gamma}$ for $1 \leq j \leq m$. Replacing z_j by $-z_j$ in (9)-(11) leads to $z_j(t, x) \leq 0$ in $\bar{\Gamma}$, this yields $z_j(t, x) = 0$, which proves $w_j(t, x) = w_j(t + T, x)$ for $1 \leq j \leq m$; hence the periodicity of w_j . Therefore $\mathbf{w}(t, x) = \mathbf{w}(t + T, x)$ and then $\mathbf{u}(t, x) = \mathbf{u}(t + T, x)$.

By (5), we observe that every solution \mathbf{u} of (1) in $(\hat{\mathbf{u}}, \bar{\mathbf{u}})$ is an upper solution as well as a lower solution. The argument in the proof of Lemma 3.2 yields $\mathbf{u} \geq \underline{\mathbf{u}}^{(k)} \geq \hat{\mathbf{u}}$ for every k . Letting $k \rightarrow \infty$ gives $\mathbf{u} \geq \underline{\mathbf{u}}$. A similar argument using \mathbf{u} and $\hat{\mathbf{u}}$ as ordered upper and lower solutions leads to $\mathbf{u} \leq \bar{\mathbf{u}}$. The same work, taking \mathbf{u} and $\hat{\mathbf{u}}$ as ordered upper and lower solutions, leads to $\mathbf{u} \leq \bar{\mathbf{u}}$.

Finally, if $\bar{\mathbf{u}}(0, x) = \underline{\mathbf{u}}(0, x) (\equiv \mathbf{u}_0(x))$, we have $\bar{\mathbf{w}}(0, x) = \underline{\mathbf{w}}(0, x)$, then when considering problem (6) with the initial condition $(\mathbf{u}(0, x), \mathbf{w}(0, x)) = (\mathbf{u}_0(x), \mathbf{w}_0(x))$, the well-known existence-uniqueness result for parabolic systems implies that $(\bar{\mathbf{u}}(t, x), \bar{\mathbf{w}}(t, x)) = (\underline{\mathbf{u}}(t, x), \underline{\mathbf{w}}(t, x))$, and $\bar{\mathbf{u}}(t, x) = \underline{\mathbf{u}}(t, x)$ on $\bar{\Gamma}$. With this we end the proof of Theorem 4.1.

5 Application

As an application of the obtained result, we give the following growth Lotka-Volterra competition model with two competing species, where the reaction rates of the competition follow the hypothesis of the Holling-Tanner interaction mechanism

$$\begin{cases} (u_1)_t - \operatorname{div}(D_1(u_1)\nabla u_1) = u_1 \left(a_1 - b_1 u_1 - c_1 \frac{u_2}{1 + \sigma_1 u_1} \right) & \text{in } \Gamma, \\ (u_2)_t - \operatorname{div}(D_2(u_2)\nabla u_2) = u_2 \left(a_2 - b_2 \frac{u_1}{1 + \sigma_2 u_1} - c_2 u_2 \right) & \text{in } \Gamma, \\ D_1(u_1) \frac{\partial u_1}{\partial \eta} = \beta_1(x) u_1, \quad D_2(u_2) \frac{\partial u_2}{\partial \eta} = \beta_2(x) u_2 & \text{on } \Sigma, \\ u_1(0, x) = u_1(T, x), \quad u_2(0, x) = u_2(T, x) & \text{in } \Omega, \end{cases} \tag{12}$$

where for each $j \in \{1, 2\}$, a_j, b_j, c_j are positive constants and $\beta_1(x) \geq 0$ on $\partial\Omega$, σ_j is nonnegative function. This system is discussed in Pao [15, 16], where there are also several other applications. One of the main concerns for problem (12) is whether, and when the two competing species can coexist. The coexistence problem is ensured if the system has a positive periodic solution.

6 Concluding Remarks and Perspectives

The fruit of this work is a result of existence and positivity of periodic solutions for a class of degenerate parabolic reaction-diffusion models. Despite some difficulties, we succeeded in obtaining several important results. It is clear from Theorem 4.1 that under hypothesis (H), system (1) admits at least one periodic solution if there exists a pair of ordered upper and lower solutions.

The results of this research paper will motivate the development of the implemented methods to different open problems in several scientific fields, such as the anisotropic

system, which consists in adding diffusion coefficients to the studied system depending on (t, x) or, more generally, depending on $(t, x, u, \nabla u)$. Moreover, we can study our problem numerically using one of the well known methods.

References

- [1] A. Abuweden. *Some Free Boundary Problems for The Nonlinear Degenerate Multidimensional Parabolic Equations Modeling Reaction-Diffusion Processes*, Ph.D. Thesis in Applied Mathematics, Florida Institute of Technology, Florida, 2019.
- [2] N. Alaa and S. Mesbahi. Existence of weak periodic solution for quasilinear parabolic problem with nonlinear boundary conditions. *An. Univ. Craiova Ser. Mat. Inform.* **37** (1) (2019) 45–57.
- [3] N. Alaa, S. Mesbahi, A. Mouida and W. Bouarifi. Existence of solutions for quasilinear elliptic degenerate systems with L^1 data and nonlinearity in the gradient. *Electron. J. Differential Equations* **142** (2013) 1–13.
- [4] J. R. Anderson. Local existence and uniqueness of solutions of degenerate parabolic equations. *Comm. Partial Differential Equations* **16** (1991) 105–143.
- [5] A. Bouzelmate and A. Gmira. Existence and Asymptotic Behavior of Unbounded Positive Solutions of a Nonlinear Degenerate Elliptic Equation. *Nonlinear Dyn. Syst. Theory* **21** (1) (2021) 27–55.
- [6] J. Carrillo. Entropy solutions for nonlinear degenerate problems. *Arch. Ration. Mech. Anal.* **147** (1999) 269–361.
- [7] E. DiBenedetto. *Degenerate Parabolic Equations*. Springer-Verlag, New York, 1993. ISBN 13: 978-1-4612-0895-2.
- [8] H. Holden, K. H. Karlsen and N. H. Risebro. On uniqueness and existence of entropy solutions of weakly coupled systems of nonlinear degenerate parabolic equations. *Electron. J. Differential Equations* **46** (2003) 1–31.
- [9] O. A. Ladyženskaja, V. A. Solonnikov and N. N. Ural'ceva. Linear and Quasi-Linear Equations of Parabolic Type. *J. Amer. Math. Soc.*, RI, 1968. (English transl.)
- [10] S. Mesbahi. *Analyse mathématique de systèmes de réaction diffusion quasi-linéaires*. Editions Universitaires Européennes, 2019. ISBN-13 : 978-6138492917.
- [11] S. Mesbahi and N. Alaa. Mathematical analysis of a reaction diffusion model for image restoration. *An. Univ. Craiova Ser. Mat. Inform.* **42** (1) (2015) 70–79.
- [12] J. D. Murray. *Mathematical Biology I: An Introduction*, Springer-Verlag, New York Inc.; 3rd edition, 2002.
- [13] J. D. Murray. *Mathematical Biology II: Spatial Models and Biochemical Applications*, Springer-Verlag, New York Inc.; 3rd edition, 2002.
- [14] C. V. Pao and W. H. Ruan. Positive solutions of quasilinear parabolic systems with nonlinear boundary conditions. *J. Math. Anal. Appl.* **333** (2007) 472–499.
- [15] C. V. Pao. Periodic solutions of parabolic systems with nonlinear boundary conditions. *J. Math. Anal. Appl.* **234** (1999) 695–716.
- [16] C. V. Pao. *Nonlinear Parabolic and Elliptic Equations*, North Carolina State University, Springer USA, 1993. ISBN 13: 978-1-4615-3034-3
- [17] K. I. Saffidine and S. Mesbahi. Existence Result for Positive Solution of a Degenerate Reaction-Diffusion System via a Method of Upper and Lower Solutions. *Nonlinear Dyn. Syst. Theory* **21** (4) (2021) 434–445.
- [18] Q. Zhang and Z. Lin. Periodic solutions of quasilinear parabolic systems with nonlinear boundary conditions. *Nonlinear Anal.* **72** (7–8) (2010) 3429–3435.



Active Fault Tolerant Synchronization of Two Hyper Chaos Lu Systems with Disturbance Input and Parametric Uncertainty

Alireza Sabaghian¹ and Saeed Balochian^{2*}

¹ *Department of Electrical Engineering, Gonabad Branch, Islamic Azad University, Gonabad, Khorasan-e-Razavi, 9691664791, Iran.*

² *Department of Electrical Engineering, Gonabad Branch, Islamic Azad University, Gonabad, Khorasan-e-Razavi, 9691664791, Iran.*

Received: April 28, 2019; Revised: February 25, 2022

Abstract: In this paper, a robust controller is proposed to synchronize two hyperchaos Lu systems with unwanted factors such as uncertainty and disturbance. In this research, first, an integral sliding mode control to synchronize two hyperchaos Lu systems with known parameters and known bound of uncertainty and disturbance is proposed. In the second part of the paper, a controller for synchronization of two hyperchaos systems with unknown parameters and unknown bound of uncertainty and disturbance is designed, and unknown parameters are estimated by an adaptation rule. The stability of the control is proved using the Lyapunov stability method in the corresponding cases. The simulation results with MATLAB software show that the designed controller is able to synchronize two systems, although they have uncertain parameters.

Keywords: *integral sliding mode; adaptive control; hyperchaos; uncertainty; parameter estimation.*

Mathematics Subject Classification (2010): 93C10, 93C40.

* Corresponding author: <mailto:saeed.balochian@gmail.com>

1 Introduction

Nonlinear dynamics is widely used in engineering, physics, biology and many other scientific areas. The interest in nonlinear dynamics and chaotic dynamics has grown rapidly since 1963, when Edward Lorenz, an American meteorologist, discovered a classic chaotic system, and the phenomenon of chaos was gradually being considered by many scholars in various fields. Given the vast applications of chaos phenomena in various sciences such as secure communications [1], nonlinear circuits [2], chemical reactions [3], power electronics [4], lasers [5], encryption [6], study and research on the inherent characteristics of this phenomenon and its control has become of importance in sciences. Due to the introduction of new chaotic systems, the problem of controlling chaos in these types of systems was considered by scientists and researchers in order to control chaos for different purposes such as removing chaos, behavior and anti-chaos control (chaos for a system), bipolar control and synchronization of two chaotic systems. A chaotic system with more than one positive Lyapunov exponent is known as a hyperchaotic system which means that its dynamics extends simultaneously in several different directions. Hyperchaos systems in the presence of more than one positive Lyapunov exponent due to more complex dynamics, which improves applications in secure communications, encryption and decryption, have attracted the attention of many researchers in recent years. Lately, several supercharged systems have been discovered with high-level dynamics. For example, Chua hyperchaos [7], Rossler system [8], Lorenz hyperchaos system [9]. In 2002, Levechin found a new chaotic system known as the Lu system which is the bridge between Lorenz's chaotic system and Chen's chaotic system. The Lu hyperchaos system is based on the chaos Lu system and state feedback [10].

One of the important applications of the hyperchaotic Lu system similar to most of the other hyperchaotic systems mentioned above in the field of secure communications is the use of hyperchaotic systems to increase the level of information security. Because of the noise-like and complex behaviors, chaotic systems have the ability to cover information with a high degree of reliability. The general idea for transmitting information by chaotic systems is based on the fact that the embedding of information in the transmitter system produces a chaotic signal.

In recent years, chaos and synchronization control have been investigated, for example, synchronization with adaptive control [11], in which the problem of synchronizing two hyperchaos systems with an adaptive controller is investigated, active control [12], fuzzy sliding mode control [13], impulsive synchronization [14], active backstepping synchronization [15], nonlinear schemes [16], [17], hybrid projective synchronization [18] and so on.

Synchronization of chaos systems has been widely discussed in recent decades, and attracted the attention of many researchers in controlling chaos. As a general synchronization definition, it is possible to synchronize the variables of a chaotic system with another chaotic system, when the primary system is called master, and the second system is slave. The first method of synchronizing two chaotic systems was proposed in [19].

In this paper, synchronization of hyperchaos systems, despite the uncertainties, disturbance and different initial conditions, was investigated. A sliding-adaptive control, regarding its advantages such as simple and easy realization, quick answer, good transient performance, and robustness against system uncertainties and disturbances, is designed as a control method for synchronization. The stability of the chaotic system has been proved by controllers designed using the Lyapunov theorem, and it is shown that the

slave system states asymptotically track the states of the master system. One of the most important applications of the presented method in this paper in nonlinear systems and systems theory is a secure communications system, where synchronization between the transmitter and the receiver is a vital problem. The overall structure of this paper is as follows. In the second section, the dynamical model of the hyperchaos system is introduced. The third part of the paper describes the issue of synchronization between two hyperchaos systems, with known bound of uncertainties and disturbances. Furthermore in this section, estimation of the unknown parameters of the hyperchaos system is investigated in spite of uncertainty and disturbance. Finally, simulation results of the proposed controller are presented in Section 4.

2 Introduction of Dynamic Model

Elabbasy et al. [20] represented dynamic equations of the hyperchaos system as follows:

$$\begin{cases} \dot{x}_1 = a(x_2 - x_1), \\ \dot{x}_2 = cx_2 - x_1x_3 + x_4, \\ \dot{x}_3 = x_1x_2 - bx_3, \\ \dot{x}_4 = x_3 - dx_4, \end{cases} \quad (1)$$

where the fourth state is a simple feedback, that is added to the second state, and $a = 20$, $b = 5$, $c = 10$, $d = 1.5$, and $X = [x_1, x_2, x_3, x_4]$ is the vector of the state variables of the master system. Both master and slave systems follow the same dynamical equations as equation (1) with different initial conditions, but the main difference is that all states of the master system should be followed by a slave system using a controller. Therefore, the slave system, with the disturbance and parametric uncertainty, is expressed as follows:

$$\begin{cases} \dot{y}_1 = a(y_2 - y_1) + \Delta f_1 + w_1 + u_1, \\ \dot{y}_2 = cy_2 - y_1y_3 + y_4 + \Delta f_2 + w_2 + u_2, \\ \dot{y}_3 = y_1y_2 - by_3 + \Delta f_3 + w_3 + u_3, \\ \dot{y}_4 = y_3 - dy_4 + \Delta f_4 + w_4 + u_4, \end{cases} \quad (2)$$

in which $u = [u_1, u_2, u_3, u_4]$ is the control vector, and $Y = [y_1, y_2, y_3, y_4]$ is the vector of states of the slave system, $\|\Delta f_i\| \leq \alpha_i, i = 1, \dots, 4$, is the parametric uncertainty with known bound and $\|w_i\| \leq \beta_i, i = 1, \dots, 4$, is the disturbance input with known bound. In Figure 1, the hyperchaos system is shown with a parametric set of $a = 20, b = 5, c = 10, d = 1.5$ [14]. These parameters, with the Lyapunov exponent $0.75, 0.03, -1.55, -15.73$ calculated in [21], cause a hyperchaos system.

3 Synchronization of Two Hyperchaos Lu Systems

In the real world, all or some of the system's parameters are unknown or uncertain. So, the synchronization issue may fail. In this section, a synchronization method for two same hyperchaos Lu systems is mentioned. Consider the master and slave systems (1) and (2). Due to the definition of the error as $e_i = y_i - x_i, i = 1, 2, 3, 4$, we have

$$\begin{cases} \dot{e}_1 = a(e_2 - e_1) + \Delta f_1 + w_1 + u_1, \\ \dot{e}_2 = ce_2 + e_4 - e_1e_3 - x_1e_3 - x_3e_1 + \Delta f_2 + w_2 + u_2, \\ \dot{e}_3 = -be_3 + e_1e_2 + x_2e_1 + x_1e_2 + \Delta f_3 + w_3 + u_3, \\ \dot{e}_4 = e_3 - de_4 + \Delta f_4 + w_4 + u_4. \end{cases} \quad (3)$$

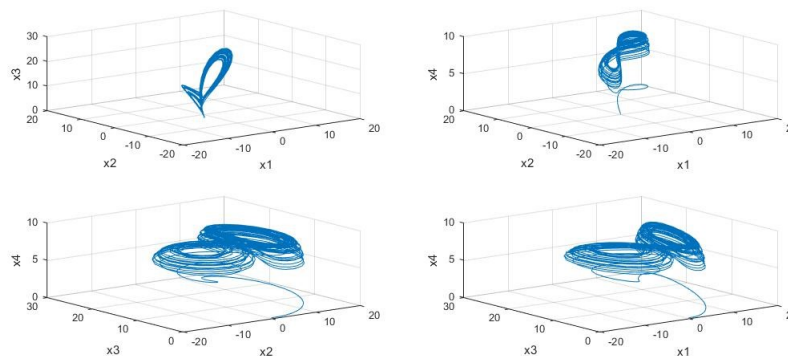


Figure 1: Images of attractor of hyperchaos Lu system.

3.1 Synchronization of two hyperchaos Lu systems with uncertainty and disturbance input

First, the problem of synchronizing two same hyperchaos systems, with known parameters is considered and the sliding mode controller is designed. The sliding mode control is a nonlinear control method that guarantees control strategy over uncertainties. In this way, stability is obtained by keeping system modes on the sliding surface.

In general, the sliding mode controller design consists of two steps:

- A. Sliding surface design that reduces the order of the closed loop system, and provides a resilient bed in the movement of the system towards the equilibrium point.
- B. Choosing the right control policy to move the system to this level and ensure that it stays on it.

Now, with the sliding surface definition, we have the following:

$$s_i = e_i + \int k_i e_i \quad i = 1, 2, 3, 4, \tag{4}$$

$$\begin{cases} \dot{s}_1 = a(e_2 - e_1) + k_1 e_1 + \Delta f_1 + w_1 + u_1, \\ \dot{s}_2 = ce_2 + e_4 - e_1 e_3 - x_1 e_3 - x_3 e_1 + k_2 e_2 + \Delta f_2 + w_2 + u_2, \\ \dot{s}_3 = -be_3 + e_1 e_2 + x_2 e_1 + x_1 e_2 + \Delta f_3 + k_3 e_3 + w_3 + u_3, \\ \dot{s}_4 = e_3 - de_4 + k_4 e_4 + \Delta f_4 + w_4 + u_4, \end{cases} \tag{5}$$

and considering $\dot{s} = 0$, we have

$$u_{eq} = \begin{cases} u_1 = -a(e_2 - e_1) - k_1 e_1, \\ u_2 = -ce_2 - e_4 + e_1 e_3 + x_1 e_3 + x_3 e_1 - k_2 e_2, \\ u_3 = be_3 - e_1 e_2 - x_2 e_1 - x_1 e_2 - k_3 e_3, \\ u_4 = -e_3 + de_4 - k_4 e_4. \end{cases} \tag{6}$$

On the other hand, the control signal of the proposed controller is considered as follows:

$$u_i = u_{eq_i} - (rs_i + \rho \text{sgn}(s_i)) - (\alpha_i + \beta_i), \tag{7}$$

in which ρ and r are greater than zero.

Theorem 3.1 *If in the control signal (7), the parameters are positive and certain, then all system states of (2) will tend to the states of system (1).*

Proof. Suppose that the Lyapunov function is considered as (8), which is a positive definite function. Given the Lyapunov stability theorem, to prove the stability of the sliding mode dynamic (5), we need to show that the derivative of the Lyapunov function is negative, so, according to the selective S , u proves the asymptotic stability by using the Lyapunov stability.

The proposed Lyapunov function is as follows:

$$V = \frac{1}{2} \sum_{i=1}^4 s_i^2 \quad (8)$$

and its derivative is as follows:

$$\begin{aligned} \dot{V} &= \sum_{i=1}^4 s_i \dot{s}_i = s_1 \dot{s}_1 + s_2 \dot{s}_2 + s_3 \dot{s}_3 + s_4 \dot{s}_4 \\ &= s_1(a(e_2 - e_1) + k_1 e_1 + \Delta f_1 + w_2 + u_1) \\ &\quad + s_2(ce_2 + e_4 - e_1 e_3 - x_1 e_3 - x_3 e_1 + k_2 e_2 + \Delta f_2 + w_2 + u_2) \\ &\quad + s_3(-be_3 + e_1 e_2 + x_2 e_1 + x_1 e_2 + \Delta f_3 + k_3 e_3 + w_3 + u_3) \\ &\quad + s_4(e_3 - de_4 + k_4 e_4 + \Delta f_4 + w_4 + u_4), \end{aligned} \quad (9)$$

$$\begin{aligned} \dot{V} &\leq s_1(a(e_2 - e_1) + k_1 e_1 + \alpha_1 + \beta_1 + u_1) \\ &\quad + s_2(ce_2 + e_4 - e_1 e_3 - x_1 e_3 - x_3 e_1 + k_2 e_2 + \alpha_2 + \beta_2 + u_2) \\ &\quad + s_3(-be_3 + e_1 e_2 + x_2 e_1 + x_1 e_2 + k_3 e_3 + \alpha_3 + \beta_3 + u_3) \\ &\quad + s_4(e_3 - de_4 + k_4 e_4 + \alpha_4 + \beta_4 + u_4), \end{aligned}$$

$$\begin{aligned} \dot{V} &\leq s_1(-rs_1 - \rho \operatorname{sgn}(s_1)) + s_2(-rs_2 - \rho \operatorname{sgn}(s_2)) \\ &\quad + s_3(-rs_3 - \rho \operatorname{sgn}(s_3)) + s_4(-rs_4 - \rho \operatorname{sgn}(s_4)), \end{aligned}$$

$$\begin{aligned} \dot{V} &\leq (-rs_1^2 - \rho |s_1|) + (-rs_2^2 - \rho |s_2|) + (-rs_3^2 - \rho |s_3|) + (-rs_4^2 - \rho |s_4|) \\ &\quad \text{for } r \geq 0, \quad \rho \geq 0 \quad \Rightarrow \quad \dot{V} \leq 0. \end{aligned} \quad (10)$$

By choosing ρ, r greater than zero, \dot{V} becomes negative, and Lyapunov's stability condition will be established. \square

3.2 Synchronization of hyperchaos Lu systems with disturbance input and unknown system parameters

Here is an estimate of the system's uncertain parameters synchronizing two same hyperchaos systems despite the uncertainty. The master systems in the form of Equation (1) and the slave system are defined as follows:

$$\begin{cases} \dot{y}_1 = \bar{a}(y_2 - y_1) + \Delta f_1 + w_1 + u_1, \\ \dot{y}_2 = \bar{c}y_2 - y_1 y_3 + y_4 + \Delta f_2 + w_2 + u_2, \\ \dot{y}_3 = y_1 y_2 - \bar{b}y_3 + \Delta f_3 + w_3 + u_3, \\ \dot{y}_4 = y_3 - \bar{d}y_4 + \Delta f_4 + w_4 + u_4, \end{cases} \quad (11)$$

where $u_i, i = 1, \dots, 4$, are the control signals used to synchronize two same hyperchaos systems and $\bar{a}, \bar{b}, \bar{c}, \bar{d}$ are unknown parameters, and to estimate them, an adaptive rule is suggested in the synchronization process.

Due to the definition of the error in the form $e_i = y_i - x_i, \quad i = 1, 2, 3, 4$, we have

$$\begin{cases} \dot{e}_1 = \bar{a}(y_2 - y_1) - a(x_2 - x_1) + \Delta f_1 + w_1 + u_1, \\ \dot{e}_2 = \bar{c}y_2 + e_4 - e_1e_3 - x_1e_3 - x_3e_1 - cx_2 + \Delta f_2 + w_2 + u_2, \\ \dot{e}_3 = -\bar{b}y_3 + e_1e_2 + x_2e_1 + x_1e_2 + bx_3 + \Delta f_3 + w_3 + u_3, \\ \dot{e}_4 = e_3 - \bar{d}y_4 + dx_4 + \Delta f_4 + w_4 + u_4. \end{cases} \tag{12}$$

Now, by defining the sliding surface as (4), we have

$$\begin{cases} \dot{s}_1 = \bar{a}(y_2 - y_1) - a(x_2 - x_1) + k_1e_1 + \Delta f_1 + w_1 + u_1, \\ \dot{s}_2 = \bar{c}y_2 - cx_2 + e_4 - e_1e_3 - x_1e_3 - x_3e_1 + k_2e_2 + \Delta f_2 + w_2 + u_2, \\ \dot{s}_3 = bx_3 - \bar{b}y_3 + e_1e_2 + x_2e_1 + x_1e_2 + k_3e_3 + \Delta f_3 + w_3 + u_3, \\ \dot{s}_4 = e_3 - \bar{d}y_4 + dx_4 + k_4e_4 + \Delta f_4 + w_4 + u_4. \end{cases} \tag{13}$$

The proposed controller is presented as follows:

$$u_i = u_{eq_i} - (rs_i + \rho \operatorname{sgn}(s_i)), \tag{14}$$

where

$$u_{eq} = \begin{cases} u_1 = -(\bar{a} + a)(e_2 - e_1) - k_1e_1 - (\tilde{\alpha}_1 + \alpha_1 + \tilde{\beta}_1 + \beta_1), \\ u_2 = -(\bar{c} + c)e_2 - e_4 + e_1e_3 + x_1e_3 + x_3e_1 + k_2e_2 - (\tilde{\alpha}_2 + \alpha_2 + \tilde{\beta}_2 + \beta_2), \\ u_3 = (\bar{b} + b)e_3 - e_1e_2 - x_2e_1 - x_1e_2 - k_3e_3 - (\tilde{\alpha}_3 + \alpha_3 + \tilde{\beta}_3 + \beta_3), \\ u_4 = (\bar{d} + d)y_4 - e_3 - k_4e_4 - (\tilde{\alpha}_4 + \alpha_4 + \tilde{\beta}_4 + \beta_4) \end{cases} \tag{15}$$

and $\tilde{a}, \tilde{b}, \tilde{c}, \tilde{d}$ are the estimation of the adaptation error.

Theorem 3.2 *If the control signal is the relation (14) with the adaptation rules of relation (22), then all system states (11) will tend to the states of system (1).*

Proof. Using the Lyapunov stability theorem, we consider the Lyapunov candidate function as (16) which is a positive definite function

$$V = \frac{1}{2} \left(\sum_{i=1}^4 s_i^2 + \tilde{a}^2 + \tilde{b}^2 + \tilde{c}^2 + \tilde{d}^2 + \tilde{\alpha}_1^2 + \tilde{\beta}_1^2 + \tilde{\alpha}_2^2 + \tilde{\beta}_2^2 + \tilde{\alpha}_3^2 + \tilde{\beta}_3^2 + \tilde{\alpha}_4^2 + \tilde{\beta}_4^2 \right) \tag{16}$$

with derivation, we have

$$\dot{V} = \sum_{i=1}^4 s_i \dot{s}_i + \dot{\tilde{a}}\tilde{a} + \dot{\tilde{b}}\tilde{b} + \dot{\tilde{c}}\tilde{c} + \dot{\tilde{d}}\tilde{d} + \dot{\tilde{\alpha}}_1\tilde{\alpha}_1 + \dot{\tilde{\beta}}_1\tilde{\beta}_1 + \dot{\tilde{\alpha}}_2\tilde{\alpha}_2 + \dot{\tilde{\beta}}_2\tilde{\beta}_2 + \dot{\tilde{\alpha}}_3\tilde{\alpha}_3 + \dot{\tilde{\beta}}_3\tilde{\beta}_3 + \dot{\tilde{\alpha}}_4\tilde{\alpha}_4 + \dot{\tilde{\beta}}_4\tilde{\beta}_4, \tag{17}$$

where

$$\begin{aligned} \tilde{a} &= \bar{a} - a, & \tilde{b} &= \bar{b} - b, & \tilde{c} &= \bar{c} - c, & \tilde{d} &= \bar{d} - d, \\ \tilde{\alpha}_1 &= \bar{\alpha}_1 - \alpha_1, & \tilde{\beta}_1 &= \bar{\beta}_1 - \beta_1, & \tilde{\alpha}_2 &= \bar{\alpha}_2 - \alpha_2, & \tilde{\beta}_2 &= \bar{\beta}_2 - \beta_2, \\ \tilde{\alpha}_3 &= \bar{\alpha}_3 - \alpha_3, & \tilde{\beta}_3 &= \bar{\beta}_3 - \beta_3, & \tilde{\alpha}_4 &= \bar{\alpha}_4 - \alpha_4, & \tilde{\beta}_4 &= \bar{\beta}_4 - \beta_4, \\ \dot{\tilde{a}} &= \dot{\bar{a}}, & \dot{\tilde{b}} &= \dot{\bar{b}}, & \dot{\tilde{c}} &= \dot{\bar{c}}, & \dot{\tilde{d}} &= \dot{\bar{d}}, & \dot{\tilde{\alpha}}_1 &= \dot{\bar{\alpha}}_1, & \dot{\tilde{\beta}}_1 &= \dot{\bar{\beta}}_1, \\ \dot{\tilde{\alpha}}_2 &= \dot{\bar{\alpha}}_2, & \dot{\tilde{\beta}}_2 &= \dot{\bar{\beta}}_2, & \dot{\tilde{\alpha}}_3 &= \dot{\bar{\alpha}}_3, & \dot{\tilde{\beta}}_3 &= \dot{\bar{\beta}}_3, & \dot{\tilde{\alpha}}_4 &= \dot{\bar{\alpha}}_4, & \dot{\tilde{\beta}}_4 &= \dot{\bar{\beta}}_4. \end{aligned} \tag{18}$$

By replacing (13) in (17), we have

$$\begin{aligned} \dot{V} = & s_1 (\bar{a}(y_2 - y_1) - a(x_2 - x_1) + k_1 e_1 + \Delta f_1 + w_1 + u_1) \\ & + s_2 (\bar{c}y_2 - cx_2 + e_4 - e_1 e_3 - x_1 e_3 - x_3 e_1 + k_2 e_2 + \Delta f_2 + w_2 + u_2) \\ & + s_3 (-\bar{b}y_3 + bx_3 + e_1 e_2 + x_2 e_1 + x_1 e_2 + k_3 e_3 + \Delta f_3 + w_3 + u_3) \\ & + s_4 (e_3 - \bar{d}y_4 + dx_4 + k_4 e_4 + \Delta f_4 + w_4 + u_4) \\ & + \dot{\bar{a}}\bar{a} + \dot{\bar{b}}\bar{b} + \dot{\bar{c}}\bar{c} + \dot{\bar{d}}\bar{d} + \dot{\bar{\alpha}}_1 \bar{\alpha}_1 + \dot{\bar{\beta}}_1 \bar{\beta}_1 + \dot{\bar{\alpha}}_2 \bar{\alpha}_2 + \dot{\bar{\beta}}_2 \bar{\beta}_2 + \dot{\bar{\alpha}}_3 \bar{\alpha}_3 + \dot{\bar{\beta}}_3 \bar{\beta}_3 + \dot{\bar{\alpha}}_4 \bar{\alpha}_4 + \dot{\bar{\beta}}_4 \bar{\beta}_4, \end{aligned} \quad (19)$$

$$\begin{aligned} \dot{V} = & s_1 (\bar{a}(y_2 - y_1) - a(x_2 - x_1) + k_1 e_1 + \Delta f_1 + w_1 + u_1 + \bar{a}(x_2 - x_1) - \bar{a}(x_2 - x_1)) \\ & + s_2 (\bar{c}y_2 - cx_2 + e_4 - e_1 e_3 - x_1 e_3 - x_3 e_1 + k_2 e_2 + \Delta f_2 + w_2 + u_2 + \bar{c}x_2 - \bar{c}x_2) \\ & + s_3 (-\bar{b}y_3 + bx_3 + e_1 e_2 + x_2 e_1 + x_1 e_2 + k_3 e_3 + \Delta f_3 + w_3 + u_3 + \bar{b}x_3 - \bar{b}x_3) \\ & + s_4 (e_3 - \bar{d}y_4 + dx_4 + k_4 e_4 + \Delta f_4 + w_4 + u_4 + \bar{d}x_4 - \bar{d}x_4) \\ & + \dot{\bar{a}}\bar{a} + \dot{\bar{b}}\bar{b} + \dot{\bar{c}}\bar{c} + \dot{\bar{d}}\bar{d} + \dot{\bar{\alpha}}_1 \bar{\alpha}_1 + \dot{\bar{\beta}}_1 \bar{\beta}_1 + \dot{\bar{\alpha}}_2 \bar{\alpha}_2 + \dot{\bar{\beta}}_2 \bar{\beta}_2 + \dot{\bar{\alpha}}_3 \bar{\alpha}_3 + \dot{\bar{\beta}}_3 \bar{\beta}_3 + \dot{\bar{\alpha}}_4 \bar{\alpha}_4 + \dot{\bar{\beta}}_4 \bar{\beta}_4, \end{aligned}$$

$$\begin{aligned} \dot{V} = & s_1 (\bar{a}(e_2 - e_1) + k_1 e_1 + \Delta f_1 + w_1 + u_1 - a(x_2 - x_1) + \bar{a}(x_2 - x_1)) \\ & + s_2 (\bar{c}e_2 - cx_2 + e_4 - e_1 e_3 - x_1 e_3 - x_3 e_1 + k_2 e_2 + \Delta f_2 + w_2 + u_2 + \bar{c}x_2) \\ & + s_3 (-\bar{b}e_3 + bx_3 + e_1 e_2 + x_2 e_1 + x_1 e_2 + k_3 e_3 + \Delta f_3 + w_3 + u_3 - \bar{b}x_3) \\ & + s_4 (e_3 - \bar{d}e_4 + dx_4 + k_4 e_4 + \Delta f_4 + w_4 + u_4 - \bar{d}x_4) \\ & + \dot{\bar{a}}\bar{a} + \dot{\bar{b}}\bar{b} + \dot{\bar{c}}\bar{c} + \dot{\bar{d}}\bar{d} + \dot{\bar{\alpha}}_1 \bar{\alpha}_1 + \dot{\bar{\beta}}_1 \bar{\beta}_1 + \dot{\bar{\alpha}}_2 \bar{\alpha}_2 + \dot{\bar{\beta}}_2 \bar{\beta}_2 + \dot{\bar{\alpha}}_3 \bar{\alpha}_3 + \dot{\bar{\beta}}_3 \bar{\beta}_3 + \dot{\bar{\alpha}}_4 \bar{\alpha}_4 + \dot{\bar{\beta}}_4 \bar{\beta}_4. \end{aligned} \quad (20)$$

By replacing (14) and (18) in (20), one gets

$$\begin{aligned} \dot{V} \leq & s_1 \left(\begin{aligned} & \bar{a}(e_2 - e_1) + ke_1 + \alpha_1 + \beta_1 - a(x_2 - x_1) + \bar{a}(x_2 - x_1) \\ & - \bar{a}(e_2 - e_1) - ke_1 - (\bar{\alpha}_1 + \bar{\beta}_1) - rs_1 - \rho \text{sgn}(s_1) \end{aligned} \right) \\ & + s_2 \left(\begin{aligned} & \bar{c}e_2 - cx_2 + e_4 - e_1 e_3 - x_1 e_3 - x_3 e_1 + ke_2 + \alpha_2 + \beta_2 + \bar{c}x_2 \\ & - \bar{c}e_2 - e_4 + e_1 e_3 + x_1 e_3 + x_3 e_1 - ke_2 - (\bar{\alpha}_2 + \bar{\beta}_2) - rs_2 - \rho \text{sgn}(s_2) \end{aligned} \right) \\ & + s_3 \left(\begin{aligned} & -\bar{b}e_3 + bx_3 + e_1 e_2 + x_2 e_1 + x_1 e_2 + ke_3 + \alpha_3 + \beta_3 + u_3 - \bar{b}x_3 \\ & + \bar{b}e_3 - e_1 e_2 - x_2 e_1 - x_1 e_2 - ke_3 - (\bar{\alpha}_3 + \bar{\beta}_3) - rs_3 - \rho \text{sgn}(s_3) \end{aligned} \right) \\ & + s_4 \left(\begin{aligned} & e_3 - \bar{d}e_4 + dx_4 + ke_4 + \alpha_4 + \beta_4 + u_4 - \bar{d}x_4 \\ & - e_3 + \bar{d}e_4 - ke_4 - (\bar{\alpha}_4 + \bar{\beta}_4) - rs_4 - \rho \text{sgn}(s_4) \end{aligned} \right) \\ & + (\bar{a} - a)\dot{\bar{a}} + (\bar{b} - b)\dot{\bar{b}} + (\bar{c} - c)\dot{\bar{c}} + (\bar{d} - d)\dot{\bar{d}} + (\bar{\alpha}_1 - \alpha_1)\dot{\bar{\alpha}}_1 + (\bar{\beta}_1 - \beta_1)\dot{\bar{\beta}}_1 \\ & + (\bar{\alpha}_2 - \alpha_2)\dot{\bar{\alpha}}_2 + (\bar{\beta}_2 - \beta_2)\dot{\bar{\beta}}_2 + (\bar{\alpha}_3 - \alpha_3)\dot{\bar{\alpha}}_3 + (\bar{\beta}_3 - \beta_3)\dot{\bar{\beta}}_3 + (\bar{\alpha}_4 - \alpha_4)\dot{\bar{\alpha}}_4 \\ & + (\bar{\beta}_4 - \beta_4)\dot{\bar{\beta}}_4. \end{aligned} \quad (21)$$

The adaptation rules are given as follows:

$$\begin{aligned} \dot{\bar{a}} &= (x_1 - x_2) s_1, & \dot{\bar{d}} &= x_4 s_4, & \dot{\bar{\alpha}}_2 &= s_2, & \dot{\bar{\beta}}_3 &= s_3, \\ \dot{\bar{b}} &= x_3 s_3, & \dot{\bar{\alpha}}_1 &= s_1, & \dot{\bar{\beta}}_2 &= s_2, & \dot{\bar{\alpha}}_4 &= s_4, \\ \dot{\bar{c}} &= -x_2 s_2, & \dot{\bar{\beta}}_1 &= s_1, & \dot{\bar{\alpha}}_3 &= s_3, & \dot{\bar{\beta}}_4 &= s_4, \end{aligned} \quad (22)$$

therefore from (21) and (22), we have

$$\begin{aligned} \dot{V} & \leq s_1 (-rs_1 - \rho \text{sgn}(s_1)) + s_2 (-rs_2 - \rho \text{sgn}(s_2)) \\ & \quad + s_3 (-rs_3 - \rho \text{sgn}(s_3)) + s_4 (-rs_4 - \rho \text{sgn}(s_4)), \\ \dot{V} & \leq (-rs_1^2 - \rho |s_1|) + (-rs_2^2 - \rho |s_2|) + (-rs_3^2 - \rho |s_3|) + (-rs_4^2 - \rho |s_4|), \\ & \quad \text{for } r \geq 0, \quad \rho \geq 0 \quad \Rightarrow \quad \dot{V} \leq 0. \end{aligned} \quad (23)$$

The hyperchaos system (11) with the initial conditions of $y_i(0) \in R^4$, by the control rules in (14), where $r, \rho > 0$, and with the adaptation rules (22), follows the trajectory of the master system. \square

4 Simulation

In this section, simulations show the effectiveness of the proposed scheme for synchronizing hyperchaos Lu systems. Simulation results are obtained using the MATLAB software.

Example 4.1 In this part, simulation with the initial conditions $[x_1, x_2, x_3, x_4]^T = [0.1, 0.1, 0.1, 0.1]^T$ and $[y_1, y_2, y_3, y_4]^T = [-9.9, -4.9, 5.1, 10.1]^T$ and $a = 20, b = 5, c = 10, d = 1.5$ is done. Parameters used in the design are $k_i = 15, r = 5, \rho = 10$. Uncertainty and bounded disturbance applied to the system are $\Delta f_i = A \sin(x_1) \cos(x_2), w_i = A \sin(t), 0.1 < A < 1$, respectively, in which $\Delta f_i \leq \alpha_i = 1, w_i \leq \beta_i = 1$.

Figures 2 and 3 show the states and error synchronization of hyperchaos system before applying the controller to the slave system. Figures 4 and 5 show the synchronization of the two systems after applying the controller of equation (7) which represents the performance of the proposed controller.

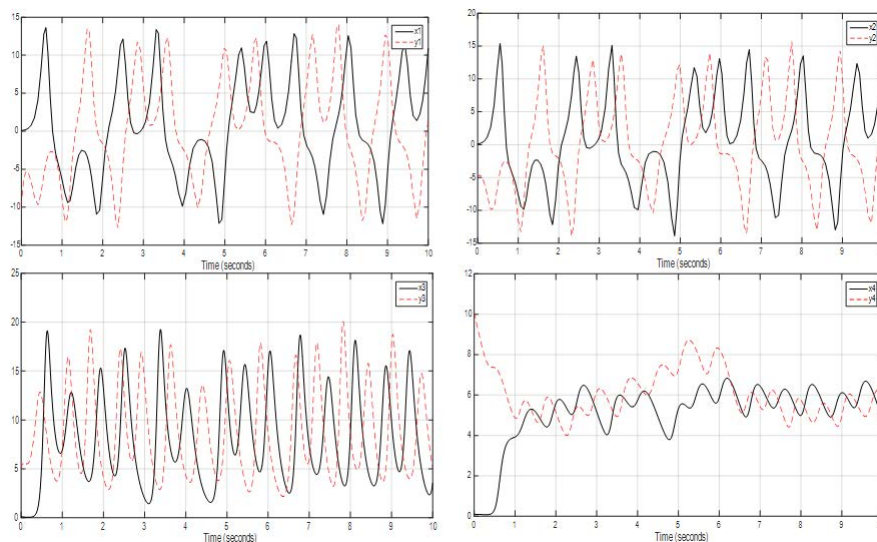


Figure 2: Master and slave system states before applying the controller.

Example 4.2 In this part, we assume unknown slave system parameters. Simulation with the initial conditions $[x_1, x_2, x_3, x_4]^T = [0.1, 0.1, 0.1, 0.1]^T$ and $[y_1, y_2, y_3, y_4]^T = [-9.9, -4.9, 5.1, 10.1]^T$ is performed. Parameters used in the design are $k_i = 15, r = 5, \rho = 10$. Uncertainty and disturbance input applied to the system are in the form of $\Delta f_i = A \sin(x_1) \cos(x_2), w_i = A \sin(t), 0.1 < A < 1$, respectively. By applying the control and estimation parameter rules of (14) and (22), respectively, and applying $\bar{\alpha}_0 = \bar{\beta}_0 = \bar{a}_0 = \bar{b}_0 = \bar{c}_0 = \bar{d}_0 = 1$, the simulation results are shown in Figures 6 and 7. Figure 6 shows the states of the master and slave systems. In Figure 7, the tendency of synchronization error to zero is depicted over time. Figure 8 also shows the estimated unknown parameters $\bar{a}, \bar{b}, \bar{c}, \bar{d}$ of the slave system.

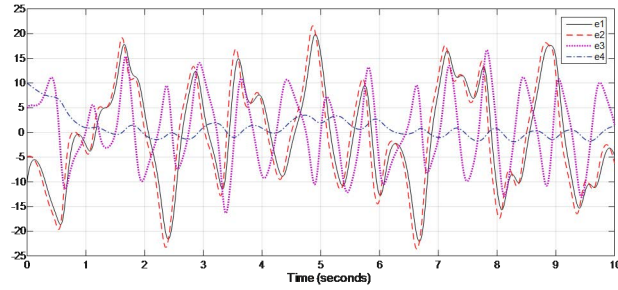


Figure 3: Synchronization error before applying the controller.

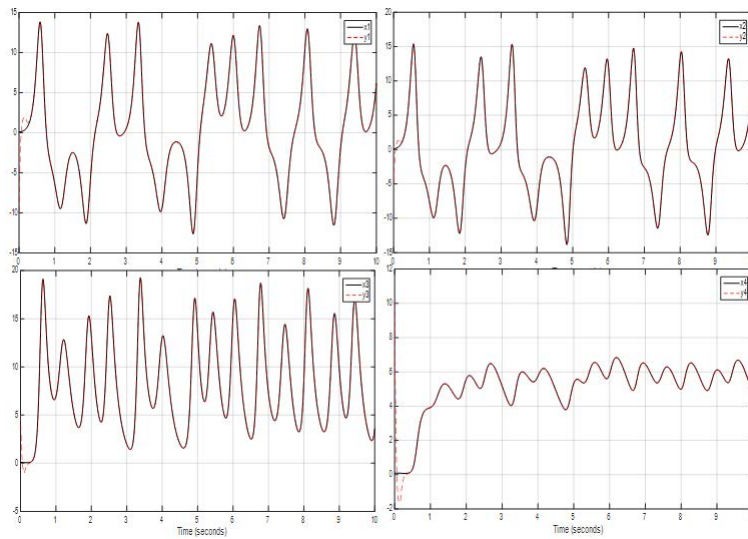


Figure 4: Master and slave system states after applying the controller equation (7).

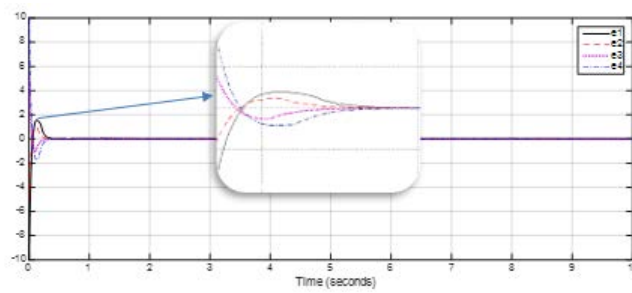


Figure 5: Synchronization error after applying the controller equation (7).

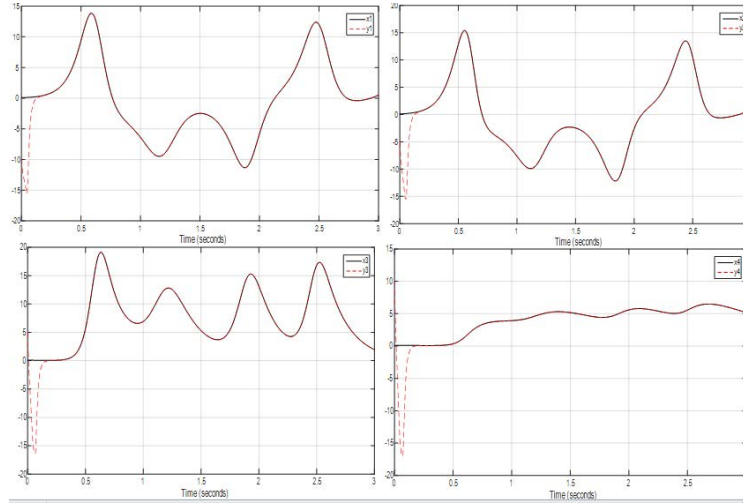


Figure 6: Master and slave system states after applying the controller equation (14).

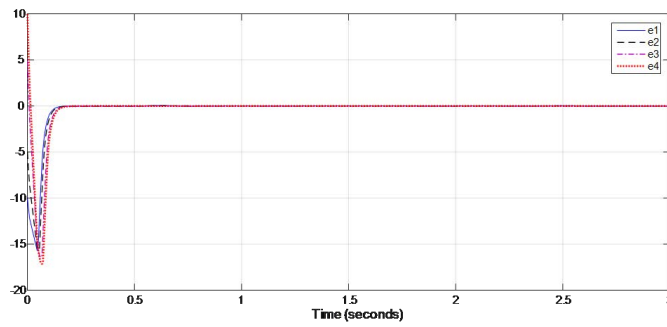


Figure 7: Synchronization error after applying the controller equation (14).

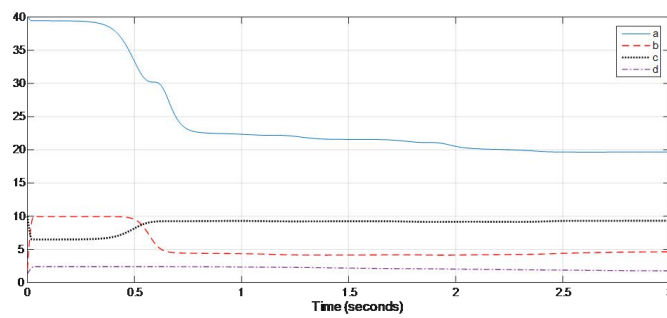


Figure 8: Estimation of \bar{a} , \bar{b} , \bar{c} , \bar{d} parameters.

5 Conclusion

The main objective of this paper is to design the adaptive controller for a hyperchaos system with unknown parameters in the presence of parametric uncertainty and disturbance input. To reach this goal, the combination of the two sliding mode control and the adaptive control methods is proposed to synchronize hyperchaos Lu systems. The stability of the chaotic system is proved using the Lyapunov theorem. To achieve synchronization, the sliding mode control method, which is a robust control against uncertainty, was used. Also, adaptive rules are used to identify the unknown slave system parameters. The results of simulation with MATLAB software showed the well-designed controllers performance in two ways.

References

- [1] W. D. Chang, S. P. Shin and C. Y. Chen. Chaotic Secure Communication Systems with an Adaptive State Observer. *Journal of Control Science and Engineering* **2015** (Article ID 471913) (2015).
- [2] J. Wang, Z. Duan and L. Huang. Dichotomy of nonlinear systems: Application to chaos control of nonlinear electronic circuit. *Physics Letters A* **351** (3) (2006) 143–152.
- [3] P. Gaspard. Microscopic Chaos and Chemical Reactions. *Physics Letters A* **263** (1) (1999) 315–328.
- [4] W. Z. Qiang, J. W. Jing, Z. L. Ru and W. C. Han. Maximum wind power tracking for PMSG chaos systems – ADHDP method. *Applied Soft Computing* **36** (16) (2015) 204–209.
- [5] G. Y. Jiang, J. Zhang and Y. Huang. Chaos and its control in semiconductor laser with delayed negative optoelectronic feedback. *Turkish Journal of Physics* **37** (3) (2013) 296–303.
- [6] E. I. Gonzalez and C. C. Hernandez. Double hyperchaotic encryption for security in biometric systems. *Nonlinear Dynamics and Systems Theory* **13** (1) (2013) 55–68.
- [7] J. Huang, C. Li, T. Huang, H. Wang and X. Wang. Synchronization and Lag synchronization of hyperchaotic memristor-based Chua's circuits. *Mathematical Problems in Engineering* **2014** (Article ID 203123) (2014).
- [8] R. Barrio, M. A. Martínez, S. Serrano and D. Wilczak. When chaos meets hyperchaos: 4D Rössler model. *Physics Letters A* **379** (38) (2015) 2300–2305.
- [9] K. Sun, X. Liu, C. Zhu and J. C. Sprott. Hyperchaos and hyperchaos control of the sinusoidally forced simplified Lorenz system. *Nonlinear Dynamics* **69** (3) (2012) 1383–1391.
- [10] G. Wang, X. Zhang and Y. Li. A new modified hyperchaotic Lü system. *Physica A* **371** (2) (2006) 260–272.
- [11] S. Vaidyanathan. Adaptive design of controller and synchronizer for Lu-xiao chaotic system with unknown parameters. *International Journal of Computer Science and Information Technology* **5** (1) (2013) 197–210.
- [12] I. Ahmad, A. Saaban, A. Ibrahim and M. Shahzad. A Research on the synchronization of two Novel chaotic systems based on a nonlinear active control algorithm. *Engineering, Technology and Applied Science Research* **5** (1) (2015) 739–747.
- [13] M. Sarailoo, Z. Rahmani and B. Rezaie. Fuzzy sliding mode control for hyper chaotic Chen system. *Advances in Electrical and Computer Engineering* **12** (1) (2012) 85–90.
- [14] J. Zhao, D. Zhau and Y. Li. A new impulsive synchronization of chen hyper-chaotic system and Lu hyperchaotic system. *Journal of Vibration and Control* **9** (12) (2013) 1773–1778.
- [15] A. Ibraheem. On multi-switching synchronization of non-identical chaotic systems via active backstepping technique. *Nonlinear Dynamics and Systems Theory* **18** (2) (2018) 170–181.

- [16] A. A. Martynyuk, and Y. A. Martynyuk-Chernienko. *Uncertain Dynamical Systems: Stability and Motion Control*. CRC Press, New York, 2012.
- [17] S. Rezzag. Boundedness results for a new hyperchaotic system and their application in chaos synchronization. *Nonlinear Dynamics and Systems Theory* **18** (4) (2018) 409–417.
- [18] A. Khan, N. Anrja, P. Tripathi and J. Biswas. A new hyper chaotic system and study of hybrid projective synchronization behavior. *Nonlinear Dynamics and Systems Theory* **17** (3) (2017) 266–278.
- [19] L. M. Pecora and T. L. Carroll. synchronization in chaotic systems. *Physical Review Letters* **64** (8) (1990) 821-825.
- [20] E. M. Elabbasy, H. N. Agiza and M. M.El-Dessoky. Adaptive synchronization of a hyperchaotic system with uncertain parameter. *Chaos, Solitons and Fractals* **30** (5) (2006) 1133–1142.
- [21] M. Sandri. Numerical calculation of Lyapunov exponents. *The Mathematica Journal* **6** (3) (1996) 78–84.



Type-II Left Censoring of Some Finite Support Family Lifetime Distributions

Mahmoud M. Smadi

*Department of Mathematics and Statistics, Jordan University of Science and Technology,
Jordan*

Received: October 31, 2021; Revised: April 3, 2022

Abstract: Reliability systems are uncertain random systems, where the failure times are random variables that follow some probability distributions. Due to the difficulty of having complete failure times data for different units in a certain given test, different censoring schemes are proposed and studied in the literature. This paper considers Type-II left censoring of certain popular members of finite support family distributions, namely, the J -family distributions, regular power function distribution, and generalized uniform distribution. The maximum likelihood estimators (MLEs) for these distributions parameters were derived under the Type-II left censoring scheme. A comprehensive simulation study was performed using different sample sizes, parameter values, and censored proportions to investigate the behavior of the estimators via bias and root mean square error (RMSE) criteria. Two lifetime data sets from engineering were analyzed to illustrate the Type-II left censoring scheme which prevailed appropriate results.

Keywords: *generalized uniform distribution; J-family distributions; power function distribution; type-II left censoring.*

Mathematics Subject Classification (2010): 62N05, 93A30, 93B40.

Corresponding author: <mailto:smadi@just.edu.jo>

1 Introduction

There are widespread applications of different censoring schemes in life-testing and reliability experiments in reliability systems, where it is impossible to follow the lifetime of the units till the end of their lifetimes. Several statistical parametric approaches and scenarios of censoring are considered in the literature based on the selected models and the available information [1]. The most popular censoring schemes are the conventional Type-I and Type-II censoring. Type-I censoring describes the situation when a test is terminated at a particular point in time in one direction (left censoring or right censoring) or two directions (interval censoring). However, the Type-II censoring scheme requires fixing the number of failures to be observed. Progressive and hybrid censoring have also been studied in the literature [2–4]. Another censoring scheme is random censoring which is used in life testing experiments and clinical trials, where both the survival and the censoring times are random. Different studies related to random censoring have been conducted [5, 6].

One of the main censoring schemes is the left censoring, which is an appropriate one when the event of interest has already occurred for the individual before the observation time. Applications involving left censoring may include survival analysis and reliability engineering. Coburn et al. [7] studied the patterns of health insurance coverage among rural and urban children with the incidence of a higher proportion of rural children whose spells were "left censored" in the sample. Also, a job duration might be incomplete because the beginning of the job spells is not observed, which is an incidence of left censoring [8]. Jiang et al. [9] conducted a semiparametric analysis on survival data with left truncation and right censoring dependent. Robert et al. [10] presented a method of handling left-censored data in quantitative microbial risk assessment. Yoshinari et al. [11] studied the Bayesian estimation using left-censored data via Markov Chain Monte Carlo simulation.

Survival analysis using various parametric models under the left censoring scheme has been considered extensively in the literature [12, 13]. Mira and Kundu [14] studied the left censored data using the generalized exponential distribution. Sindhu et al. [15] considered the Bayesian estimation of the left censored data using the inverse Rayleigh distribution. Asgharzadeh et al. [16] performed estimation and reconstruction based on the left censored data using the Pareto model. Sindhu et al. [17] applied the Gumbel Type II distribution under the Bayesian approach to the left censored data.

The J -shaped family distributions were introduced by Toop and Lone [18]. The applications of the J -shaped family distributions were considered by Nadarajah and Kotz [19] who showed that the hazard rate function is bathtub shaped. An advantage of the J -shaped family distributions, which have a bathtub shaped hazard rate function, is attributed to the possession of only two parameters, whereas other distributions with a bathtub shaped hazard function involve three or four parameters. Bathtub shaped hazard rate functions have a wide range of applications in reliability engineering and reliability analysis. The bathtub shaped hazard rate function can be applied to human populations. For example, at the infant age, the death rate is high due to birth defects or infant diseases, then the death rate remains constant up to the age of thirty, then it increases again. Also, some manufactured items such as televisions, handheld calculators, and microprocessors follow this pattern.

The power function distribution is commonly used in survival analysis. It is a flexible distribution as it can be used to model various types of data. Different versions of the

power function distribution were reported in the literature [20]. In this work, we consider two versions of power function distribution, namely, the regular power function distribution, and the generalized uniform distribution; both distributions have two parameters: a scale parameter, and a shape parameter. Meniconi and Barry [21] compared the power function distribution with the exponential, lognormal, and Weibull distributions to measure the reliability. They concluded that the power function distribution is the best one to model such types of data. The power function distribution is characterized by the simplicity of its mathematical form and can be handled easily by medical researchers and reliability engineers to obtain failure rates and reliability data. The generalized uniform distribution was used as a model of plant growth [22]. Lee [23] studied the estimation of the generalized uniform distribution (GUD). Bhatt [22] discussed the consistent characterization of the GUD through expectation. Khan and Khan [24] obtained the characterization of the GUD based on lower record values.

This paper considers Type-II left censoring of some popular finite support family distributions, namely, the J -family distributions, regular power function distribution, and generalized uniform distribution. The maximum likelihood estimators (MLEs) for the model parameters were derived. A simulation study was performed using different sample sizes, parameter values, and censored proportions to observe the behavior of the estimators in terms of bias and root mean square error (RMSE) criteria. Finally, two real lifetime data sets from engineering were analyzed to illustrate the derived results.

2 Finite Family Support Distributions

2.1 J -Family distribution

The cumulative distribution function (CDF) of the J -shaped family of distributions is given by

$$F(x; \theta, \beta) = \begin{cases} 0, & x < 0, \\ \left(\frac{x}{\theta}\left(2 - \frac{x}{\theta}\right)\right)^\beta, & 0 \leq x < \theta, \quad 0 < \beta < 1, \\ 1, & \theta \leq x, \end{cases} \quad (1)$$

with the corresponding probability density function (PDF) given by

$$f(x; \theta, \beta) = \frac{2\beta}{\theta} \left(1 - \frac{x}{\theta}\right) \left(\frac{x}{\theta}\left(2 - \frac{x}{\theta}\right)\right)^{\beta-1}; \quad 0 < x \leq \theta, \quad 0 < \beta < 1, \quad (2)$$

where θ is the scale parameter and β is the shape parameter. The reliability function of the distribution is given by

$$R(t) = P(T > t) = 1 - \left(\frac{t}{\theta}\left(2 - \frac{t}{\theta}\right)\right)^\beta$$

and the hazard rate function is given by

$$h(t) = \frac{f(t)}{R(t)} = \frac{\frac{2\beta}{\theta} \left(1 - \frac{t}{\theta}\right) \left(\frac{t}{\theta}\left(2 - \frac{t}{\theta}\right)\right)^{\beta-1}}{1 - \left(\frac{t}{\theta}\left(2 - \frac{t}{\theta}\right)\right)^\beta},$$

2.2 Regular power function distribution

The cumulative distribution function (CDF) of the regular power function distribution is given by

$$F(x; \theta, \beta) = \left(\frac{x}{\theta}\right)^p, \quad 0 < x \leq \theta, \quad p > 0, \theta > 0 \tag{3}$$

with the corresponding probability density function (PDF) given by

$$f(x; \theta, \beta) = \frac{p}{\theta^p} x^{p-1}, \quad 0 < x \leq \theta, \quad p > 0, \theta > 0, \tag{4}$$

where θ is the scale parameter and p is the shape parameter. It is denoted by $X \sim PFF(p, \theta)$. The reliability function of the distribution can be expressed as

$$R(t) = P(T > t) = 1 - \left(\frac{t}{\theta}\right)^p$$

and the hazard rate function is given by

$$h(t) = \frac{f(t)}{R(t)} = \frac{pt^{p-1}}{\theta^p - t^p}.$$

2.3 Generalized uniform distribution

The cumulative distribution function (CDF) of the generalized uniform distribution is given by Lee [23]

$$F(x; \theta, \beta) = \left(\frac{x}{\theta}\right)^{p+1}, \quad 0 < x \leq \theta, \quad -1 < p, \theta > 0 \tag{5}$$

with the corresponding probability density function (PDF) given by

$$f(x, \theta, \beta) = \left(\frac{p+1}{\theta}\right) \left(\frac{x}{\theta}\right)^p, \quad 0 < x \leq \theta, \quad -1 < p, \theta > 0, \tag{6}$$

where θ is the scale parameter, and p is the shape parameter. It is denoted by $X \sim GUD(p, \theta)$. The generalized uniform distribution is a uniform distribution over $(0, \theta)$ if $p = 0$. It should be noted that the density function (6) is decreasing with x if $-1 < p < 0$, and constant if $p = 0$, and increasing if $p > 0$.

The reliability function of the distribution can be expressed as

$$R(t) = P(T > t) = 1 - \left(\frac{t}{\theta}\right)^{p-1}$$

and the hazard rate function is given by

$$h(t) = \frac{f(t)}{R(t)} = \frac{\left(\frac{p+1}{\theta}\right) \left(\frac{t}{\theta}\right)^p}{1 - \left(\frac{t}{\theta}\right)^{p-1}}.$$

3 Maximum Likelihood Estimation

The Type-II left censoring scheme is considered. Suppose the initial r observations are censored or unobserved and the largest $n-r$ lifetimes $X_{(r+1)} < X_{(r+2)} < \dots < X_{(n)}$ have only been observed. Then the joint probability density function of $X_{(r+1)}, X_{(r+2)}, \dots, X_{(n)}$ is given by

$$f(x_{(r)}, \dots, x_{(n)}; \theta, p) = \frac{n!}{r!} \left(F(x_{(r+1)}) \right)^r f(x_{(r+1)}) \dots f(x_{(n)}). \tag{7}$$

3.1 Maximum likelihood estimation of J -family distribution

When using equation (7), the joint probability density function of $X_{(r+1)}, \dots, X_{(n)}$ is given by

$$f(x_{(r)}, \dots, x_{(n)}; \theta, \beta) = \frac{n!}{r!} \left(\left(\frac{x_{(r)}}{\theta} \left(2 - \frac{x_{(r)}}{\theta} \right) \right)^\beta \right)^r \prod_{i=r+1}^n \left[\frac{2\beta}{\theta} \left(1 - \frac{x_{(i)}}{\theta} \right) \left(\frac{x_{(i)}}{\theta} \left(2 - \frac{x_{(i)}}{\theta} \right) \right)^{\beta-1} \right],$$

where

$$0 < x_{(r)} \leq x_{(r+1)} \leq \dots \leq x_{(n)} \leq \theta, \quad 0 < \beta < 1.$$

The likelihood function is given by

$$L(x_{(r+1)}, \dots, x_{(n)}, \theta, \beta) = \frac{n!}{r!} \frac{x_{(r)}^{r\beta}}{\theta^{r\beta}} \left(2 - \frac{x_{(r)}}{\theta} \right)^{r\beta} \frac{(2\beta)^{n-r}}{n-r} \prod_{i=r+1}^n \left(1 - \frac{x_{(i)}}{\theta} \right) \left(\frac{x_{(i)}}{\theta} \right)^{\beta-1} \left(2 - \frac{x_{(i)}}{\theta} \right)^{\beta-1},$$

where

$$0 < x_{(r)} \leq x_{(r+1)} \leq \dots \leq x_{(n)} \leq \theta,$$

It is noticed that for fixed $0 < \beta < 1$,

$$\lim_{\theta \rightarrow x_{(n)}} L(\theta, \beta | x_{(r+1)}, \dots, x_{(n)}) = \lim_{\theta \rightarrow \infty} L(\theta, \beta | x_{(r+1)}, \dots, x_{(n)}).$$

Thus, for a fixed value of β , the value of θ that maximizes the likelihood function lies in the interval $(x_{(n)}, \infty)$. Therefore, the MLE of (θ, β) is the solution of the likelihood equations, such that

$$\frac{\partial L}{\partial \beta} = 0 \quad \text{and} \quad \frac{\partial L}{\partial \theta} = 0$$

or, equivalently, $\frac{\partial \log L(\beta, \theta)}{\partial \beta} = 0$ and $\frac{\partial \log L(\beta, \theta)}{\partial \theta} = 0$.

The log-likelihood function can be expressed as

$$\begin{aligned} \log L(\theta, \beta; x_{(r+1)}, \dots, x_{(n)}) = & \log \frac{n!}{r!} + r\beta \log x_{(r)} - r\beta \log \theta + r\beta \log \left(2 - \frac{x_{(r)}}{\theta} \right) + (n-r) \log 2\beta \\ & - (n-r) \log \theta + \sum_{i=r+1}^n \log \left(1 - \frac{x_{(i)}}{\theta} \right) + (\beta-1) \sum_{i=r+1}^n \log \left(\frac{x_{(i)}}{\theta} \right) \\ & + (\beta-1) \sum_{i=r+1}^n \log \left(2 - \frac{x_{(i)}}{\theta} \right). \end{aligned}$$

The derivative of the log-likelihood function for β gives the following normal equation:

$$r \log x_{(r)} - r \log \theta + r \log \left(2 - \frac{x_{(r)}}{\theta} \right) + \frac{(n-r)}{\beta} + \sum_{i=r+1}^n \log \left(\frac{x_{(i)}}{\theta} \right) + \sum_{i=r+1}^n \log \left(2 - \frac{x_{(i)}}{\theta} \right) = 0, \quad (8)$$

while the derivative of the log-likelihood function for θ results in the following normal equation

$$\frac{r\beta x_{(r)}}{\theta(2\theta - x_{(r)})} + \sum_{i=r+1}^n \frac{x_{(i)}}{\theta(\theta - x_{(i)})} + (\beta-1) \sum_{i=r+1}^n \frac{x_{(i)}}{\theta(2\theta - x_{(i)})} - \frac{n\beta}{\theta} = 0. \quad (9)$$

The maximum likelihood estimates $\hat{\beta}$ and $\hat{\theta}$ of the unknown parameters β and θ can be obtained by solving equations 8 and 9 numerically.

3.2 Maximum likelihood estimation of power function distribution

When using equation (7), the joint probability density function of $x_{(r+1)}, \dots, x_{(n)}$ and the likelihood function can be, respectively, expressed as

$$f(x_{(r)}, \dots, x_{(n)}; \theta, \beta) = \frac{n!}{r!} \left(\left(\frac{x_{(r+1)}}{\theta} \right)^p \right)^r \prod_{i=r+1}^n \frac{p}{\theta p} x_{(i)}^{p-1},$$

$$L(x_{(r+1)}, \dots, x_{(n)}; \theta, \beta) = \frac{n!}{r!} \frac{(x_{(r+1)})^{rp}}{\theta^{rp}} \frac{p^{n-r}}{\theta^{p(n-r)}} \prod_{i=r+1}^n x_{(i)}^{p-1}. \tag{10}$$

The MLEs of p and θ can be derived by maximizing the function L in equation 10. Since this likelihood function is a decreasing function of θ , the MLE of θ is

$$\hat{\theta} = X_{(n)} = \max(X_1, X_2, \dots, X_n),$$

while the MLE of p can be obtained by solving

$$\frac{d \log L_1(p, \hat{\theta})}{dp}.$$

The log-likelihood function in this case is given by

$$\ln L(\hat{\theta}, p; (r + 1), \dots, x_{(n)}) = \log \frac{n!}{r!} + rp \ln x_{(r+1)} + (n-r) \ln p - np \ln \hat{\theta} + (p-1) \sum_{i=r+1}^n \ln x_{(i)}.$$

The derivative of the log-likelihood function for p gives the following normal equation: $r \ln x_{(r+1)} - n \ln \hat{\theta} + \sum_{i=r+1}^n \ln x_{(i)} + \frac{n-r}{p} = 0$. Thus, the maximum likelihood estimator (MLE) of p can be derived:

$$\hat{p} = \frac{n-r}{n \log \hat{\theta} - r \log x_{(r+1)} - \sum_{i=r+1}^n \ln x_{(i)}}.$$

3.3 Maximum likelihood estimation of generalized uniform distribution

When using equation 7, the joint probability density function of $X_{(r+1)}, X_{(r+2)}, \dots, X_{(n)}$ and the likelihood function, respectively, can be expressed as

$$f(x_{(r)}, \dots, x_{(n)}; \theta, p) = \frac{n!}{r!} \left(\left(\frac{x_{(r+1)}^{p+1}}{\theta} \right)^{p+1} \right)^r \prod_{i=r+1}^n \frac{p+1}{\theta^{p+1}} x_{(i)}^p,$$

$$L(x_{(r+1)}, \dots, x_{(n)}; \theta, \beta) = \frac{n!}{r!} \frac{(x_{(r+1)})^{r(p+1)}}{\theta^{r(p+1)}} \frac{p^{n-r}}{\theta^{p(n-r)}} \prod_{i=r+1}^n x_{(i)}^{p-1},$$

$$L(x_{(r+1)}, \dots, x_{(n)}; \theta, p) = \frac{n!}{r!} \frac{(x_{(r+1)})^{r(p+1)} ((p+1)^{n-r}}{\theta^{r(p+1)} \theta^{(n-r)(p+1)}} \prod_{i=r+1}^n x_{(i)}^p. \tag{11}$$

The MLEs of p and θ can be derived by maximizing the function L in equation 11. Since this likelihood function is a decreasing function of θ , the MLE of θ is

$$\hat{\theta} = X_{(n)} = \max(X_1, X_2, \dots, X_n),$$

while the MLE of p can be obtained by solving

$$\frac{d \log L_1(p, \hat{\theta})}{dp} = 0.$$

In this case, the log-likelihood function is given by

$$\begin{aligned} \log L(\hat{\theta}, p; x_{(r+1)}, \dots, x_{(n)}) = \\ \log \frac{n!}{r!} - n(p+1) \ln \hat{\theta} + r(p+1) \ln x_{(r+1)} + (n-r) \ln p + 1 + p \sum_{i=r+1}^n \ln x_{(i)}. \end{aligned}$$

The derivative of the log-likelihood function for p gives the following normal equation:

$$-n \ln x_{(n)} + r \ln x_{(r+1)} + \frac{n-r}{p+1} + \sum_{i=r+1}^n \ln x_{(i)} = 0.$$

Thus, the maximum likelihood estimator (MLE) of p can be derived:

$$\hat{p} = \frac{n-r}{n \ln x_{(n)} - r \ln x_{(r+1)} - \sum_{i=r+1}^n \ln x_{(i)}} - 1.$$

4 Simulation Study

A simulation study was performed to deduce the behavior of the estimators. Different sample sizes, namely, $n = 25, 50$ and 100 , different combinations of the parameter values and different censored proportions were considered. The simulation results were based on 1000 replicates. The means and root mean square errors (RMSE) of the maximum likelihood estimators of the shape parameters were calculated. The simulation results for the J -shaped family, power function, and generalized uniform distribution are displayed in Tables 1-3, respectively.

The following remarks can be drawn based on the simulation results:

- a. The performance of the estimators improves in terms of bias and RMSE due to the increase in the sample size.
- b. As the number of censored observations increases, the biases and RMSEs increase and vice versa.
- c. The bias and RMSE increase with increasing values of the shape parameter.

5 Applications

In this section, two applications of Type-II left censoring lifetime data sets are presented. The first application is related to the J -shaped family distributions and the second application is related to the power function distribution.

Table 1: Mean and RMSE for MLE of β for different combinations of r, n, β and θ of the J -shaped family distribution.

θ	β	$n = 25$			$n = 50$			$n = 100$		
		r	Mean	RMSE	r	Mean	RMSE	r	Mean	RMSE
2	0.5	3	0.62421	0.16763	5	0.56925	0.09498	10	0.54283	0.06246
		5	0.63776	0.17955	10	0.57903	0.10371	20	0.54937	0.06819
	0.7	3	0.88971	0.24339	5	0.80039	0.13669	10	0.76625	0.08940
		5	0.91057	0.26119	10	0.82138	0.14954	20	0.77623	0.09778
	1.0	3	1.29608	0.36162	5	1.16690	0.20129	10	1.10455	0.13093
		5	1.32866	0.38876	10	1.19022	0.22061	20	1.11998	0.14342
4	0.5	3	0.62421	0.16763	5	0.56925	0.09498	10	0.54283	0.06246
		5	0.63776	0.17955	10	0.57903	0.10371	20	0.54937	0.06819
	0.7	3	0.88971	0.24339	5	0.80039	0.13669	10	0.76625	0.08940
		5	0.91057	0.26119	10	0.82138	0.14954	20	0.77622	0.09777
	1.0	3	1.29608	0.36162	5	1.16690	0.20129	10	1.10455	0.09777
		5	1.32866	0.38876	10	1.19022	0.22061	20	1.11998	0.14342

Table 2: Mean and RMSE for MLE of β for different combinations of r, n, β and θ of the power function distribution.

θ	β	$n = 25$			$n = 50$			$n = 100$		
		r	Mean	RMSE	r	Mean	RMSE	r	Mean	RMSE
2	0.5	3	0.55191	0.12795	5	0.53020	0.08585	10	0.51294	0.05625
		5	0.55363	0.13522	10	0.52976	0.08607	20	0.51495	0.06071
	0.7	3	0.77271	0.17914	5	0.74220	0.12021	10	0.71811	0.07875
		5	0.77516	0.18931	10	0.74167	0.12050	20	0.72093	0.08500
	1.0	3	1.10399	0.25591	5	1.06040	0.17173	10	1.02588	0.11249
		5	1.10737	0.27044	10	1.05953	0.17214	20	1.02990	0.12142
4	0.5	3	0.55191	0.12795	5	0.53020	0.08586	10	0.51294	0.05625
		5	0.55368	0.13522	10	0.52976	0.08607	20	0.51495	0.06071
	0.7	3	0.77210	0.17914	5	0.74228	0.12021	10	0.71811	0.07875
		5	0.77516	0.18931	10	0.74167	0.12050	20	0.72093	0.08500
	1.0	3	1.10310	0.25591	5	1.06040	0.17173	10	1.02509	0.11249
		5	1.10737	0.27044	10	1.05953	0.17214	20	1.02990	0.12142

5.1 Application (1)

This application considers the use of the Type-II left censored J -shaped family distributions to fit a real-life data set which represents the number of cycles to failure for a group of 60 electrical appliances [25]. The failure times are

14 34 61 69 80 123 165 210 381 464 479 556
 574 839 917 969 991 1064 1088 1091 1174 1270 1275 1355
 1397 1477 1578 1649 1702 1893 1932 2011 2161 2292 2326 2337
 2628 2785 2811 2886 2993 3122 3248 3715 3790 3857 3912 4100
 4106 4116 4315 4510 4584 5267 5299 5583 6065 9701.

Table 3: Mean and RMSE for MLE of β for different combinations of r, n, β and θ of the generalized uniform distribution.

θ	β	$n = 25$			$n = 50$			$n = 100$		
		r	Mean	RMSE	r	Mean	RMSE	r	Mean	RMSE
2	0.5	3	0.65210	0.38329	5	0.57583	0.23810	10	0.53565	0.1684
		5	0.67379	0.41918	10	0.58752	0.26122	20	0.54136	0.17896
	0.7	3	0.87339	0.43439	5	0.78594	0.27084	10	0.74041	0.19055
		5	0.89696	0.47507	10	0.79919	0.29604	20	0.74876	0.20284
	1.0	3	1.20399	0.51105	5	1.10110	0.31864	10	1.04754	0.22417
		5	1.23171	0.55891	10	1.11670	0.34829	20	1.05515	0.23861
4	0.5	3	0.65299	0.38329	5	0.57587	0.23900	10	0.53565	0.16814
		5	0.67379	0.41918	10	0.58752	0.26122	20	0.54136	0.17896
	0.7	3	0.87339	0.43439	5	0.78534	0.27084	10	0.74041	0.19055
		5	0.89696	0.47507	10	0.79919	0.29604	20	0.74876	0.20281
	1.0	3	1.20399	0.51105	5	1.10110	0.31864	10	1.04754	0.22418
		5	1.23172	0.55891	10	1.11669	0.34829	20	1.05515	0.23861

The last observation was ignored as it is about 4 standard deviations above the mean and thus can be considered as an outlier. Thus, the data was rescaled by dividing each observation by 7000 [26]. The maximum likelihood estimates for θ and β were found to be 0.8664 and 0.8425, respectively. The Kolmogorov-Smirnov ($K - S$) test was used for this data set. The Kolmogorov-Smirnov test statistic value was found to be 0.11 and the theoretical critical value at $\alpha = 0.05$ was 0.17. Thus, fitting the J -shaped family distribution is adequate for the above data set. In the reliability analysis, the first 10 observations were censored, i.e., $r = 10$. The maximum likelihood estimates using the remaining data were 0.8664 for θ and 0.9086 for β . The estimated hazard function of the J -shaped family distribution using the complete and censored samples is shown in Figure 1. It is seen that the estimated hazard functions for the complete and censored samples are very close.

5.2 Application (2)

This application considers the use of the Type-II left censored power function distribution to fit a real-life data set which represents the failure times (in minutes) for a sample of 15 electronic components in an accelerated life test [25]. The failure times were analyzed to illustrate the Type-II left censoring scheme. The failure times are

1.4 5.1 6.3 10.8 12.1 18.5 19.7 22.2 23.0
30.6 37.3 46.3 53.9 59.8 66.2.

The validity of the power function distribution was checked. Based on the maximum likelihood estimates of θ and p , the parameters of 66.2 and 0.792, respectively, were obtained. The Kolmogorov-Smirnov ($K - S$) test was used for this data set. It is observed that the K-S distance between the fitted and the empirical distribution functions, and the corresponding critical value at $\alpha = 0.05$ are 0.167 and 0.33, respectively. Thus, the fit of power function distribution fits the above data reasonably well.

In the analysis, the first three observations, $r = 3$, were censored, namely, $x_{(1)} = 1.4, x_{(2)} = 5.1$ and $x_{(3)} = 6.3$. The maximum likelihood estimate of θ was 66.2 and p

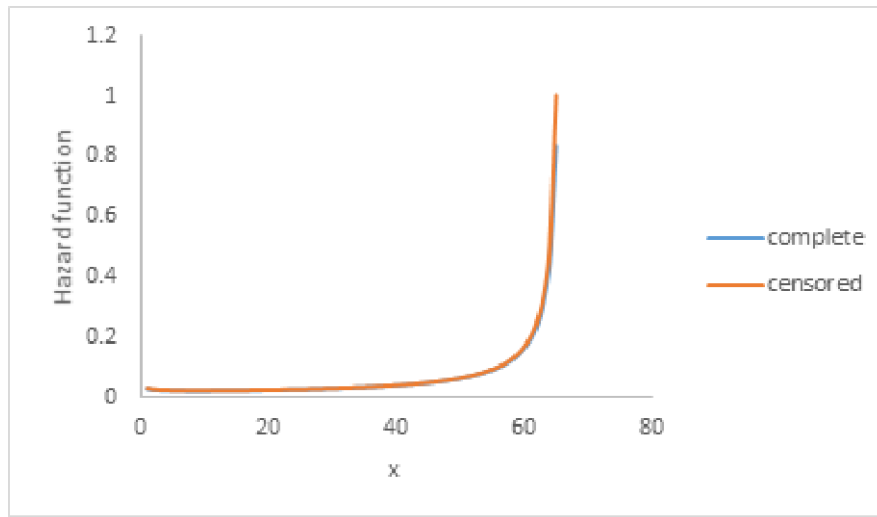


Figure 1: Hazard function of J -shaped distribution using complete and censored sample.

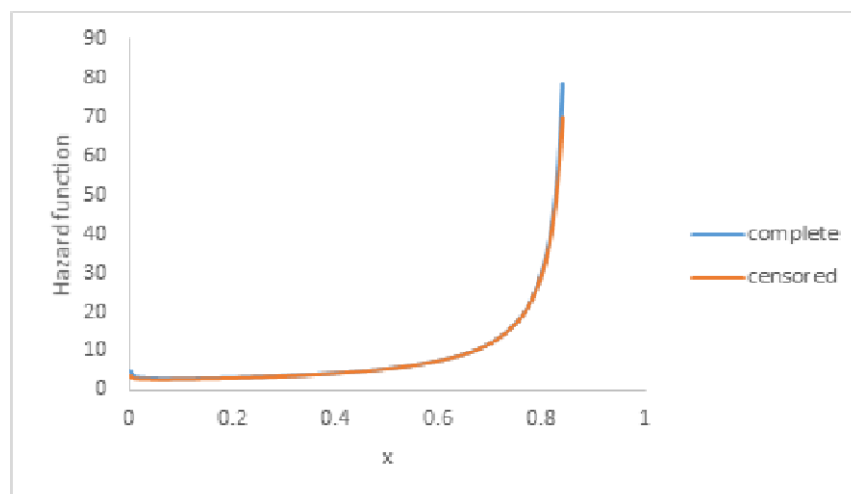


Figure 2: Hazard function of power function distribution using complete and censored samples.

was 0.7693. The estimated hazard functions for the complete and censored samples are shown in Figure 2. It is seen that the estimated hazard functions for the complete and censored samples are very close.

6 Conclusion

Type-II left censoring of three popular finite support family distributions, namely, the J -family distributions, the regular power function distribution and the generalized uniform

distribution have been considered. The maximum likelihood estimators (MLEs) were derived for these distributions. A comprehensive simulation study was conducted for different sample sizes, parameter values, and censored proportions. Two lifetime data sets were analyzed to illustrate the Type-II left censoring scheme under the power function distribution and J -shaped family distributions and showed appropriate results.

References

- [1] M. M. Smadi and A. A. Jaradat. System reliability of Ailamujia model and additive failure rate models. *Nonlinear Dynamics and Systems Theory* **21** (2) (2021) 193–201.
- [2] N. Balakrishnan and R. Aggarwala. *Progressive Censoring: Theory, Methods and Applications*, Birkhauser, Boston, 2000.
- [3] N. Balakrishnan and D. Kundu. Hybrid censoring: Models, inferential results and applications. *Computational Statistics and Data Analysis* **57** (1) (2013) 166–209.
- [4] A. A. Abu-Taleb and M. M. Smadi. Asymptotic efficiencies of the survival functions estimators for the exponential distribution. *International Mathematical Forum* **1** (38) (2006) 1861–1869.
- [5] M. M. Smadi, A. Zghoul, M. H. Alrefaei. Progressive type-II censoring power function distribution under binomial removals. *Nonlinear Dynamics and Systems Theory* **21** (4) (2021) 510–524.
- [6] H. Krishna, Vivckanad and K. Kumar. Estimation in Maxwell distribution with randomly censored data. *Journal of Statistical Computing and Simulation* **85** (17) (2015) 3560–3578.
- [7] A. F. Coburn, T. McBride and E. Ziller. Patterns of health insurance coverage among rural and urban children. *Medical Care Research review* **59** (3) (2002) 272–292.
- [8] J. Bagger. *Wage Growth and Turnover in Denmark*. University of Aarhus, Denmark, 2005.
- [9] H. Jiang, P. J. Fine and R. Chappell. Semiparametric analysis of survival data with left truncation and dependent right censoring. *Biometrics* **61** (2005) 567–575.
- [10] A. C. Robert, M. W. Amanda, I. P. Jennifer, P. V. Marc and R. A. Kelly. Methods for handling left-censored data in quantitative microbial risk assessment. *Applied and Environmental Microbiology* **84** (20) (2018) 1–10.
- [11] S. Yoshinari, T. Noriko and A. Hiroshi. Attempt of Bayesian estimation from left-censored data using the Markov Chain Monte Carlo method: Exploring Cr(VI) concentrations in mineral water products. *Food Safety* **8** (4) (2020) 67–89.
- [12] N. Balakrishnan and J. V. Varadan. Approximate maximum likelihood estimation of the location and scale parameters of the extreme value distribution based on complete and censored samples. *IEEE Transactions on Reliability* **40** (1991) 146–151.
- [13] S. S. Wagner and S. A. Altmann. What time do the baboons come down from the trees? (An estimation problem). *Biometrics* (1973) 623–635.
- [14] S. Mitra and D. Kundu. Analysis of left censored data from the generalized exponential distribution. *Journal of Statistical Computing and Simulation* **78** (7) (2008) 669–679.
- [15] N. S. Sindhu, M. Asalam and N. Feroze. Bayes estimation of the parameters of the inverse Rayleigh distribution for left censored data. *ProbStat Forum* **6** (2013) 42–59.
- [16] M. Asgharzadeh, M. Mohammadpour and Z. M. Ganji. Estimation and reconstruction based on left censored data from Pareto model. *Journal of Iranian Statistical Society* **13** (2) (2014) 151–175.
- [17] T. N. Sindhu, N. Feroze and M. Aslam. Study of the Left Censored Data from the Gumbel Type II Distribution under a Bayesian Approach. *Journal of Modern Applied Statistical Methods* **15** (2) (2016) 112–134.

- [18] C. W. Topp and F. C. Leone. A family of J -shaped frequency functions. *Journal of the American Statistical Association* **50** (1955) 209–219.
- [19] S. Nadarajah and S. Kotz. Moments of some J -shaped distributions. *Journal of Applied Statistics* (2003) 311–317.
- [20] M. H. Tahir, M. Alizadeh, M. Mansoor, C. M. Cordeiri and M. Zubair. The Weibull-power function distribution with applications. *Hacettepe Journal of Mathematics and Statistics* **45** (1) (2016) 245–265.
- [21] M. Meniconi and D. M. Barry. The Power Function Distribution: A Useful and Simple Distribution to Assess. Electrical Component Reliability. *Journal Microelectron Reliability* **36**(9) (1996) 1207–1212.
- [22] M. B. Bhatt. Characterization of Generalized Uniform Distribution. *Open Journal of Statistics* **8** (4) (2014) 563–569.
- [23] C. Lee. Estimations in the generalized uniform distribution. *Journal of the Korean Data & Information Science Society* **11**(2) (2000) 319–325.
- [24] M. I. Khan and M. A. R. Khan. Characterization of Generalized Uniform Distribution Based on Lower Record Values. *Prob Stat Forum* **10** (2017) 23–26.
- [25] J. F. Lawless. *Statistical Models and Methods for Lifetime Data*, 2nd Ed. John Wiley and Sons, New York, USA, 2003.
- [26] A. A. Zghoul. Record values from a family of J -shaped distributions. *Statistica* **3** (2011) 355–365.

CAMBRIDGE SCIENTIFIC PUBLISHERS

AN INTERNATIONAL BOOK SERIES
STABILITY OSCILLATIONS AND OPTIMIZATION OF SYSTEMS

Advances in Stability and Control Theory for Uncertain Dynamical Systems

Stability, Oscillations and Optimization of Systems: Volume 11

317+xxii pp., 2021 ISBN 978-1-908106-73-5 £60/\$80/€67

C. Cruz-Hernández (Ed.)

Department of Electronics and Telecommunications, Scientific Research and Advanced Studies Center of Ensenada (CICESE), Ensenada, México.

A.A. Martynyuk (Ed.)

Institute of Mechanics, National Academy of Sciences of Ukraine, Kyiv, Ukraine

A.G. Mazko (Ed.)

Institute of Mathematics, National Academy of Sciences of Ukraine, Kyiv, Ukraine

This volume presents the latest investigations in stability and control theory for uncertain dynamical systems, incorporating the main engineering applications. The volume consists of 16 chapters containing the results of theoretical research and engineering applications of some uncertain systems and provides new trends for future promising researches. Some issues covered in the volume include:

- stability and control in uncertain systems: optimal design of robust control, generalization of direct Lyapunov method, robust output feedback stabilization and optimization of control systems, optimal control of nonlinear systems over an infinite horizon;
- stability and stabilization in discrete-time systems: stability conditions for discrete-time positive switched systems with delay, quadratic stabilization for nonlinear perturbed discrete time-delay systems, robust output feedback stabilization and optimization of discrete-time control systems, stability of singularly perturbed nonlinear Lur'e discrete-time systems;
- synchronization in dynamical systems: function projective dual synchronization of chaotic systems with uncertain parameters, anti-synchronization and hybrid synchronization of 3D discrete generalized Hénon map, adaptive hybrid function projective synchronization;
- engineering applications: attitude stabilization of a rigid body, adaptive control of continuous bioreactors, wavelet adaptive tracking control, adaptive fuzzy control of nonlinear systems, robust active control for structural systems with structured uncertainties.

The **Advances in Stability and Control Theory for Uncertain Dynamical Systems** may be useful for graduate students and researchers in applied mathematics and physics, control, nonlinear science, and engineering.

CONTENTS: Introduction to the series • Preface • Contributors • An Overview • Stability and Control in Uncertain Systems • Stability and Stabilization in Discrete-Time Systems • Synchronization in Dynamical Systems • Engineering applications • Index

Please send order form to:

Cambridge Scientific Publishers

45 Margett Street, Cottenham, Cambridge CB24 8QY, UK

Telephone: +44 (0) 1954 251283; Fax: +44 (0) 1954 252517

Email: janie.wardle@cambridgescientificpublishers.com

Or buy direct from our secure website: www.cambridgescientificpublishers.com
